# Ore vectoring in IOCG systems: trace elements in garnets from the Groundhog skarn, Punt Hill, South Australia

Thesis submitted in accordance with the requirements of the University of Adelaide for an Honours Degree in Geology

Diana-Sophia Nikolakopoulos

November 2013


THE UNIVERSITY of ADELAIDE

**Trace elements in garnet from Groundhog, S.A.**


## ABSTRACT

The Groundhog Cu-Pb-Zn prospect, Punt Hill district, eastern Gawler Craton, South Australia, is a recently discovered ore system located within the 1.6 Ga Olympic iron oxide-copper-gold (IOCG) Province. The prospect is characterized by a retrogressive calcic skarn/IOCG-type footprint. Laser-ablation inductively-coupled plasma mass spectrometry spot analyses and grain-scale element mapping of garnet and accessory minerals, supported by optical and scanning electron microscopy and electron probe microanalysis, determines distributions of rare earth (REE), incompatible and ore-forming elements within skarn and marker horizons.

Distinct textural categories of garnet, each reflecting stages in the evolution of the skarn system, are recognised. Fe-rich prograde andradite is oscillatory-zoned, with high W and As, relatively low ΣREY, and low HREE/LREE ratio. Retrograde garnet is Al-rich, characterised by ΣREY concentrations an order of magnitude higher, high HREE/LREE, and high concentrations of incompatible and high field strength elements. Marked Cr enrichment defines the garnet rim.

Trace element distributions in texturally-distinct categories of garnet are applied as mineralization vectors along the two controlling structures. Based on Cr concentrations in rim garnet, the NNE-trending structure is interpreted to control fluid flow, with increasing intensity of mineralization towards NNE. Vectors defined by REY- and W-concentrations in prograde and retrograde garnets indicate that NW-SE structures drive skarn-forming fluids on the regional scale. This has potential for defining metallogenic patterns in the broader Punt Hill area. Application of such vectors requires, however, that the data is adequately interpreted in the contexts of textures and of prograde-to-retrograde evolution of the system. Groundhog is an oxidised IOCG system with skarn alteration positioned distal to a deep magmatic fluid source. Comparison of garnet chemistry at Groundhog and Hillside points to a possible N-S, W- to Sn-enriched trend within the Olympic Province. Results may offer a basis for defining specific settings for magma generation within the province.



## KEYWORDS

Ore vectoring, garnet, skarn, IOCG, Groundhog, Punt Hill, mineral trace element signature

## TABLE OF CONTENTS

## LIST OF FIGURES

## LIST OF TABLES

# Trace elements in garnet from Groundhog, S.A.

## INTRODUCTION

Detailed investigation of the mineralogy and geochemistry of alteration and mineralization phases are important for tracking the evolution of an ore system and can be used as framework for distinguishing regional versus local signatures of Iron Oxide Copper-Gold (IOCG) footprints (Haywood & Skirrow 2010). Characterization of minerals specific to the IOCG-hosting environment also allows for interpretation of the dynamic evolution of a specific ore system in time and space. In turn, this can be implemented as a tool for exploring the footprints of IOCG-skarn systems in heterogeneous sample media. Distinguishing alteration and mineralization signatures within an IOCG-skarn system, relative to those outside the main deposit, carries significant implications for vectoring towards high-grade ore zones within the mineral system. Garnet skarns, in particular, represent an excellent host for a wide variety of trace elements, including rare earth elements (REE) (Smith *et al.* 2004; Gaspar *et al.* 2008; Ismail *et al.* in press), and as a refractory mineral, may record discrete prograde and retrograde events.

The Groundhog Cu (+Au-Ag-Zn-Pb-REE) prospect is located within retrogressive calcic exoskarn host rocks of the Punt Hill district (Reid *et al.* 2011). Skarn formation is favoured by the presence of a calcareous sedimentary and volcaniclastic protolith, approximately 200-400 m thick, deposited within local sediment-filled basins comparable to either Moonta-Wallaroo or Hutchinson Group sequences (Reid *et al.* 2011). Groundhog is located within the Olympic Province (Skirrow *et al.* 2007; Figure 1A), where IOCG-style mineralization is linked to hydrothermal fluids associated with

**Trace elements in garnet from Groundhog, S.A.**

~1.6 Ga Hiltaba Intrusive Suite (HIS) and Gawler Range Volcanics (GRV) (Hand *et al.* 2007; Hand & Reid 2012). This magmatic package has been considered as a Large Igneous Province by some authors (e.g. Allen *et al*. 2008).

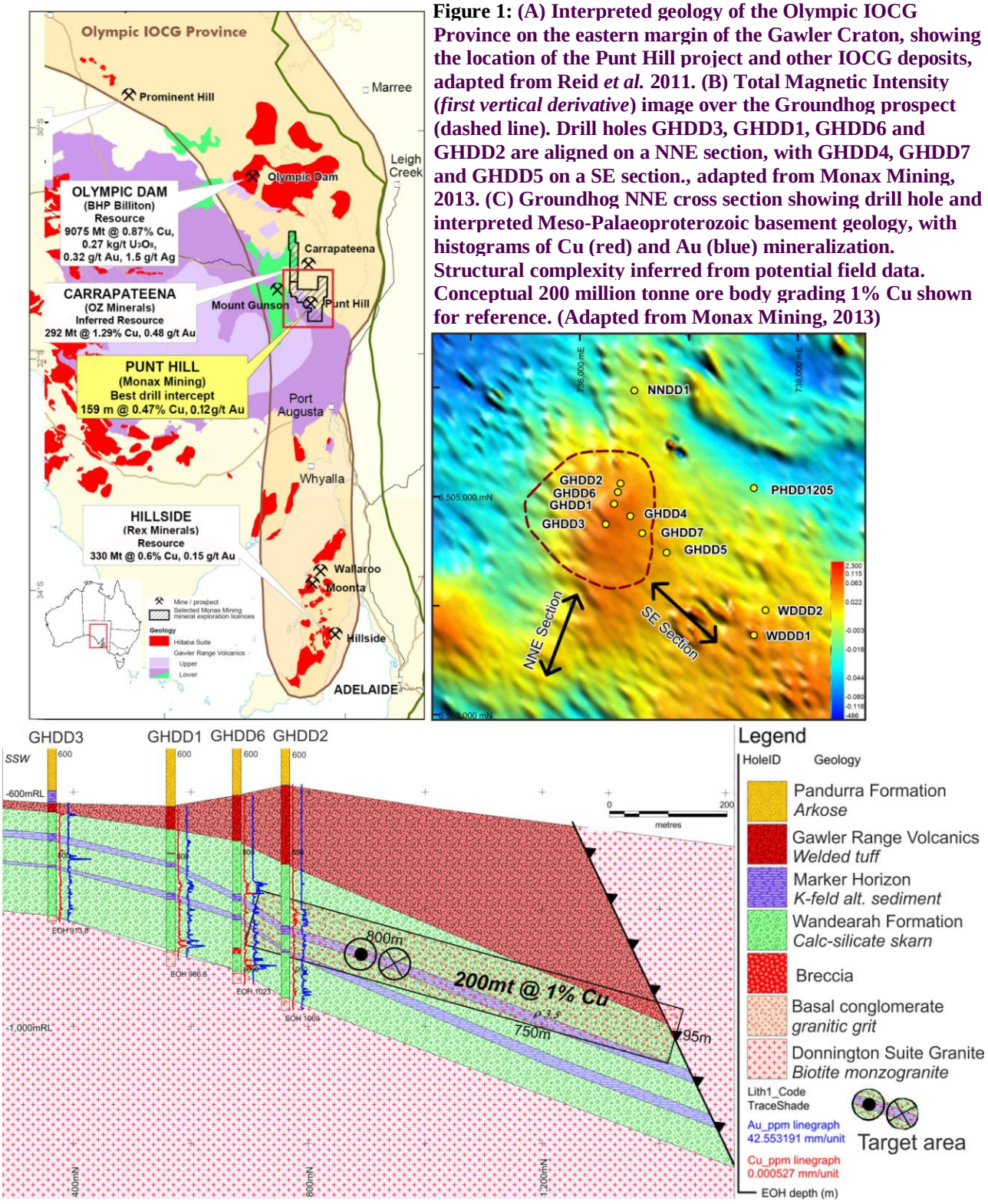


**Figure 1: (A) Interpreted geology of the Olympic IOCG Province on the eastern margin of the Gawler Craton, showing the location of the Punt Hill project and other IOCG deposits, adapted from Reid *et al.* 2011. (B) Total Magnetic Intensity (*first vertical derivative*) image over the Groundhog prospect (dashed line). Drill holes GHDD3, GHDD1, GHDD6 and GHDD2 are aligned on a NNE section, with GHDD4, GHDD7 and GHDD5 on a SE section., adapted from Monax Mining, 2013. (C) Groundhog NNE cross section showing drill hole and interpreted Meso-Palaeoproterozoic basement geology, with histograms of Cu (red) and Au (blue) mineralization. Structural complexity inferred from potential field data. Conceptual 200 million tonne ore body grading 1% Cu shown for reference. (Adapted from Monax Mining, 2013)**

**Trace elements in garnet from Groundhog, S.A.**

This paper considers variation in garnet chemistry along NW- and NNE-trending drill hole sections at Punt Hill as a potential vector for fluid-flow, alteration and high-grade mineralization. Using optical and scanning electron microscopy (SEM), electron probe microanalysis (EPMA) and laser ablation inductively-coupled plasma mass spectrometry (LA-ICP-MS), the evolution of the IOCG-skarn system is tracked in both time and space. Trace and Rare Earth Element (REE) distribution is also applied to distinguish mineralised from non-mineralised, and proximal from distal, skarn and ore assemblages. Characterisation of mineral element chemistry at Punt Hill has potential benefits beyond the specific geological setting at Groundhog and can assist with establishing the regional-scale alteration footprint of IOCG mineralization elsewhere in the Olympic Province and beyond.

## GEOLOGICAL SETTING

The Punt Hill project is located in the Olympic IOCG Province, positioned along the eastern margin of the Gawler Craton, South Australia (Figure 1a). The Gawler Craton embodies an Archaean to Mesoproterozoic crystalline basement comprising volcanic, granitic and metasedimentary rocks which have been subjected to a protracted crustal growth and tectonic history (Parker, 1990, 1993; Ferris *et al.* 2002; Hand *et al.* 2007). The Palaeoproterozoic crystalline basement at Punt Hill consists of ca. 1850 Ma Donington Suite granite, overlain by the Wandearah Metasiltstone which is interpreted to be equivalent to the ca. 1850-1735 Ma Wallaroo and/or Hutchinson Groups (Reid *et al.* 2010). A significant episode in the geologic evolution of the Gawler Craton was emplacement of the ca. 1600-1580 Ma Hiltaba Intrusive Suite (HIS) and extrusion of the Gawler Range Volcanics (GRV) (e.g., Skirrow *et al.* 2007), with deposition of

coeval IOCG mineralization at Olympic Dam, Prominent Hill, Carrapateena, Hillside and Moonta-Wallaroo (Skirrow *et al.* 2002; Belpeiro & Freeman 2004; Skirrow *et al.* 2007; Conor *et al.* 2010). The Proterozoic crystalline basement is unconformably overlain by Adelaidean rock units of the Stuart Shelf, comprising arenaceous redbeds, amygdaloidal basalts, shale limestone, quartzite and sandstone (Parker 1990; Reid *et al.* 2011).

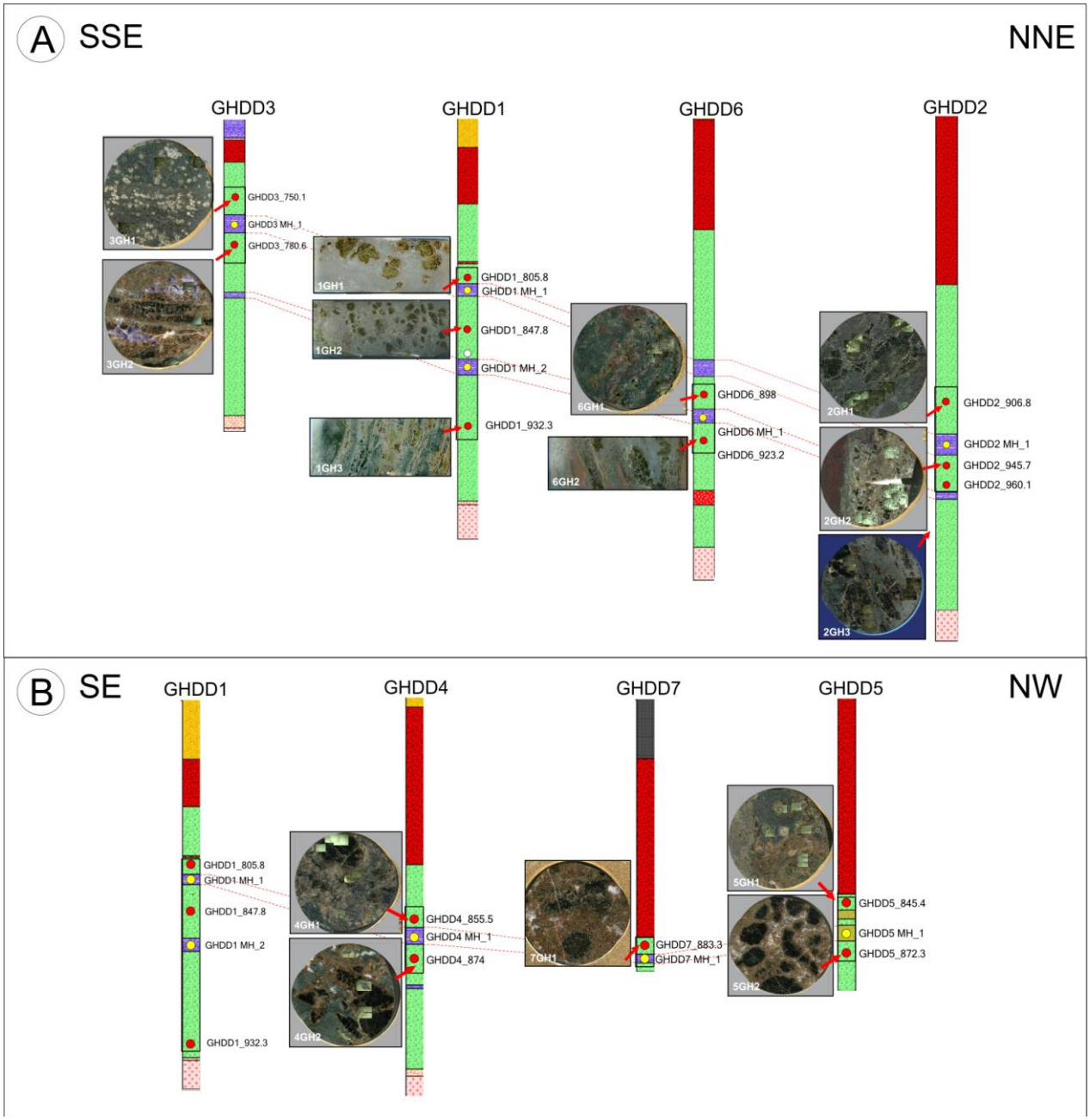


**Figure 2: (A) NNE trending section showing proximal drillcores GHDD3, GHDD1, GHDD6 and GHDD2 with images of garnet skarn samples that have undergone LA-ICP-MS analysis from above and below the marker horizon. (B) SE section (NNW trending) including distal drill holes GHDD1, GHDD4, GHDD7 and GHDD5 with images of garnet skarn samples that have undergone LA-ICP-MS analysis from above and below the marker horizon. (Distances between drill holes are not to scale)**

**Trace elements in garnet from Groundhog, S.A.**

Punt Hill comprises skarn alteration with associated Cu-Au-Ag-Zn-Pb-REE mineralization, sharing many similarities with other alteration systems within the Olympic IOCG Province. The best intercept of mineralization at the Groundhog prospect from drill hole GHDD6 included 159 m @ 0.47 Cu, 5.3 g/t Ag, 0.12 g/t Au, 0.48% Zn & 0.12% Pb, including 17 m @ 1.1% Cu, 1.2% Zn & 8.5 g/t Ag (Monax Mining Limited 2011). Mineralised skarns are positioned within a 250-400 m-thick interval beneath the GRV and above the Donington Suite granite, with no Hiltaba-related intrusion known in the area (Reid *et al.* 2011). Considering that the Donington Suite granite has been dated at ~1.8 Ga (Reid & Hand 2012), the much younger age of skarn alteration at Punt Hill implies there is no genetic correlation between hydrothermal fluids derived from the Donington Suite granite and the skarn. The Donington Suite granite may, however, play an important role in providing structural or lithological traps for fluid flow along structures as inferred from the models put forward to explain formation of the Carrapateena IOCG prospect, ~27 km NW from Groundhog (Porter 2010). Two types of structures are recognised in the Punt Hill district: NW- and NNE-trending features. Fluid flow modelling indicates that effective mineralization traps can develop at the junction between the different trending structures (Monax Mining Ltd. 2013).

A garnet-diopside-whole rock Sm-Nd isochron from the skarn mineral assemblage at Groundhog yielded an age of 1577 ± 7 Ma (Reid *et al.* 2011). The latter authors interpret this to be the age of crystallisation of cogenetic garnet-diopside aggregates, which comprise the bulk of the Punt Hill skarn. This links Groundhog mineralization to all the other major IOCG deposits in the Olympic Province, within the geodynamic

context of Columbia supercontinent break-up during Middle-Late Proterozoic (Reid *et al.* 2011).

The Groundhog mineralization is currently confined within an 887 $km^2$ area (Figure 1a, b), based on drill results from intersections along NW- and NNE-trending structures (Monax Mining Ltd. 2013). It is also recognized that an uplifted, barren Donington Suite granite block is present along the NNE-trending corridor. Thus, a current approach in developing the Groundhog prospect considers a 'Carrapateena' analogue model in which a high-grade, breccia-hosted ore should be found close to the uplifted Donington block along the NNE structure (Figure 1c).

A prominent impermeable feldspathic unit occurs within the skarn interval (Figs. 1c and 2). This was used in the present study as a marker horizon (MH) to ensure that analysed garnets, whether from above or below MH, were taken from comparable stratigraphic levels. The MH was also sampled in some of the drill cores. In order to understand variation of the skarn-mineralization with depth, the skarn sequence was also sampled from the overlying GRV to the Donington granite in one drill core located at the junction between SE- and NNE-trending sections (Figure 2).

## METHODOLOGY

Mineralogical and petrographic studies were undertaken on skarn and feldspathic marker horizon samples from 7 drill holes within the Groundhog prospect. A total of 31 samples were collected from the Groundhog drill holes GHDD1 to GHDD7 (Table 1).

**Trace elements in garnet from Groundhog, S.A.**

The samples are representative of mineralized (notably in drill holes GH1 and GH6) and non-mineralized calc-silicate skarn, metasediments and Gawler Range Volcanics.

Each sample was prepared as a one-inch polished block or polished thin sections. These were examined under a Nikon LV100 polarizing microscope in transmitted and reflected light mode, and using a FEI Quanta 450 scanning electron microscope (SEM) with energy dispersive X-ray spectrometry and back-scattered electron (BSE) imaging capabilities (Adelaide Microscopy, University of Adelaide). BSE imaging was used to characterise mineral parageneses, to document significant textures and mineralogical relationships, as well as to identify inclusions of REE-bearing phases within iron oxides, calc-silicates and accessory minerals.

Garnet and other minerals which vary in composition, including accessory minerals, were analysed in selected samples to obtain quantitative major and minor element compositional data. A Cameca SX-Five electron probe microanalyser (Adelaide Microscopy) was used. Operating conditions, standards, X-ray lines and typical minimum detection limits are given in Appendix A.

Laser-Ablation Inductively-Coupled Mass Spectrometry (LA-ICP-MS) was used on selected polished thin sections and polished blocks to provide trace element concentrations in calc-silicate and accessory minerals. Spot analysis was performed on a Resonetics M-50-LR 193-nm Excimer laser microprobe coupled to an Agilent 7700cx Quadrupole ICP-MS (Adelaide Microscopy). This new-generation laser system offers excellent spatial resolution coupled with sub-ppm level sensitivity. LA-ICP-MS element

mapping of approximately 4 $mm^2$ – 1 $cm^2$ sized areas of samples from drill holes GHDD1-GHDD7 provided a visual image of trace element distribution at the grain scale. The same Resonetics LA-ICP-MS system was used. Full details of analytical methodology used for LA-ICP-MS spot analysis and element mapping are given in Appendix A.

Results of this project are of current or future interest to end-users in the minerals industry. For this reason, additional element maps and petrographic images not included in the main body of the paper, are presented as Appendices B, D & E.

**Table 1: Sample suite showing sample ID, description, dril hole and intervals**

| Drill hole | Sample ID | Description | Interval (m) |
|---|---|---|---|
| GHDD1 | GH1-1 | Gawler Range Volcanics | 729.4 – 729.5 |
| GHDD1 | GH1-2 | Quartz-K-feldspar-chlorite veined metasediment | 730.3 – 760.4 |
| GHDD1 | GH1-3 | Talc-garnet-actinolite skarn | 805.8-805.9 |
| GHDD1 | GH1-4 | 'Marker horizon' calcite-hematite rock | 808.9- 809.0 |
| GHDD1 | GH1-5 | Mineralised- garnet-calcite skarn | 839.7- 839.8 |
| GHDD1 | GH1-6 | Mineralised garnet-calcite-feldspar skarn | 853.9- 854.0 |
| GHDD1 | GH1-7 | Mineralised-calcite-chlorite skarn | 857.8- 857.9 |
| GHDD1 | GH1-8 | 'Marker horizon' K-feldspar-chlorite metasediment | 857.8- 857.9 |
| GHDD1 | GH101_1 | Mineralized-hematite skarn | 847.8- 847.09 |
| GHDD1 | GH101_2 | Mineralised garnet-carbonate skarn | 889.9- 890.0 |
| GHDD1 | GH101_3 | Mineralised- actinolite- clinopyroxene skarn | 952- 952.1 |
| GHDD1 | GH101_4 | Biotite-talc-actinolite rock | 958.30- 958.3 |
| GHDD2 | GHDD2_1 | Mineralised-garnet skarn | 906.8 – 906.9 |
| GHDD2 | GHDD2_2 | 'Marker horizon' rimmed pyrites | 931.1 – 931.2 |
| GHDD2 | GHDD2_3 | Red banded Mineralised-garnet skarn | 945.8 – 945.8 |
| GHDD2 | GHDD2_4 | Massive garnet skarn | 960.1- 960.2 |
| GHDD3 | GHDD3_1 | Retrogressed amphibole-feldspar-pyrite skarn | 750.1- 750.2 |
| GHDD3 | GHDD3_2 | 'Marker horizon' banded feldspar-fluorite-sulphides | 771.2 – 771.3 |
| GHDD3 | GHDD3_3 | Banded garnet-calcite-fluorite skarn | 780.6 – 780.7 |
| GHDD4 | GHDD4_1 | Mineralised- massive garnet-calcite skarn | 855.5 |
| GHDD4 | GHDD4_2 | 'Marker horizon' mineralised and banded layers | 867.9 |
| GHDD4 | GHDD4_3 | Massive garnet-calcite skarn | 874.0 |
| GHDD5 | GHDD5_1 | Retrogressive amphibole skarn | 845.4 – 845.5 |
| GHDD5 | GHDD5_2 | Mineralised skarn (garnet absent) | 871.2- 871.3 |
| GHDD5 | GHDD5_3 | Massive garnet-calcite-feldspar skarn | 872.3- 872.4 |
| GHDD6 | GHDD6_1 | Mineralized-actinolite-garnet skarn | 864.1- 864.2 |
| GHDD6 | GHDD6_2 | 'Marker horizon' unbanded-pyrite | 879 |
| GHDD6 | GHDD6_3 | Retrogressive hematite-amphibole skarn | 898 |
| GHDD6 | GHDD6_4 | Mineralized-garnet- feldspar-calcite skarn | 923.2- 923.3 |
| GHDD7 | GHDD7_1 | Massive garnet-feldspar-calcite skarn | 883.3- 883.4 |
| GHDD7 | GHDD7_2 | 'Marker horizon' disseminated pyrite-green banded | 895.1- 895.2 |

## OBSERVATIONS AND RESULTS

### Petrography

Two lithologies have been studied: garnet-rich skarn and dominantly feldspathic rocks from the marker horizons (MH) (Figure 2, Table 1). The skarn is mineralised except in drill holes GHDD3, -5 and -7. Representative textures are shown in Figures 3 and 5, and compositional data (EPMA) for garnet, amphibole, talc and accessory apatite is included in Tables 2-5. Compositional variation in garnet is shown on Figure 4.

#### SKARN

The skarn is well-defined as a 200-300 m interval between the overlying Gawler Range Volcanics (GRV) unit and the subjacent Donington granite in all drill holes except GHDD5 and -7 where only the upper part of the skarn is intersected (Figure 2). The skarn is typified by green and brown colours and the presence of garnet in variable amounts (from ~50% to ~90%), of variable sizes (cm- to mm-size) and with textures ranging from massive, to banded (with other minerals forming the skarn matrix, see below) or porphyroblastic (Figure 2). Various degrees of brecciation and rounding of garnet are observed, especially in the skarn intervals from the mineralised drill holes. The skarn from the non-mineralized drill holes is more massive (garnetite) and shows variation in colour from dark (grain- or aggregate-cores) to light (margins) brown (Figure 2).

#### SKARN GARNET – TEXTURAL AND COMPOSITIONAL VARIATION

Skarn garnet is characterised by a variety of morphologies and textures; the most characteristic are shown in Figure 3. Some of the textures are present throughout all

drill holes whereas others are typical of the mineralised skarn only. Garnet is represented by members of the andradite (And) – grossular (Gr) – spessartine (Sp) solid solution series with compositions in the interval $And_{99-38}Gr_{0-58}Sp_{1-4}$, indicating dominant grandite compositions with minor Sp component (Figure 4; Table 2). Minor elements (<1 wt. %) but measurable by EPMA are Ti, F and Cl, as well as W and P.

Two main types of garnet are represented throughout all the intervals: I) oscillatory-zoned with bright (B) and dark (D) bands of composition (on BSE images; Figure 3a-c) in the ranges $And_{99-75}Gr_{0-24}Sp_{\sim 1}$ and $And_{74-60}Gr_{25-38}Sp_{1-2}$, respectively (Figure 4, Table 2), and II) weakly-zoned (Figure 3d) garnet, often inclusion-rich (pyroxene replaced by talc, apatite, titanite) with compositional range $And_{58-37}Gr_{40-60}Sp_{2-3}$ (Figure 3d, Table 2). The density of the inclusions varies widely, and, in some cases, the texture has a poikilitic appearance where the randomly-oriented inclusions appear to have grown within the garnet matrix.

These types of garnet and in particular type-I (B+D) form some of the largest single grains (up to 3-4 cm) and aggregates that are often preserved only as cores within domains that undergo replacement by more Al-rich, undifferentiated (U) garnet (indistinguishable in composition from type II) (Figure 3e). Often, type-I garnet also shows reworking of the oscillatory zoning with darker zones (Al-richer) superimposed onto initial Fe-richer cores (Figure 3c).

In addition to the above, in the mineralized skarn, a prominent type of texture is recognised as rim (R) to the larger garnets (type-I especially). The rim overlaps

compositionally with type-II and undifferentiated garnet (Figure 4; Table 2) and is thus unrecognisable on BSE images (Figure 3a). It is however optically distinct in that the garnet is strongly anisotropic and occurs as small garnet-grains outgrowing the larger garnet (Figure 3b). Such rims appear to be bracketed by chalcopyrite replacement of garnet (e.g. sample 2GH1, see also below). In some of the samples, small, subhedral garnets are also seen throughout the matrix of the skarn (M; see below).

Various aspects of gradational brittle to fluidisation textures are observed relating to garnet brecciation. These are accompanied by rim overgrowths and re-crystallization underlined by subtle oscillatory zoning post-dating the brecciation. One of the most outstanding textures observed in the mineralised skarn (4GH1) consists of an emulsion-like texture formed by dense apatite inclusions (< 1µm to a few µm) in garnet (Figure 3f; sample 4GH1). The margins of such garnet are rounded and show a darker rim on BSE images, also full of inclusions of quartz, coarser apatite (tens of µm) and hematite. Locally, pockets of larger still apatite, cemented by hematite, occur along preferentially-oriented zones of strong milling of garnet. This garnet is compositionally in the middle of the grandite series (Figure 4), i.e. average ~ $And_{49}Gr_{49}Sp_2$.

Garnet categories, as defined above, provide a basis for constraining temporal evolution from early-prograde (type-I and -II) to late-retrograde stages (U, R, M, emulsion-rich) during skarn development. Secondly, the trend in which the intensity of retrograde development increases towards NNW and NNE suggests a spatial vector from un-mineralised to mineralised skarn along the sampled profiles (Figure 2).

SKARN MATRIX: AMPHIBOLE, CHLORITE, TALC AND ACCESSORY MINERALS

Aside from garnet, the other component of the skarn is a relatively fine-grained (<1 mm) matrix consisting of variable proportions of green amphibole, chlorite, talc, carbonates, quartz (Figure 5a), and in some cases, fluorite (sample 3GH2). Potassium feldspar can also be present, in particular in samples adjacent to the MH. This matrix can be very rich in accessory minerals such as apatite, titanite (Figure 5b) and lesser zircon, especially in the mineralised skarn. Apatite alone can also be very abundant in samples adjacent to the MH, e.g. GHDD1-7 (see below). These accessory minerals are also found as inclusions within garnet. Crystallisation of matrix minerals appears to be late relative to garnet based on replacement relationships. Such replacement starts with corrosion of garnet boundaries and expands within the garnet as seen from clusters of inclusions of minerals typical of the matrix spreading inwards from the garnet margins (Figure 5a).

Amphibole is an important component of the matrix and its abundance increases with depth throughout the skarn intervals (e.g. 1GH3). Where abundant, the amphibole forms bundles of radial aggregates with dark blue-green colours (Figure 5c). The amphibole is also found as acicular inclusions crosscutting boundaries between sulphides and quartz (Figure 5d). Based on the ferro-index (0.73-0.21; Table 2) the amphibole varies in composition from ferro-actinolite to actinolite (Verkouteren & Wylie 2000). However, this amphibole is Al-rich (up to 9 wt. % $Al_2O_3$) and the calculated crystal chemical formulae show Al varying from 0.4 to 3.6 apfu. This suggests that the amphibole consists of interstratified layers of actinolite varieties (dominant) and hornblende (minor). Amphibole compositions are also characterized by few wt. % MnO (up to 4 wt.

%), as well as Cl contents (up to 1 wt. % Cl) (Table 3). Based on these observations, the crystallisation of amphibole appears to be late, i.e. post-dating sulphides.

The other important components of the matrix are talc (Table 4) and chlorite. Both are also seen replacing garnet even though talc is mostly constrained within euhedral shapes of a pre-existing, short-prismatic mineral (pseudomorphosis) found as inclusions in garnet. It is interesting to note that the abundance of these minerals relative to one another varies markedly from one sample to another (i.e. the sample is either chlorite- or talc-dominant). Chlorite, like amphibole, can be also Mn-enriched (Figure 5e; up to few wt. % MnO based on EDAX analyses). As in the garnet, talc in the matrix is often observed to replace a pre-existing short-prismatic mineral (Figure 5f).

These observations infer that pyroxenes from the diopside-hedenbergite-johannsenite series, with compositions varying from Mg-dominant (diopside) to Fe-dominant (hedenbergite), were present in the skarn associations. Pyroxene has been described by previous authors (e.g. Reid *et al.* 2011) but is extensively replaced by either talc (if Mg-rich) or chlorite (if Fe-rich) in the intervals sampled here. In the present samples the only pyroxene identified was seen in the deeper parts of the skarn intervals (e.g. 1GH3); such relics were too small to be analysed.

Of the accessory minerals, fluorapatite (Table 5) is by far the most abundant and is ubiquitously found throughout the skarn and MH samples.

**Trace elements in garnet from Groundhog, S.A.**

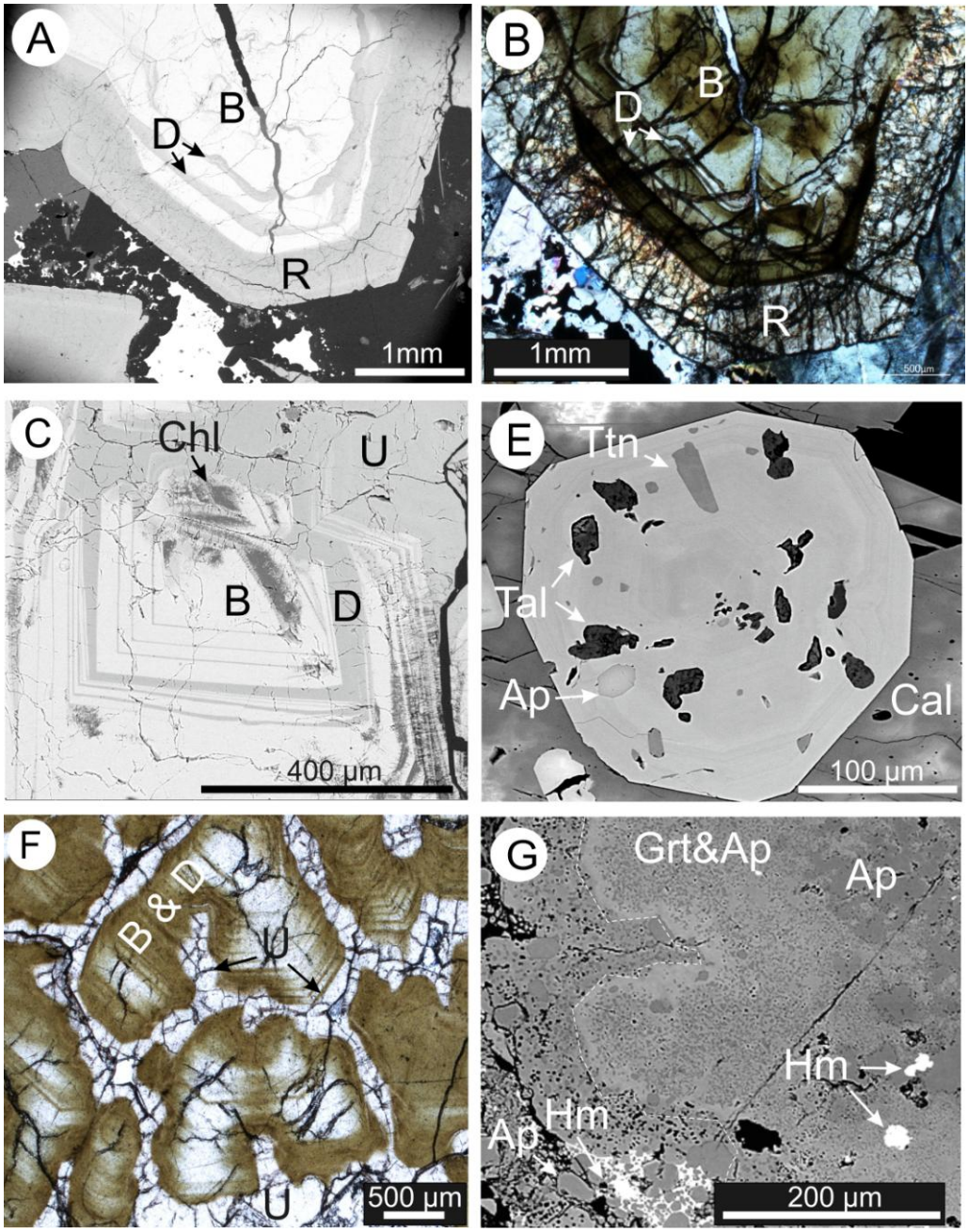


**Figure 3: Backscatter electron images (A, C, D, F) and transmitted light photomicrographs (B, E) showing main textural aspects of skarn garnet. (A) Garnet porphyroblast showing bright, oscillatory-zoned, andradite-rich core (B), darker, Al-rich mantle zone (D), and outermost rim (R). Major element compositions are similar in the 'D' and 'R' zones. (B) Image of the same grain as in (A) but in transmitted light, highlighting the dark green andradite core mantled by Al-rich garnet and the distinct outermost rim. Note that the latter consists of an aggregate of garnet microcrystals and has been extensively micro-fractured. (A) and (B) typify type-I garnet with rim overgrowth. (C) Undifferentiated garnet surrounding a reworked core showing oscillatory zoning between Fe-rich and Al-poor compositions. (D) Weakly-zoned idiomorphic garnet grain with inclusions of coarser Ap cemented by hematite (Hm). Abbreviations: Ap - apatite, cal – calcite, Grt- garnet, Hm- hematite and Ttn- titanite**

SKARN MINERALIZATION

The skarn hosts base metal mineralization consisting of chalcopyrite, bornite, chalcocite, (Fe-poor) sphalerite and galena. Minor components include members of the tetrahedrite-tennantite series (fahlore), wittichenite ($Cu_3BiS_3$) and native silver. Hematite is widespread throughout skarn but increases in abundance in the mineralised intervals. Scheelite was identified as minute inclusions trailing along/across zones of brecciated garnet.

Sulphides occur mostly as patches (up to few mm), veinlets and disseminations throughout the skarn matrix, generally concentrated within the middle part of the skarn intervals. There is, however, a strong spatial association between sulphides and garnet, in particular in cases where the latter is intensively brecciated (see also above). The relationships vary from advanced replacement of garnet by chalcopyrite (Figure 5g) to inclusions of bornite and galena in the core of the garnet (Figure 5h). In the former case, chalcopyrite shows skeletal growth parallel to compositional banding in garnet. A garnet rim overgrows such chalcopyrite replacement (Figure 5g). The majority of sulphides, mostly consisting of chalcopyrite and sphalerite (and minor galena) are placed in the matrix. Two stages of sulphide deposition can thus be inferred: (i) early Cu±Pb (replacement of garnet) and (ii) late Cu-Zn±Pb (co-existing or post-dating garnet rims).

Another notable characteristic of the sulphide ore is the presence of symplectites, e.g. bornite-galena, bornite+chalcocite, chalcocite-wittichenite or chalcopyrite-sphalerite±fahlore (Figure 5h-k). The latter are found as 10-100 µm-sized pockets

outside the garnet rim (Figure 5i). In detail, the symplectite texture between the sulphides and sulphosalts is reproduced by compositional variation within the sulphosalts themselves (Figure 5l). Such textures among Cu-Fe±Bi±Pb-sulphides are suggestive of sequential exsolution from higher-temperature bornite solid solutions (~400 °C) (e.g. Cook *et al.* 2011). The Cu-Zn-As-Sb-S associations could be instead related to (re)mobilisation of trace-elements from sulphides during superimposed stages of fluid-mineral reaction.

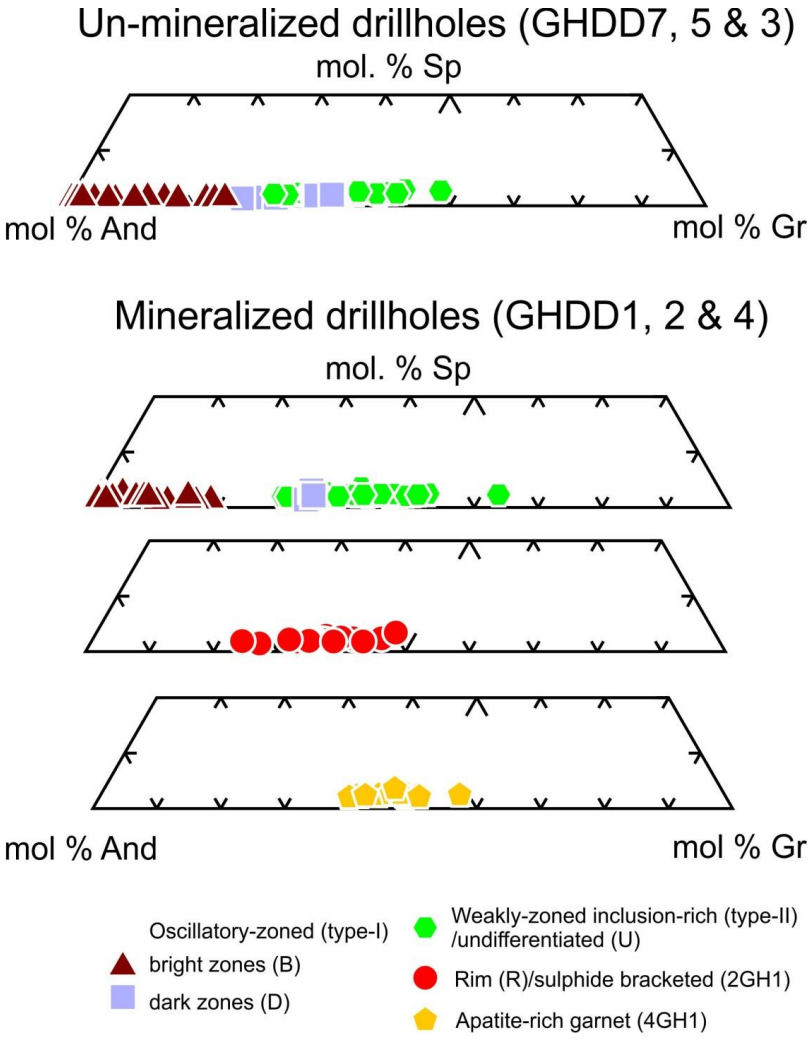


**Figure 4: Ternary compositional diagram for garnet expressed in terms of andradite (And), grossular (Gr) and spessartine (Sp) end-members (see Table 2). Data shown on diagram is compiled from EPMA results on sub-types of garnet throughout six drill cores (all except GHDD6). The diagram depicts evolution from an early, Fe-rich, initial prograde stage to an Al-rich retrograde stage. It also shows the overlap between all garnet categories except bright zones in type-I garnet. The compositional ranges are the same throughout the extent of the profiles as seen from garnet from non-mineralised and mineralised drill cores**

Hematite predates and co-exists with sulphides. It can be seen in association with bornite (Figure 5m) in an unusual apatite-rich carbonate rock found above one of the MH in drill hole GHDD1 (Figure 2). Native silver was identified as inclusions in bornite (Figure 5n).

## MARKER HORIZONS

The middle-upper part of the skarn intervals are bracketed by a pair of MH intervals (10-20 m thick, pink to grey, fine-grained rocks) positioned 30-40 m apart from one another. Exceptions are GHDD5 and 7 where the MH is positioned very close to the GRV limit (Figure 2). Marker horizons are considered almost impermeable units and have been described either as feldspathic, quartzitic, or shaly rocks (Reid *et al.* 2011). In the present samples MH are represented by end-member K-feldspar, minor quartz and carbonates as well as common fluorite, coarse (up to 500 µm) accessory minerals such as apatite, titanite, abundant zircon and hematite. Importantly, the MHs contain disseminations of sulphide, in some cases included within the fluorite. Sulphides are mostly represented by abundant pyrite (Figure 5o), arsenopyrite and minor sulpharsenides (cobaltite and gersdorffite); the presence of native gold and thorite has also been documented from MH samples. These rocks also contain dissemination of minerals that are common within the skarn intervals, e.g. chalcopyrite, sphalerite, tetrahedrite-tennantite and galena.

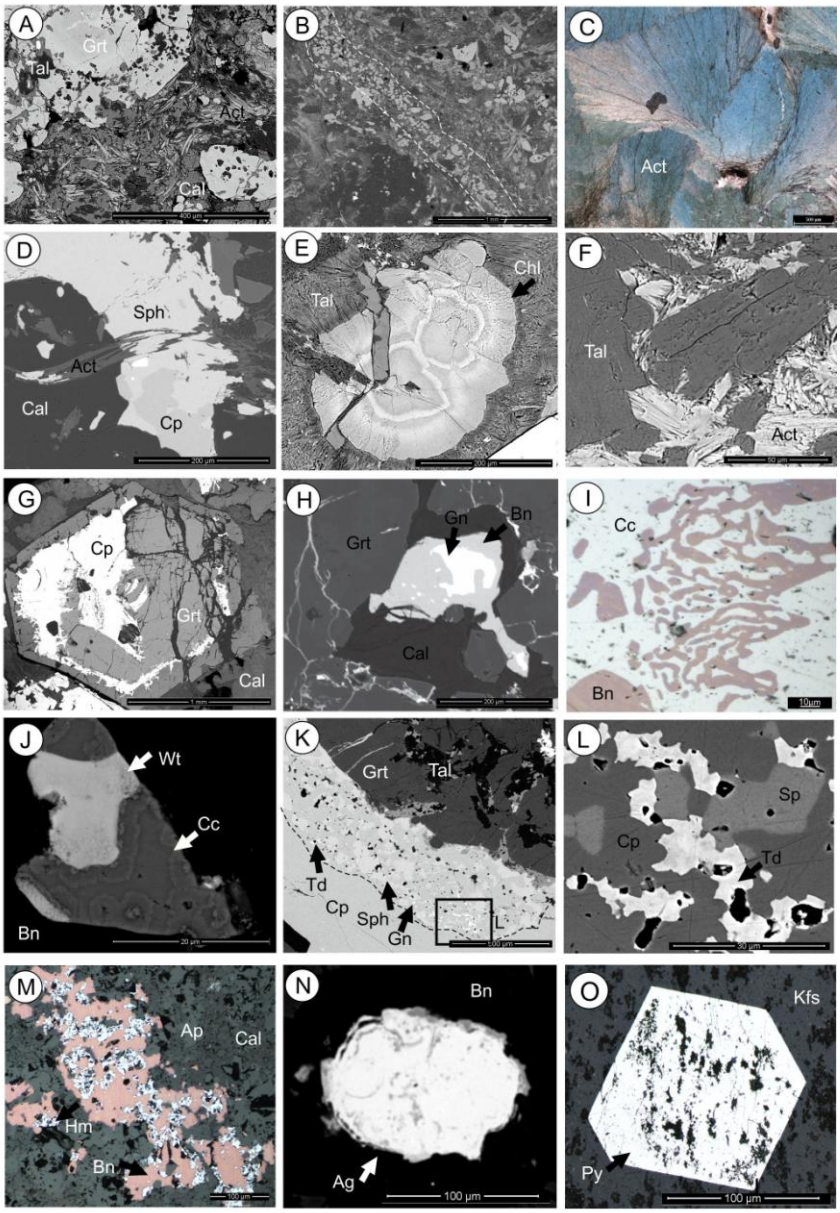


**Figure 5: Backscatter electron images (A, B, D-H, J-L, N, O) and reflected light photomicrographs (C, I, M) showing mineralogy and key textures of skarn matrix (A-F), mineralization (G-N) and marker horizon (O). (A) Fine-grained skarn matrix consisting of amphibole (Amph), talc (Tal), calcite (Cal) and coarse garnet (Grt). Note replacement of Grt by minerals from the matrix shown by boundary corrosion and inclusion formation. (B) Apatite (Ap)-rich band within the skarn matrix. Note small, subhedral grains of garnet (type M) on the margin of such bands. (C) Acicular ferro-actinolite (Fe-Act) aggregate with radial growth (shown by the undulatory pleochroism). (D) Amphibole crosscutting boundaries of quartz (Qz) and sphalerite (Sph); Cp=chalcopyrite. (E) Mn-rich radial aggregate of chlorite (Chl) in Fe-rich chlorite. (F) Pseudomorphic replacement of a pre-existing short prismatic mineral (pyroxene?) by talc. (G) Replacement of Grt by Cp. Note the outer rim of Grt outside the Cp. (H) Bornite (Bn)-galena (Gn) inclusions within Grt core. (I-K) Symplectites between various sulphides, Bn-chalcocite (Cc) in (I), wittichenite (Wit)-Cc in (J), Cp-Sph and tetrahedrite-tennantite (Ttn) in (K). (L) Detail of Ttn domain (marked by rectangle on (K), showing compositional heterogeneity in terms of Sb-(brighter) and As-rich (darker) domains. (M) Bornite with Hm inclusions within Ap-rich carbonate rock. (N) Native silver (Ag) inclusion in Bn from the same rock as (K). (O) Euhedral pyrite (Py) in K-feldspar (Kfs)-rich rocks from the marker horizon**

## Trace elements in garnet from Groundhog, S.A.

**Table 2: Electron probe microanalyses of garnet types from prograde through to retrograde stage**

| | Un-mineralised skarn | | | | | | Mineralised skarn | | | | | | | | | | | |
|---|---|---|---|---|---|---|---|---|---|---|---|---|---|---|---|---|---|---|
| | Prograde | | | | | | Prograde | | | | | | Retrograde | | | | | |
| | type I (oscillatory-zoned) | | type II (inclusion-rich and undifferentiated) | | | | type I (oscillatory-zoned) | | | | type II (inclusion-rich and undifferentiated) | | Rim | | | | Apatite-rich inclusions | |
| | | | | | | | | | | | | | sulphide bracketed | | | | | |
| | 7GH1 | 7GH1 | 7GH1 | 5GH2 | | 3GH2 | 1GH1 | 1GH1 | 2GH1 | 2GH1 | 4GH1 | | 2GH1 | | 4GH1 | | 4GH2 | |
| | B | D | | area 1 | area 2 | | B | D | B | D | area 1 | area 2 | area 1 | area 2 | area 1 | area 2 | area 1 | area 2 |
| (Wt. %) | (n=22) | (n=13) | (n=11) | (n=8) | (n=14) | (n=10) | (n=7) | (n=1) | (n=21) | (n=2) | (n=10) | (n=16) | (n=8) | (n=11) | (n=5) | (n=17) | (n=6) | (n=3) |
| CaO | 32.52 | 33.48 | 32.77 | 32.91 | 32.85 | 33.42 | 33.20 | 33.90 | 32.88 | 33.83 | 34.14 | 33.42 | 33.54 | 33.75 | 33.83 | 33.39 | 32.57 | 33.48 |
| $Na_2O$ | | | | | 0.02 | 0.06 | | | | | | | 0.12 | | | | | |
| $K_2O$ | | | | | | | | | | | | | | 0.03 | | | | |
| $Fe_2O_3$ | 28.37 | 21.34 | 19.34 | 20.33 | 17.89 | 16.84 | 26.77 | 21.39 | 29.78 | 20.89 | 18.27 | 17.10 | 19.64 | 19.68 | 19.08 | 17.61 | 18.48 | 15.36 |
| $TiO_2$ | 0.11 | 0.21 | 0.27 | 0.24 | 0.38 | 0.32 | 0.05 | | 0.08 | 0.39 | 0.51 | 0.69 | 0.32 | 0.54 | 0.60 | 0.64 | 0.38 | 0.58 |
| MgO | 0.03 | 0.03 | 0.04 | 0.06 | 0.05 | 0.07 | 0.09 | 0.08 | 0.07 | 0.06 | 0.09 | 0.27 | 0.11 | 0.24 | 0.06 | 0.09 | 0.23 | 0.11 |
| $SiO_2$ | 34.85 | 35.89 | 36.12 | 36.07 | 35.64 | 36.89 | 35.28 | 35.79 | 34.82 | 36.45 | 35.48 | 37.18 | 35.59 | 35.57 | 36.36 | 36.64 | 35.77 | 35.60 |
| MnO | 0.56 | 0.66 | 0.99 | 1.00 | 0.95 | 1.09 | 0.51 | 0.63 | 0.83 | 1.16 | 0.91 | 1.04 | 0.96 | 0.92 | 0.96 | 1.03 | 1.01 | 1.25 |
| $Al_2O_3$ | 2.18 | 7.29 | 8.94 | 8.14 | 9.83 | 10.88 | 3.17 | 7.45 | 0.71 | 7.29 | 9.10 | 9.97 | 8.14 | 8.08 | 8.97 | 10.10 | 9.44 | 9.55 |
| F | 0.27 | 0.48 | | | | 0.23 | | 0.56 | | | 0.41 | 0.30 | 0.32 | 0.82 | | 0.20 | | 0.24 |
| Cl | 0.02 | | | | | | | | 0.03 | | | | 0.04 | 0.03 | | | | |
| $P_2O_5$ | 0.04 | 0.04 | | | | 0.03 | | | 0.05 | 0.05 | 0.03 | | 0.05 | 0.03 | | 0.09 | | 0.08 |
| $WO_3$ | 0.12 | | | | | | | | | | | | | | | | | |
| **Total** | **99.10** | **99.42** | **98.47** | **98.74** | **97.63** | **99.69** | **99.08** | **99.82** | **99.24** | **100.11** | **98.96** | **99.98** | **98.83** | **99.68** | **99.86** | **99.80** | **97.89** | **96.23** |
| ***Formulae*** $(Ca,Mg,Mn)_6(Fe,Al)_4Si_6O_{24}$ | | | | | | | | | | | | | | | | | | |
| Mg | 0.009 | 0.008 | 0.011 | 0.014 | 0.013 | 0.016 | 0.022 | 0.021 | 0.017 | 0.014 | 0.021 | 0.064 | 0.026 | 0.058 | 0.016 | 0.021 | 0.057 | 0.026 |
| Mn | 0.081 | 0.091 | 0.137 | 0.139 | 0.133 | 0.148 | 0.073 | 0.088 | 0.120 | 0.161 | 0.127 | 0.142 | 0.134 | 0.129 | 0.132 | 0.141 | 0.141 | 0.177 |
| Ca | 5.924 | 5.914 | 5.760 | 5.795 | 5.804 | 5.752 | 5.986 | 5.975 | 6.011 | 5.906 | 6.016 | 5.750 | 5.937 | 5.953 | 5.870 | 5.771 | 5.746 | 6.004 |
| **Total** | **6.014** | **6.014** | **5.908** | **5.948** | **5.950** | **5.917** | **6.082** | **6.083** | **6.148** | **6.080** | **6.164** | **5.956** | **6.097** | **6.140** | **6.017** | **5.934** | **5.944** | **6.207** |

**Trace elements in garnet from Groundhog, S.A.**

| | | | | | | | | | | | | | | | | | | |
|---|---|---|---|---|---|---|---|---|---|---|---|---|---|---|---|---|---|---|
| Fe | 3.630 | 2.648 | 2.387 | 2.514 | 2.220 | 2.036 | 3.389 | 2.648 | 3.823 | 2.562 | 2.261 | 2.067 | 2.441 | 2.438 | 2.325 | 2.138 | 2.289 | 1.935 |
| Al | 0.365 | 1.335 | 1.654 | 1.506 | 1.789 | 1.987 | 0.568 | 1.334 | 0.084 | 1.340 | 1.600 | 1.860 | 1.467 | 1.424 | 1.603 | 1.832 | 1.722 | 1.843 |
| Ti | 0.015 | 0.026 | 0.034 | 0.029 | 0.048 | 0.038 | 0.007 | 0.000 | 0.011 | 0.048 | 0.064 | 0.084 | 0.040 | 0.067 | 0.073 | 0.078 | 0.047 | 0.073 |
| Cr | 0.000 | 0.000 | 0.000 | 0.000 | 0.000 | 0.000 | 0.000 | 0.000 | 0.000 | 0.000 | 0.000 | 0.000 | 0.000 | 0.000 | 0.000 | 0.000 | 0.000 | 0.000 |
| **Total** | **4.010** | **4.010** | **4.075** | **4.049** | **4.056** | **4.061** | **3.964** | **3.982** | **3.917** | **3.950** | **3.924** | **4.011** | **3.949** | **3.930** | **4.001** | **4.048** | **4.058** | **3.851** |
| | | | | | | | | | | | | | | | | | | |
| Si | 5.928 | 5.918 | 5.926 | 5.928 | 5.878 | 5.926 | 5.938 | 5.889 | 5.942 | 5.940 | 5.835 | 5.973 | 5.881 | 5.857 | 5.890 | 5.912 | 5.890 | 5.959 |
| Al | 0.072 | 0.082 | 0.074 | 0.072 | 0.122 | 0.074 | 0.062 | 0.111 | 0.058 | 0.060 | 0.165 | 0.027 | 0.119 | 0.143 | 0.110 | 0.088 | 0.110 | 0.041 |
| **Total** | **6.000** | **6.000** | **6.000** | **6.000** | **6.000** | **6.000** | **6.000** | **6.000** | **6.000** | **6.000** | **6.000** | **6.000** | **6.000** | **6.000** | **6.000** | **6.000** | **6.000** | **6.000** |
| | | | | | | | | | | | | | | | | | | |
| Na | 0.000 | 0.000 | 0.000 | 0.000 | 0.006 | 0.018 | 0.000 | 0.000 | 0.000 | 0.000 | 0.000 | 0.000 | 0.037 | 0.000 | 0.000 | 0.000 | 0.000 | 0.000 |
| K | 0.000 | 0.000 | 0.000 | 0.000 | 0.000 | 0.000 | 0.000 | 0.000 | 0.000 | 0.000 | 0.000 | 0.000 | 0.000 | 0.005 | 0.000 | 0.000 | 0.000 | 0.000 |
| | | | | | | | | | | | | | | | | | | |
| **TOTAL** | **16.024** | **16.023** | **15.983** | **15.997** | **16.006** | **15.978** | **16.045** | **16.065** | **16.065** | **16.031** | **16.089** | **15.967** | **16.046** | **16.070** | **16.018** | **15.981** | **16.002** | **16.058** |
| | | | | | | | | | | | | | | | | | | |
| ***Mol.% end-members*** | | | | | | | | | | | | | | | | | | |
| Andradite | 90.5 | 66.0 | 58.6 | 62.1 | 54.7 | 50.1 | 85.5 | 66.5 | 97.6 | 64.9 | 57.6 | 51.5 | 61.8 | 62.0 | 58.1 | 52.8 | 56.4 | 50.2 |
| Grossular | 9.1 | 33.3 | 40.6 | 37.2 | 44.1 | 48.9 | 14.3 | 33.5 | 2.1 | 33.9 | 40.8 | 46.4 | 37.2 | 36.2 | 40.1 | 45.3 | 42.4 | 47.9 |
| Spessartine | 1.3 | 1.5 | 2.3 | 2.3 | 2.2 | 2.5 | 1.2 | 1.4 | 2.0 | 2.6 | 2.1 | 2.4 | 2.2 | 2.1 | 2.2 | 2.4 | 2.4 | 2.8 |

**Table 3: Electron probe analytical data for ferroactinolite and actinolite within skarn samples**

| | FERROACTINOLITE | | | | | | ACTINOLITE |
|---|---|---|---|---|---|---|---|
| | 1GH3 | | 4GH2 | | 5GH2 | | 4GH2 |
| | Area 1 | Area 2 | Area 1 | Area 2 | | | Area 3 |
| | mean | mean | mean | mean | mean | | mean |
| | (n=10) | (n=10) | (n=14) | (n=14) | (n=4) | | (n=3) |
| F | 0.41 | | 0.23 | 0.21 | | | 0.06 |
| Cl | 0.75 | 0.78 | 0.53 | 0.58 | 0.54 | | 0.31 |
| $Na_2O$ | 0.95 | 0.31 | 0.37 | 0.34 | 0.26 | | 0.30 |
| MgO | 8.64 | 7.96 | 9.38 | 9.44 | 9.90 | | 11.86 |
| $Al_2O_3$ | 7.70 | 4.05 | 3.92 | 4.04 | 2.88 | | 3.63 |
| $SiO_2$ | 43.73 | 47.88 | 48.46 | 48.26 | 49.70 | | 48.77 |
| $P_2O_5$ | | | | | 0.02 | | |
| $K_2O$ | 1.39 | 1.04 | 0.85 | 0.95 | 0.67 | | 0.58 |
| CaO | 11.74 | 11.62 | 11.96 | 11.84 | 11.28 | | 11.77 |
| $TiO_2$ | 0.02 | 0.06 | 0.07 | 0.07 | 0.09 | | 0.05 |
| MnO | 0.37 | 0.84 | 1.73 | 1.14 | 2.68 | | 1.70 |
| FeO | 21.75 | 23.90 | 20.75 | 21.31 | 20.14 | | 17.62 |
| **Total** | **97.44** | **98.43** | **98.07** | **98.07** | **98.16** | | **96.64** |
| | | | | | | | |
| ***Formulae based on $Ca_2(Mg,Fe2+,Mn)_5(Si,Al)_8O_{22}(OH,F,Cl)_2$*** | | | | | | | |
| Si | 6.848 | 7.392 | 7.408 | 7.388 | 7.555 | | 7.421 |
| Al | 1.152 | 0.608 | 0.592 | 0.612 | 0.445 | | 0.579 |
| **Total** | **8.000** | **8.000** | **8.000** | **8.000** | **8.000** | | **8.000** |
| | | | | | | | |
| Mg | 2.016 | 1.831 | 2.136 | 2.153 | 2.243 | | 2.690 |
| Fe | 2.848 | 3.085 | 2.652 | 2.728 | 2.560 | | 2.242 |
| Ti | 0.005 | 0.013 | 0.015 | 0.017 | 0.021 | | 0.012 |
| Mn | 0.049 | 0.110 | 0.224 | 0.148 | 0.344 | | 0.220 |
| **Total** | **4.919** | **5.040** | **5.027** | **5.046** | **5.169** | | **5.163** |
| | | | | | | | |
| Ca | 1.970 | 1.923 | 1.959 | 1.941 | 1.837 | | 1.918 |
| Na | 0.144 | 0.046 | 0.054 | 0.050 | 0.038 | | 0.045 |
| K | 0.000 | 0.000 | 0.000 | 0.000 | 0.000 | | 0.000 |
| **Total** | **2.114** | **1.969** | **2.013** | **1.991** | **1.875** | | **1.963** |
| | | | | | | | |
| **Ferro index** | 0.59 | 0.64 | 0.57 | 0.57 | 0.56 | | 0.48 |
| | | | | | | | |
| F | 0.201 | 0.000 | 0.111 | 0.102 | 0.000 | | 0.029 |
| Cl | 0.198 | 0.205 | 0.137 | 0.151 | 0.138 | | 0.081 |
| OH | 0.601 | 0.795 | 0.751 | 0.747 | 0.862 | | 0.891 |
| **Total** | **1.000** | **1.000** | **1.000** | **1.000** | **1.000** | | **1.000** |

**Table 4: Electron probe microanalyses of talc inclusions within garnet**

| | **3GH2** | **4GH1** | **4GH2** |
|---|---|---|---|
| | (GH3 780m) | (GH4 855m) | (GH4 874m) |
| | mean | mean | mean |
| | (n=5) | (n=4) | (n=7) |
| F | 0.62 | 0.46 | 0.16 |
| Cl | 0.03 | 0.03 | 0.03 |
| $Na_2O$ | 0.20 | 2.04 | 0.16 |
| $K_2O$ | 0.06 | 0.07 | 0.03 |
| $SiO_2$ | 58.73 | 54.74 | 58.58 |
| MgO | 26.59 | 22.62 | 26.27 |
| $Al_2O_3$ | 1.25 | 1.18 | 1.14 |
| $P_2O_5$ | | 0.04 | |
| CaO | 0.64 | 2.21 | 0.91 |
| $TiO_2$ | 0.05 | | |
| $Fe_2O_3$ | 5.63 | 6.77 | 6.63 |
| MnO | 0.71 | 2.76 | 0.92 |
| **Total** | **94.35** | **92.92** | **94.82** |
| | | | |
| ***Formulae base on 10 O and 1 OH*** | | | |
| Si | 3.901 | 3.817 | 3.887 |
| Al | 0.220 | 0.219 | 0.200 |
| Total | 4.121 | 4.036 | 4.087 |
| | | | |
| Mg | 2.631 | 2.350 | 2.597 |
| Fe | 0.313 | 0.394 | 0.368 |
| Mn | 0.040 | 0.163 | 0.051 |
| Ca | 0.046 | 0.165 | 0.064 |
| Na | 0.013 | 0.138 | 0.010 |
| K | 0.003 | 0.003 | 0.001 |
| Cr | 0.005 | 0.000 | 0.000 |
| Ti | 0.000 | 0.004 | 0.000 |
| Total | 3.051 | 3.218 | 3.092 |
| | | | |
| F | 0.130 | 0.102 | 0.033 |
| Cl | 0.003 | 0.003 | 0.004 |

**Table 5: Electron probe microanalyses of fluorapatite**

| | 3GH MH1 | 1GH Ap-rich | 4GH1 |
|---|---|---|---|
| | (GH3 771m) | (GH1-7) | (GH4 855m) |
| | mean | mean | mean |
| | (n=5) | (n=5) | (n=4) |
| F | 3.85 | 4.11 | 4.74 |
| Cl | 0.06 | 0.07 | 0.05 |
| $Na_2O$ | 0.34 | | |
| $SiO_2$ | 0.24 | 0.14 | 0.30 |
| $Al_2O_3$ | 0.20 | | 0.06 |
| MgO | 0.50 | | 0.26 |
| $P_2O_5$ | 41.98 | 44.22 | 43.47 |
| $SO_2$ | 0.03 | 0.10 | 0.10 |
| CaO | 53.69 | 50.01 | 51.79 |
| MnO | 0.05 | 0.04 | 0.05 |
| $Fe_2O_3$ | 0.15 | 0.04 | 0.28 |
| SrO | 0.05 | 0.04 | 0.04 |
| $Ce_2O_3$ | 0.31 | | |
| $Pr_2O_3$ | 0.15 | 0.13 | 0.11 |
| $Nd_2O_3$ | 0.26 | 0.14 | 0.13 |
| $Eu_2O_3$ | 0.13 | 0.12 | 0.11 |
| $Dy_2O_3$ | 0.33 | 0.26 | 0.28 |
| **Total** | **102.34** | **99.42** | **101.76** |
| | | | |
| ***Formulae based on $Ca_5(PO_4)_3(OH,F,Cl)$, apfu*** | | | |
| Ca | 4.987 | 4.654 | 4.722 |
| Sr | 0.002 | 0.002 | 0.002 |
| Mg | 0.065 | 0.000 | 0.032 |
| Mn | 0.004 | 0.003 | 0.003 |
| Ce | 0.010 | 0.000 | 0.000 |
| Pr | 0.005 | 0.004 | 0.003 |
| Nd | 0.008 | 0.004 | 0.004 |
| Eu | 0.004 | 0.004 | 0.003 |
| Dy | 0.009 | 0.007 | 0.008 |
| Na | 0.056 | 0.000 | 0.000 |
| Total | 5.150 | 4.678 | 4.778 |
| **ΣREY** | **0.036** | **0.019** | **0.018** |
| | | | |
| Fe | 0.010 | 0.002 | 0.018 |
| Al | 0.021 | 0.000 | 0.006 |
| Total | 0.031 | 0.002 | 0.024 |
| | | | |
| P | 3.081 | 3.251 | 3.131 |
| S | 0.003 | 0.008 | 0.008 |
| Si | 0.021 | 0.012 | 0.025 |
| **Total** | **3.104** | **3.272** | **3.164** |
| | | | |
| F | 1.056 | 1.130 | 1.275 |
| Cl | 0.009 | 0.010 | 0.007 |

**Trace elements in garnet from Groundhog, S.A.**

## Concentrations and distributions of trace elements in garnet and accessory minerals: LA-ICP-MS data

Garnet and accessory minerals were analysed. Each displays a range of characteristic patterns for REE+Y (ΣREY), and other elements. Some of these patterns reflect characteristic trends for each mineral, governed by inherent crystal-chemistry. It is emphasized, however, that the size of the LA-ICP-MS spot is often an order of magnitude greater than that of individual (zoned) bands in some of the analysed grains, thus leading to an inevitable averaging of compositional variations in such zones (particularly for oscillatory-zoned type-I D garnets, in which individual bands are only a couple of μm in width).

When characterising REE concentrations, Y has been included in the tables and figures, positioned between Dy and Ho on the chondrite-normalised fractionation trends following practise elsewhere (Bau 1996). ΣREY is defined as the sum of measured La+Ce+Pr+Nd+Sm+Eu+Gd+Tb+Dy+Y+ Ho+Er+Tm+Yb+Lu. Normalization to chondrite follows McDonough & Sun (1995).

### RARE EARTH ELEMENTS AND YTTRIUM

Calc-silicate minerals in skarns can incorporate significant concentrations of REE (Smith *et al.* 2004, Gaspar *et al.* 2008, Ismail *et al.* in press). In the Punt Hill skarn, garnet is abundant and is the major REE-host. LA-ICP-MS spot analysis of garnet in 15 samples (Table 6) show varying ΣREY concentrations, ranging across three orders of magnitude (tens to thousands of ppm). Importantly, the different categories of garnet within the Punt Hill system (as defined in the petrography section above) display distinct and generally consistent ranges of composition. The chondrite-normalised REE

fractionation trends, showing the behaviour of LREE relative to HREE (Figure 6) are thus valuable for petrogenetic interpretation.

Figure 6 shows the clear difference in the REE patterns for garnet from the prograde and retrograde stages, as well as the increase in absolute ΣREY concentrations towards the retrograde stage. ΣREY concentrations in the latest generation of garnets (overgrowth rim) are among the highest.

Prograde garnet, including oscillatory-zoned type-I and undifferentiated garnet (type II) display modest LREE-enrichment with ΣREY concentrations varying from ~30 ppm up to 1,500 ppm. Iron-rich Type-I garnets display flat to downwards-sloping REE fractionation pattern, with a marked positive Eu-anomaly. There is no major difference in range of concentration, or of REE fractionation trend between type-I garnets from mineralised and non-mineralised skarn. In samples located below the marker horizon, both mineralized and non-mineralized prograde garnet also show a distinct negative Y-anomaly that increases with depth. Of further interest is that ΣREY concentrations in type-I B garnet from non-mineralised skarn are generally somewhat higher in ΣREY above the marker horizon than below.

Aluminium-rich type-I D garnets and type-II garnets contain greater ΣREY and show a very different REE fractionation pattern which is common to mineralized and non-mineralized samples. This pattern is characterised by relative LREE-depletion and an upwards-sloping (or slightly convex shape for most undifferentiated garnets) curve, without or with only small (positive) Eu- and/or Y-anomalies.

**Trace elements in garnet from Groundhog, S.A.**

The LREE-poor patterns shown by Al-rich prograde garnet closely resemble those shown by all retrograde garnet categories. The general fractionation trend shown by retrograde garnet is LREE-poor, REE-rich, albeit with a tendency towards a slightly more convex shape (relative depletion of the heaviest REE) among the latest garnet generation (rim, mineralized skarn category).

Less common garnet sub-types display trends that diverge from the above and which may be interpreted in terms of local conditions. Notably, garnets showing pronounced brecciated-fluidal textures, and in particular those with apatite emulsions, show a tendency towards a flatter trend. In the latter case, the enrichment in LREE relative to other retrograde garnet is clearly tied to the presence of apatite as the strength of the LREE-enrichment increases with the density of apatite inclusions. The presence of microscopic apatite may also explain the modest LREE enrichment shown by other retrograde garnet (type 1 B, brecciated and rim, mineralized skarn categories).

Overall, the trends obtained for garnet correlate with their composition, where partitioning between LREE and HREE is controlled by their Fe- and Al-rich character. This supports incorporation of REY into garnets via substitution mechanisms of YAG (yttrogarnet)-type substitution (Smith *et al.* 2004, Gaspar *et al.* 2008) as will be discussed below. The data here also shows that oscillatory zoning in terms of major components (Fe, Al) is not a necessary condition for the REY partitioning trends since most retrograde categories lack such an attribute.

# Trace elements in garnet from Groundhog, S.A.

**Table 6**: Summary of LA-ICP-MS trace element data for garnet (ppm)

| | La | Ce | Pr | Nd | Sm | Eu | Gd | Tb | Dy | Y | Ho | Er | Tm | Yb | Lu | ΣREY | Pb | Th | U |
|---|---|---|---|---|---|---|---|---|---|---|---|---|---|---|---|---|---|---|---|
| **1GH1 BRIGHT** | | | | | | | | | | | | | | | | | 0.05 | 0.01 | 0.11 |
| Min | 0.7 | 0.71 | 0.01 | 0.13 | 0.11 | 0.02 | 0.06 | 0.01 | 0.04 | 0.15 | 0.01 | 0.01 | 0.01 | 0.06 | <0.00 | 2.0 | 2.2 | 1.1 | 62 |
| Max | 12 | 54 | 9.4 | 37 | 3.1 | 3.7 | 1.5 | 0.24 | 1.2 | 1.1 | 0.19 | 21 | 0.11 | 0.6 | 0.09 | 122 | 0.57 | 0.13 | 18 |
| **Mean(11)** | 4.5 | 16 | 2.3 | 8.2 | 0.79 | 1.4 | 0.4 | 0.05 | 0.19 | 0.5 | 0.04 | 2.1 | 0.03 | 0.15 | 0.02 | 37 | 0.7 | 0.34 | 17 |
| S.D. | 4.0 | 17 | 2.9 | 12 | 0.99 | 1.0 | 0.47 | 0.07 | 0.35 | 0.28 | 0.05 | 6.4 | 0.03 | 0.15 | 0.02 | 39 | 0.09 | 0.02 | 1.7 |
| **1GH1 DARK** | | | | | | | | | | | | | | | | | | | |
| Min | 0.3 | 2.4 | 0.17 | 0.47 | 0.1 | 0.12 | 0.13 | 0.02 | 0.10 | 0.34 | 0.02 | 0.05 | 0.02 | 0.07 | 0.01 | 12 | 2.7 | 5.7 | 44 |
| Max | 23 | 24 | 3.5 | 28 | 14 | 4.4 | 22 | 4.9 | 40 | 8.3 | 9.9 | 32 | 4.7 | 31 | 4.5 | 535 | 1.4 | 2.3 | 22 |
| **Mean (8)** | 4.9 | 9.5 | 1.7 | 13 | 7.6 | 2.8 | 14 | 2.6 | 19 | 1.5 | 4.2 | 13 | 1.9 | 13 | 1.9 | 247 | 0.97 | 2.6 | 18 |
| S.D. | 7.3 | 6.7 | 1.3 | 10 | 5.0 | 1.6 | 7.8 | 1.6 | 13 | 2.7 | 3.2 | 10 | 1.61 | 11 | 1.8 | 159 | 0.02 | - | 1.2 |
| **1GH1 RIM** | | | | | | | | | | | | | | | | | | | |
| Min | <0.0 | 0.14 | 0.05 | 0.81 | 1.5 | 1.3 | 5.8 | 1.3 | 7.1 | 0.03 | 0.91 | 1.3 | 0.22 | 0.84 | 0.11 | 53 | 2.4 | 0.11 | 4.4 |
| Max | 21 | 20 | 2.0 | 8.7 | 11 | 3.8 | 28 | 5.9 | 45 | 353 | 12 | 43 | 6.7 | 51 | 8.8 | 534 | 0.13 | 0.02 | 2.3 |
| **Mean (59)** | 0.77 | 1.2 | 0.33 | 3.9 | 6.6 | 2.8 | 18 | 3.8 | 27 | 147 | 5.9 | 18 | 2.5 | 19 | 2.9 | 282 | 0.32 | 0.02 | 0.71 |
| STDV | 3 | 2.9 | 0.28 | 1.5 | 2.3 | 0.47 | 6.2 | 1.5 | 12 | 96 | 2.9 | 9.8 | 1.5 | 11 | 1.9 | 129 | 0.03 | - | 0.62 |
| **1GH2 BRIGHT** | | | | | | | | | | | | | | | | | | | |
| Min | 3.0 | 1.9 | 0.05 | 0.08 | 0.02 | 0.01 | 0.02 | <0.01 | 0.01 | 0.01 | <0.01 | 0.01 | <0.01 | <0.01 | <0.01 | 6 | 0.8 | 0.65 | 143 |
| Max | 17 | 59 | 9.5 | 36 | 7.5 | 11 | 4.9 | 0.5 | 2.7 | 14 | 0.41 | 1.6 | 0.4 | 1.5 | 0.4 | 147 | 0.2 | 0.08 | 43 |
| **Mean (78)** | 7.6 | 22 | 2.7 | 8.7 | 1.2 | 2.9 | 0.72 | 0.07 | 0.3 | 1.2 | 0.05 | 0.13 | 0.03 | 0.12 | 0.03 | 48 | 0.12 | 0.13 | 34 |
| S.D. | 3.2 | 13 | 2.2 | 8.7 | 1.6 | 2.4 | 1 | 0.11 | 0.48 | 2.5 | 0.08 | 0.25 | 0.06 | 0.21 | 0.06 | 31 | 0.03 | - | 1.9 |
| **1GH2 DARK** | | | | | | | | | | | | | | | | | | | |
| Min | 0.01 | 0.04 | 0.02 | 0.2 | 0.63 | 1.3 | 0.09 | 0.02 | 0.02 | 0.01 | <0.00 | 0.03 | 0.03 | 0.04 | 0.01 | 14 | 3.9 | 1.1 | 68 |
| Max | 66 | 98 | 8.3 | 24 | 13 | 6.6 | 33 | 7.5 | 63 | 488 | 18 | 59 | 9.4 | 72 | 10 | 766 | 0.3 | 0.06 | 9.6 |
| **Mean(104)** | 2.1 | 4.3 | 0.72 | 5.6 | 6.1 | 3.4 | 18 | 4.3 | 36 | 264 | 9.1 | 29 | 4.4 | 33 | 4.7 | 344 | 0.57 | 0.13 | 11 |
| S.D. | 9.9 | 15 | 1.3 | 5 | 3.3 | 1.4 | 8.7 | 2.1 | 19 | 155 | 5.4 | 18 | 2.9 | 23 | 3.3 | 268 | 0.04 | - | 1.9 |
| **1GH2 RIM** | | | | | | | | | | | | | | | | | | | |
| Min | 0.02 | 0.09 | 0.05 | 0.81 | 1.9 | 1.6 | 4.4 | 0.73 | 3.8 | 20 | 0.66 | 1.6 | 0.19 | 1.1 | 0.14 | 40 | 15 | 22 | 17 |
| Max | 1034 | 1703 | 138 | 364 | 33 | 6.4 | 24 | 5.3 | 45 | 352 | 12 | 38 | 6.0 | 45 | 6.35 | 3629 | 1.4 | 1.2 | 4.1 |
| **Mean(20)** | 54 | 89 | 7.5 | 22 | 6.5 | 2.8 | 13 | 2.8 | 20 | 138 | 4.8 | 15 | 2.2 | 17 | 2.5 | 397 | 3.8 | 4.9 | 3.6 |
| S.D. | 231 | 380 | 31 | 81 | 6.9 | 1.2 | 7.4 | 1.7 | 13 | 101 | 3.4 | 12 | 1.8 | 14 | 2.1 | 778 | 0.04 | 0.01 | 19 |
| **1GH3 BRIGHT** | | | | | | | | | | | | | | | | | | | |
| Min | 3.1 | 7.5 | 0.7 | 1.3 | 0.06 | 0.46 | 0.05 | 0.01 | 0.02 | 0.3 | 0.01 | <0.00 | <0.00 | 0.03 | 0.01 | 14 | 0.89 | 2.3 | 100 |
| Max | 5.7 | 20 | 4.3 | 27 | 7.6 | 6.1 | 6.2 | 0.67 | 2.4 | 0.82 | 0.32 | 0.81 | 0.2 | 0.85 | 0.07 | 89 | 0.27 | 0.48 | 58 |
| **Mean(5)** | 4.3 | 15 | 2.3 | 9.8 | 1.8 | 2.8 | 1.3 | 0.14 | 0.51 | 0.47 | 0.09 | 0.19 | 0.05 | 0.22 | 0.02 | 42 | 0.35 | 1.0 | 35 |
| S.D. | 1.2 | 5.8 | 1.5 | 10 | 3.2 | 2.2 | 2.8 | 0.29 | 1.0 | 0.22 | 0.14 | 0.35 | 0.08 | 0.35 | 0.03 | 30 | 0.27 | - | 3.5 |
| **1GH3 DARK** | | | | | | | | | | | | | | | | | | | |
| Min | 0.03 | 0.13 | 0.15 | 2.4 | 6.4 | 2.9 | 3.0 | 0.2 | 0.74 | 0.16 | 0.09 | 0.33 | 0.03 | 0.05 | 0.02 | 60 | 8.7 | 0.4 | 74 |
| Max | 0.9 | 8.5 | 2.7 | 23 | 9.7 | 10 | 29 | 7.6 | 57 | 12 | 13 | 39 | 5.7 | 36 | 3.9 | 606 | 1.9 | 0.09 | 17 |
| **Mean(6)** | 0.2 | 1.8 | 0.68 | 7.0 | 8.1 | 4.6 | 20 | 4.5 | 33 | 2.2 | 7.1 | 20 | 2.8 | 18 | 2.2 | 347 | 3.3 | 0.15 | 28 |
| S.D. | 0.35 | 3.3 | 0.98 | 7.7 | 1.3 | 2.8 | 9.2 | 2.4 | 19 | 4.6 | 4.3 | 13 | 1.9 | 13 | 1.5 | 183 | <0 | 0.1 | 1.0 |
| **2GH1 UNDIFFERENTIATED** | | | | | | | | | | | | | | | | | | | |
| Min | 3.6 | 3.0 | 0.25 | <0.00 | <0.00 | 0.12 | 0.49 | 0.06 | 0.3 | 0.46 | 0.08 | 0.22 | 0.07 | 0.34 | 0.08 | 17 | 1985 | 1.0 | 44 |
| Max | 18 | 69 | 12 | 52 | 11 | 8.6 | 22 | 2.8 | 15 | 52 | 2.0 | 5.8 | 0.82 | 4.8 | 0.61 | 239 | 106 | 0.39 | 21 |
| **Mean(32)** | 12 | 33 | 4.2 | 13 | 2.1 | 3.1 | 5.6 | 0.79 | 4.2 | 18 | 0.76 | 1.9 | 0.28 | 1.7 | 0.26 | 101 | 352 | 0.23 | 12 |
| S.D. | 3.8 | 18.7 | 3.3 | 13 | 2.1 | 2.2 | 5.4 | 0.69 | 3.4 | 15 | 0.63 | 1.5 | 0.18 | 1.1 | 0.14 | 62 | 0.04 | 0.01 | 1.1 |
| **2GH1 BRIGHT** | | | | | | | | | | | | | | | | | | | |
| Min | 2.7 | 6.8 | 0.24 | 0.17 | 0.03 | 0.1 | 0.07 | 0.01 | 0.06 | 0.1 | 0.01 | 0.02 | 0.01 | 0.01 | 0.01 | 14 | 544 | 6.2 | 74 |
| Max | 37 | 157 | 21 | 61 | 13 | 8.1 | 17 | 2.8 | 20 | 93 | 3.5 | 11 | 1.1 | 7.7 | 0.84 | 290 | 24 | 1.0 | 26 |
| **Mean(41)** | 15 | 57 | 7.7 | 24 | 3.1 | 4.1 | 3.4 | 0.47 | 2.4 | 11 | 0.45 | 1.2 | 0.23 | 1.1 | 0.21 | 131 | 89 | 1.2 | 15 |
| S.D. | 7.4 | 32 | 4.6 | 16 | 2.9 | 2.1 | 3.6 | 0.56 | 3.4 | 15 | 0.59 | 1.8 | 0.19 | 1.3 | 0.17 | 71 | 0.27 | 0.16 | 21 |
| **2GH1 DARK** | | | | | | | | | | | | | | | | | | | |
| Min | 7.7 | 23 | 2.3 | 6.2 | 1.6 | 2.1 | 2.0 | 0.34 | 2.0 | 10 | 0.42 | 1.2 | 0.16 | 1.1 | 0.16 | 63 | 1.2 | 1.5 | 30 |
| Max | 14 | 38 | 5.1 | 20 | 5.5 | 3.7 | 3.8 | 0.52 | 3.0 | 15 | 0.64 | 1.7 | 0.24 | 1.5 | 0.22 | 106 | 0.48 | 0.71 | 25 |
| **Mean(5)** | 11 | 29 | 3.3 | 11 | 2.7 | 2.5 | 2.9 | 0.42 | 2.5 | 12 | 0.51 | 1.5 | 0.19 | 1.3 | 0.18 | 80 | 0.38 | 0.64 | 4.5 |
| S.D. | 2.6 | 7.3 | 1.3 | 5.6 | 1.7 | 0.68 | 0.72 | 0.09 | 0.49 | 2.0 | 0.08 | 0.18 | 0.03 | 0.15 | 0.03 | 21 | 0.37 | 0.12 | 1.9 |
| **2GH1 MATRIX** | | | | | | | | | | | | | | | | | | | |
| Min | 0.1 | 0.15 | 0.28 | 1.3 | 1.6 | 2.0 | 2.8 | 0.65 | 5.0 | 34 | 1.1 | 3.1 | 0.21 | 1.3 | 0.38 | 59 | 108 | 0.8 | 6.4 |
| Max | 10 | 5.1 | 1.1 | 5.3 | 6.2 | 3.0 | 26 | 3.7 | 25 | 152 | 5.2 | 16 | 2.42 | 20 | 2.4 | 264 | 17 | 0.3 | 3.5 |
| **Mean(9)** | 1.7 | 1.1 | 0.52 | 2.8 | 4.1 | 2.5 | 11 | 1.9 | 13 | 69 | 2.6 | 6.8 | 0.97 | 7.3 | 0.95 | 126 | 35 | 0.2 | 1.5 |
| S.D. | 3.3 | 1.5 | 0.24 | 1.4 | 1.8 | 0.39 | 6.7 | 0.86 | 6.0 | 38 | 1.4 | 4.1 | 0.76 | 6.4 | 0.68 | 65 | 0.16 | <0 | 1.1 |
| **2GH1 RIM** | | | | | | | | | | | | | | | | | | | |
| Min | 0.1 | 0.22 | 0.1 | 0.93 | 0.2 | 1.08 | 5.3 | 1.0 | 5.8 | 25 | 0.84 | 2.1 | 0.10 | 1.0 | 0.12 | 55 | 641 | 0.87 | 8.7 |
| Max | 1.6 | 69 | 0.79 | 9.0 | 16 | 5.8 | 34 | 6.7 | 49 | 355 | 14 | 39 | 6.1 | 34 | 5.7 | 551 | 25 | 0.32 | 2.7 |
| **Mean(45)** | 0.29 | 2.2 | 0.39 | 4.4 | 7.1 | 2.7 | 18 | 3.5 | 24 | 143 | 4.8 | 14 | 2.0 | 14 | 2.4 | 243 | 96 | 0.17 | 1.6 |
| S.D. | 0.25 | 10 | 0.18 | 2.2 | 3.9 | 1.0 | 8.3 | 1.7 | 11.3 | 76 | 2.7 | 8.3 | 1.3 | 8.1 | 1.4 | 119 | 0.04 | 0.01 | 1.1 |

# Trace elements in garnet from Groundhog, S.A.

**Table 6**: Summary of LA-ICP-MS trace element data for garnet (ppm) (continued)

| | La | Ce | Pr | Nd | Sm | Eu | Gd | Tb | Dy | Y | Ho | Er | Tm | Yb | Lu | ΣREY | Pb | Th | U |
|---|---|---|---|---|---|---|---|---|---|---|---|---|---|---|---|---|---|---|---|
| **2GH2 BRIGHT** | | | | | | | | | | | | | | | | | | | |
| Min | 4.3 | 6.8 | 0.24 | 0.17 | 0.03 | 0.1 | 0.07 | 0.01 | 0.06 | 0.1 | 0.01 | 0.02 | 0.01 | 0.01 | 0.01 | 14 | 0.52 | 0.94 | 74 |
| Max | 18 | 57 | 6.7 | 29 | 7.8 | 7.1 | 6 | 0.72 | 3.5 | 17 | 0.73 | 1.9 | 0.19 | 1.5 | 0.2 | 130 | 0.15 | 0.11 | 27 |
| **Mean(10)** | 9.5 | 25 | 2.7 | 8 | 1.5 | 2.2 | 1.2 | 0.17 | 0.9 | 4.6 | 0.19 | 0.48 | 0.06 | 0.38 | 0.05 | 57 | 0.15 | 0.29 | 27 |
| S.D. | 4.4 | 17 | 2.4 | 9.1 | 2.3 | 2.2 | 1.8 | 0.21 | 1 | 5.1 | 0.21 | 0.55 | 0.06 | 0.43 | 0.06 | 41 | 0.04 | <0 | 3.1 |
| **2GH2 BRECCIATED BRIGHT** | | | | | | | | | | | | | | | | | | | |
| Min | 0.02 | 0.21 | 0.11 | 0.64 | 0.18 | 0.81 | 0.1 | 0.02 | 0.11 | 0.63 | 0.02 | 0.06 | 0.02 | 0.06 | 0.01 | 25 | 0.95 | 0.21 | 41 |
| Max | 8.4 | 34 | 3.5 | 6.8 | 7.4 | 2.8 | 15 | 2.6 | 12 | 84 | 3.1 | 9.9 | 1.1 | 11 | 0.82 | 139 | 0.19 | 0.08 | 13 |
| **Mean(10)** | 3.5 | 9.4 | 0.97 | 3.3 | 3.3 | 2.2 | 6.6 | 1.1 | 5.3 | 21 | 0.81 | 1.9 | 0.2 | 1.6 | 0.14 | 61 | 0.27 | 0.07 | 15 |
| S.D. | 3.8 | 14 | 1.4 | 2.1 | 2.7 | 0.74 | 6.2 | 0.98 | 5 | 25 | 0.93 | 2.9 | 0.32 | 3.2 | 0.24 | 34 | 0.04 | 0.05 | 2.9 |
| **2GH2 BRECCIATED DARK** | | | | | | | | | | | | | | | | | | | |
| Min | 0.02 | 0.26 | 0.17 | 1.7 | 3.2 | 2.2 | 6.3 | 0.78 | 3.6 | 15 | 0.51 | 1.1 | 0.1 | 0.57 | 0.06 | 37 | 0.27 | 0.23 | 6 |
| Max | 0.14 | 1.1 | 0.51 | 6.7 | 12 | 3.5 | 27 | 5.7 | 40 | 248 | 8.7 | 28 | 4.2 | 30 | 4.7 | 419 | 0.12 | 0.13 | 3.8 |
| **Mean(10)** | 0.06 | 0.6 | 0.3 | 3.9 | 6.8 | 2.7 | 15 | 3 | 20 | 127 | 4.4 | 14 | 2.1 | 15 | 2.3 | 217 | 0.08 | 0.06 | 1.1 |
| S.D. | 0.04 | 0.31 | 0.14 | 1.9 | 3.2 | 0.46 | 7.9 | 1.9 | 14 | 87 | 3.1 | 9.8 | 1.5 | 11 | 1.7 | 143 | 0.09 | 0.05 | 2.7 |
| **2GH2 RIM** | | | | | | | | | | | | | | | | | | | |
| Min | <0.00 | 0.19 | 0.09 | 1.4 | 2.9 | 2 | 7.3 | 1.2 | 5.8 | 20 | 0.73 | 1.3 | 0.11 | 0.69 | 0.08 | 44 | 0.65 | 0.83 | 27 |
| Max | 0.64 | 5.6 | 2 | 19 | 14 | 7.1 | 22 | 3.5 | 21 | 109 | 3.8 | 10 | 1.36 | 9.5 | 1.3 | 207 | 0.26 | 0.22 | 7.6 |
| **Mean(16)** | 0.12 | 1.2 | 0.5 | 5.4 | 6.1 | 3.3 | 11 | 1.7 | 8.5 | 36 | 1.3 | 3 | 0.34 | 2.2 | 0.29 | 81 | 0.15 | 0.26 | 7.9 |
| S.D. | 0.19 | 1.9 | 0.67 | 6.3 | 3.9 | 1.8 | 4 | 0.55 | 3.5 | 20 | 0.69 | 2 | 0.29 | 2.1 | 0.29 | 40 | 0.03 | 0.01 | 3.4 |
| **2GH3 BRIGHT** | | | | | | | | | | | | | | | | | | | |
| Min | 1.9 | 4.6 | 0.11 | 0.24 | 0.04 | 0.03 | 0.02 | <0.00 | 0.02 | 0.01 | <0.00 | 0.02 | <0.00 | 0.01 | <0.00 | 8 | 2.1 | 6.9 | 155 |
| Max | 15 | 51 | 11 | 55 | 12 | 13 | 11 | 0.88 | 2.8 | 7.4 | 0.3 | 0.68 | 0.5 | 0.6 | 0.5 | 150 | 0.22 | 0.43 | 60 |
| **Mean(53)** | 6.3 | 28 | 4.6 | 18 | 2.9 | 4.6 | 1.3 | 0.1 | 0.31 | 0.82 | 0.05 | 0.12 | 0.07 | 0.09 | 0.05 | 68 | 0.34 | 1 | 37 |
| S.D. | 2.5 | 12 | 2.8 | 15 | 3.6 | 4.1 | 2.1 | 0.16 | 0.48 | 1.6 | 0.07 | 0.16 | 0.14 | 0.13 | 0.1 | 37 | 0.04 | 0.01 | 2.9 |
| **2GH3 BRECCIATED BRIGHT** | | | | | | | | | | | | | | | | | | | |
| Min | 0.02 | 0.21 | 0.11 | 0.64 | 0.18 | 0.81 | 0.1 | 0.02 | 0.11 | 0.63 | 0.02 | 0.06 | 0.02 | 0.06 | 0.01 | 25 | 0.95 | 0.23 | 41 |
| Max | 8.4 | 34 | 3.5 | 6.8 | 12 | 3.5 | 27 | 5.7 | 40 | 248 | 8.7 | 28 | 4.2 | 30 | 4.7 | 419 | 0.16 | 0.12 | 8.4 |
| **Mean(20)** | 1.4 | 5 | 0.64 | 3.6 | 5.1 | 2.4 | 11 | 2 | 13 | 74 | 2.6 | 7.9 | 1.1 | 8.3 | 1.2 | 139 | 0.2 | 0.07 | 11 |
| S.D. | 2.8 | 10 | 1 | 2 | 3.4 | 0.67 | 8 | 1.7 | 13 | 83 | 2.9 | 9.3 | 1.4 | 10 | 1.6 | 129 | 0.54 | 0.6 | 8.3 |
| **2GH3 DARK** | | | | | | | | | | | | | | | | | | | |
| Min | 1.7 | 7.1 | 1.2 | 6.7 | 0.98 | 2.4 | 0.2 | 0.23 | 0.37 | 0.3 | 0.25 | 0.1 | 0.08 | 0.63 | 0.08 | 112 | 2581 | 5.1 | 31 |
| Max | 35 | 114 | 16 | 59 | 10 | 7.2 | 20 | 2 | 13 | 69 | 3.3 | 7 | 1.2 | 8.6 | 0.74 | 248 | 176 | 1.7 | 19 |
| **Mean(16)** | 17 | 66 | 8.9 | 28 | 4.8 | 4.9 | 7.4 | 0.84 | 5.7 | 30 | 1.2 | 2.8 | 0.4 | 3.4 | 0.38 | 188 | 641 | 1.3 | 8.4 |
| S.D. | 11 | 39 | 5.3 | 15 | 2.7 | 1.3 | 4.8 | 0.52 | 4.2 | 24 | 1.1 | 2.3 | 0.32 | 3.1 | 0.19 | 47 | 0.04 | 0.02 | 0.88 |
| **2GH3 RIM** | | | | | | | | | | | | | | | | | | | |
| Min | <0.00 | 0.19 | 0.09 | 1.4 | 1.7 | 1 | 3.9 | 0.62 | 3 | 17 | 0.6 | 1.3 | 0.11 | 0.69 | 0.08 | 15 | 4 | 0.83 | 27 |
| Max | 1.1 | 5.6 | 2 | 19 | 14 | 7.1 | 22 | 3.8 | 24 | 130 | 4.5 | 13 | 1.8 | 13 | 1.9 | 207 | 0.61 | 0.15 | 5.1 |
| **Mean(41)** | 0.18 | 0.98 | 0.36 | 3.9 | 5.2 | 2.6 | 10 | 1.7 | 9.4 | 46 | 1.6 | 4.2 | 0.56 | 3.8 | 0.55 | 55 | 0.99 | 0.2 | 5.5 |
| S.D. | 0.25 | 1.3 | 0.45 | 4.2 | 3.2 | 1.3 | 4.4 | 0.82 | 5.4 | 33 | 1.1 | 3.5 | 0.53 | 3.9 | 0.58 | 38 | 0.03 | <0 | 1.7 |
| **3GH1 UNDIFFERENTIATED** | | | | | | | | | | | | | | | | | | | |
| Min | <0.00 | 0.23 | 0.08 | 1.8 | 4.1 | 2 | 11 | 2 | 18 | 117 | 3.9 | 12 | 1.5 | 13 | 1.9 | 199 | 11 | 0.51 | 4.8 |
| Max | 2.1 | 5.1 | 0.65 | 10 | 13 | 3.1 | 26 | 5.5 | 40 | 314 | 10 | 38 | 5.8 | 45 | 7.6 | 489 | 0.94 | 0.04 | 2.5 |
| **Mean(15)** | 0.2 | 0.95 | 0.31 | 4 | 6.6 | 2.6 | 18 | 4.3 | 34 | 257 | 8.7 | 30 | 4.6 | 35 | 5.8 | 412 | 2.7 | 0.13 | 0.76 |
| S.D. | 0.52 | 1.2 | 0.18 | 2.2 | 2.4 | 0.36 | 4 | 0.83 | 6.6 | 53 | 1.8 | 6.5 | 1.3 | 9.3 | 1.66 | 83 | 0.04 | 0.01 | 3.1 |
| **3GH1 BRECCIATED BRIGHT** | | | | | | | | | | | | | | | | | | | |
| Min | 0.02 | 0.21 | 0.11 | 0.64 | 0.18 | 0.81 | 0.1 | 0.02 | 0.11 | 0.63 | 0.02 | 0.06 | 0.02 | 0.06 | 0.01 | 25 | 0.95 | 0.21 | 41 |
| Max | 8.4 | 34 | 3.5 | 6.8 | 7.4 | 2.8 | 15 | 2.6 | 12 | 84 | 3.1 | 9.9 | 1.1 | 11 | 0.82 | 139 | 0.19 | 0.1 | 13 |
| **Mean(10)** | 2.7 | 9.4 | 0.97 | 3.3 | 3.3 | 2.2 | 6.6 | 1.1 | 5.3 | 21 | 0.81 | 1.9 | 0.2 | 1.6 | 0.14 | 61 | 0.27 | 0.08 | 15 |
| S.D. | 3.6 | 14 | 1.4 | 2.1 | 2.7 | 0.74 | 6.2 | 0.98 | 5 | 25 | 0.93 | 2.9 | 0.32 | 3.2 | 0.24 | 34 | 0.04 | 0.05 | 2.9 |
| **3GH1 BRECCIATED DARK** | | | | | | | | | | | | | | | | | | | |
| Min | 0.02 | 0.26 | 0.17 | 1.7 | 3.2 | 2.2 | 6.3 | 0.78 | 3.6 | 15 | 0.51 | 1.1 | 0.1 | 0.57 | 0.06 | 37 | 0.27 | 0.23 | 6 |
| Max | 0.14 | 1.1 | 0.51 | 6.7 | 12 | 3.5 | 27 | 5.7 | 40 | 248 | 8.7 | 28 | 4.2 | 30 | 4.7 | 419 | 0.12 | 0.13 | 3.8 |
| **Mean(10)** | 0.06 | 0.6 | 0.3 | 3.9 | 6.8 | 2.7 | 15 | 3 | 20 | 127 | 4.4 | 14 | 2.1 | 15 | 2.3 | 217 | 0.08 | 0.06 | 1.1 |
| S.D. | 0.04 | 0.31 | 0.14 | 1.9 | 3.2 | 0.46 | 7.9 | 1.9 | 14 | 87 | 3.1 | 9.8 | 1.5 | 11 | 1.7 | 143 | 0.03 | <0 | 2.3 |
| **3GH1 BRECCIATED UNDIFFERENTIATED** | | | | | | | | | | | | | | | | | | | |
| Min | 0.01 | 0.12 | 0.12 | 1.2 | 2.2 | 2.1 | 6.4 | 1.2 | 8.2 | 37 | 1.3 | 2.9 | 0.35 | 1.7 | 0.21 | 67 | 0.05 | 0.02 | 3.1 |
| Max | 0.04 | 0.55 | 0.44 | 4.3 | 9.2 | 3.5 | 26 | 5.6 | 41 | 298 | 9.7 | 33 | 5.1 | 39 | 6.5 | 459 | 0.04 | 0.01 | 2.7 |
| **Mean(7)** | 0.02 | 0.26 | 0.22 | 2.2 | 4.3 | 2.5 | 14 | 3.2 | 25 | 172 | 5.9 | 18 | 2.8 | 20 | 3.1 | 273 | 0.01 | <0 | 0.27 |
| S.D. | 0.01 | 0.14 | 0.12 | 1 | 2.4 | 0.48 | 7.3 | 1.8 | 16 | 125 | 4.2 | 14 | 2.2 | 17 | 2.7 | 191 | 0.04 | 0.02 | 0.88 |
| **3GH1 RIM** | | | | | | | | | | | | | | | | | | | |
| Min | <0.00 | 0.14 | 0.1 | 1.5 | 1.7 | 1 | 3.9 | 0.62 | 3 | 17 | 0.6 | 1.4 | 0.18 | 1.1 | 0.13 | 35 | 4 | 0.77 | 9.4 |
| Max | 1.1 | 3 | 0.92 | 7.7 | 10 | 3.7 | 19 | 3.8 | 24 | 130 | 4.5 | 13 | 1.8 | 13 | 1.9 | 231 | 0.83 | 0.11 | 3.4 |
| **Mean(26)** | 0.21 | 0.79 | 0.26 | 2.9 | 4.5 | 2.2 | 9.4 | 1.6 | 9.8 | 51 | 1.8 | 4.9 | 0.7 | 4.8 | 0.7 | 95 | 1.2 | 0.15 | 1.9 |
| S.D. | 0.28 | 0.69 | 0.19 | 1.7 | 2.4 | 0.7 | 4.5 | 0.95 | 6.2 | 38 | 1.3 | 3.9 | 0.6 | 4.4 | 0.65 | 64 | 0.05 | 0.03 | 17 |

# Trace elements in garnet from Groundhog, S.A.

**Table 6**: Summary of LA-ICP-MS trace element data for garnet (ppm) (continued)

| | La | Ce | Pr | Nd | Sm | Eu | Gd | Tb | Dy | Y | Ho | Er | Tm | Yb | Lu | ΣREY | Pb | Th | U |
|---|---|---|---|---|---|---|---|---|---|---|---|---|---|---|---|---|---|---|---|
| **3GH2 BRIGHT** | | | | | | | | | | | | | | | | | | | |
| Min | 4.1 | 12 | 1.4 | 2.6 | 0.1 | 0.59 | <0.00 | 0.02 | 0.12 | 0.1 | 0.02 | 0.06 | 0.02 | 0.14 | 0.04 | 27 | 54 | 0.3 | 77 |
| Max | 12 | 45 | 5.2 | 14 | 1.3 | 2.4 | 0.76 | 0.13 | 0.63 | 4 | 0.24 | 0.63 | 0.3 | 0.86 | 0.5 | 78 | 9.2 | 0.14 | 36 |
| **Mean(6)** | 5.8 | 21 | 2.6 | 7.8 | 0.41 | 1.2 | 0.33 | 0.06 | 0.32 | 1.6 | 0.1 | 0.27 | 0.1 | 0.38 | 0.12 | 42 | 22 | 0.1 | 22 |
| S.D. | 2.9 | 12 | 1.4 | 5.1 | 0.44 | 0.66 | 0.25 | 0.04 | 0.2 | 1.7 | 0.1 | 0.23 | 0.11 | 0.28 | 0.19 | 19 | 0.11 | 0.12 | 17 |
| **3GH2 DARK** | | | | | | | | | | | | | | | | | | | |
| **(1)** | 0.08 | 0.75 | 0.2 | 4.6 | 8.3 | 5.4 | 17 | 4.1 | 21 | 77 | 2.5 | 6 | 0.59 | 3.1 | 0.48 | 150 | <0 | <0 | <0 |
| **4GH1 BRECCIATED BRIGHT** | | | | | | | | | | | | | | | | | | | |
| Min | 0.79 | 3.7 | 0.71 | 1.4 | 0.32 | 1.1 | 0.35 | 0.07 | 0.24 | 0.14 | 0.03 | 0.08 | 0.05 | 0.12 | 0.03 | 14 | 4.9 | 1.1 | 71 |
| Max | 2 | 10 | 2.8 | 18 | 8.5 | 4.5 | 7.8 | 0.76 | 4.6 | 16 | 0.69 | 1.5 | 0.2 | 1.2 | 0.7 | 78 | 1.4 | 0.46 | 47 |
| **Mean(8)** | 1.5 | 8.3 | 1.8 | 11 | 2.9 | 2.8 | 2.2 | 0.24 | 1.1 | 3.8 | 0.25 | 0.47 | 0.1 | 0.45 | 0.17 | 33 | 1.9 | 0.41 | 23 |
| S.D. | 0.47 | 2.6 | 0.84 | 7.2 | 2.9 | 1.1 | 2.5 | 0.23 | 1.4 | 5.3 | 0.23 | 0.47 | 0.06 | 0.32 | 0.23 | 22 | 0.62 | 0.78 | 4.5 |
| **4GH1 BRECCIATED DARK** | | | | | | | | | | | | | | | | | | | |
| Min | 0.14 | 0.33 | 0.21 | 2.2 | 4.8 | 0.92 | 7 | 1.7 | 8.3 | 43 | 1.7 | 3.5 | 0.45 | 2.7 | 0.39 | 49 | 26 | 1.2 | 13 |
| Max | 4.7 | 5.1 | 1.4 | 9 | 9.8 | 2.3 | 14 | 2.4 | 16 | 72 | 2.8 | 6.6 | 1.3 | 7.5 | 1.3 | 164 | 6.8 | 0.9 | 8.8 |
| **Mean(5)** | 1.5 | 2.5 | 0.57 | 4.6 | 6.6 | 1.5 | 9.8 | 2.1 | 13 | 60 | 2.3 | 5.2 | 0.77 | 5.4 | 0.88 | 120 | 11 | 0.18 | 3.4 |
| S.D. | 1.8 | 2.1 | 0.48 | 2.7 | 1.9 | 0.55 | 2.8 | 0.29 | 2.9 | 11 | 0.43 | 1.2 | 0.31 | 2.4 | 0.41 | 43 | 4.5 | 0.13 | 2.1 |
| **4GH1 RIM** | | | | | | | | | | | | | | | | | | | |
| Min | 0.18 | 0.14 | 0.05 | 0.91 | 2 | 0.96 | 4.3 | 0.81 | 3.7 | 21 | 0.53 | 1.8 | 0.14 | 0.93 | 0.16 | 50 | 12 | 5.6 | 41 |
| Max | 12 | 22 | 2 | 11 | 10 | 3.7 | 30 | 8.3 | 75 | 580 | 20 | 73 | 9.6 | 66 | 6.9 | 925 | 7.5 | 1.4 | 8.2 |
| **Mean(8)** | 4.7 | 5.8 | 0.54 | 4 | 5.3 | 2.2 | 12 | 2.9 | 20 | 137 | 5.1 | 16 | 2.3 | 15 | 1.8 | 234 | 2.6 | 2.1 | 13 |
| S.D. | 5.5 | 7.7 | 0.64 | 3.3 | 3 | 0.91 | 11 | 3 | 25 | 194 | 6.8 | 24 | 3.3 | 23 | 2.5 | 304 | 0.13 | 0.04 | 14 |
| **4GH2 BRIGHT** | | | | | | | | | | | | | | | | | | | |
| Min | 1.4 | 6.2 | 0.63 | 1.3 | 0.26 | 0.92 | 0.3 | 0.02 | 0.09 | 0.04 | 0.02 | 0.07 | 0.02 | 0.11 | 0.02 | 16 | 12 | 0.3 | 136 |
| Max | 7.1 | 27 | 4.3 | 20 | 6.8 | 9.3 | 10 | 1.9 | 8.9 | 46 | 1.7 | 3.8 | 0.65 | 3.6 | 0.55 | 276 | 0.73 | 0.12 | 78 |
| **Mean(29)** | 4.6 | 16.2 | 2.4 | 9.7 | 2.6 | 5.1 | 2.5 | 0.36 | 1.8 | 7.6 | 0.29 | 0.72 | 0.12 | 0.7 | 0.15 | 91 | 2.1 | 0.06 | 39 |
| S.D. | 1.6 | 6.1 | 1.1 | 5.3 | 2 | 2.5 | 2.7 | 0.48 | 2.5 | 14 | 0.48 | 1.08 | 0.14 | 0.96 | 0.13 | 85 | 0.19 | 0.04 | 19 |
| **4GH2 BRECCIATED BRIGHT** | | | | | | | | | | | | | | | | | | | |
| Min | 3.3 | 10.9 | 1.5 | 3.3 | 0.54 | 1.3 | 0.15 | 0.04 | 0.19 | 0.08 | 0.02 | 0.15 | 0.02 | 0.32 | 0.03 | 27 | 0.27 | 0.16 | 53 |
| Max | 3.7 | 14 | 2.7 | 11 | 1.4 | 3.4 | 1.3 | 0.26 | 1.4 | 4 | 0.22 | 0.52 | 0.07 | 0.79 | 0.11 | 41 | 0.22 | 0.11 | 32 |
| **Mean(5)** | 3.5 | 13 | 1.9 | 7.2 | 0.92 | 2.4 | 0.51 | 0.12 | 0.57 | 1.6 | 0.14 | 0.35 | 0.06 | 0.5 | 0.07 | 35 | 0.04 | 0.04 | 13 |
| S.D. | 0.19 | 1.2 | 0.51 | 3.3 | 0.42 | 0.78 | 0.47 | 0.08 | 0.53 | 1.9 | 0.09 | 0.14 | 0.02 | 0.2 | 0.03 | 7 | 1.2 | 0.13 | 5.4 |
| **4GH2 BRECCIATED DARK** | | | | | | | | | | | | | | | | | | | |
| **(1)** | 15 | 18 | 1.7 | 5.3 | 2.9 | 1.8 | 9.8 | 2.5 | 19 | 142 | 4 | 16 | 2.4 | 20 | 2.3 | 263 | <0 | <0 | <0 |
| **4GH2 BRECCIATED DARK FLUIDAL** | | | | | | | | | | | | | | | | | | | |
| Min | 0.09 | 0.32 | 0.07 | 1.6 | 1.6 | 1.5 | 6.5 | 2.1 | 18 | 56 | 2.3 | 2.8 | 0.39 | 2.3 | 0.1 | 121 | 6.7 | 1.2 | 9.3 |
| Max | 50 | 58 | 5.9 | 18 | 9.2 | 4.2 | 22 | 4.4 | 37 | 298 | 9.8 | 35 | 6 | 41 | 6.4 | 516 | 2.9 | 0.32 | 4.5 |
| **Mean(14)** | 6 | 7.4 | 0.98 | 4.8 | 4.7 | 2.7 | 15 | 3.5 | 26 | 182 | 6.1 | 19 | 2.7 | 20 | 2.8 | 303 | 2 | 0.29 | 2.2 |
| S.D. | 15 | 17 | 1.6 | 4.4 | 2 | 0.68 | 4.5 | 0.62 | 6.7 | 56 | 1.7 | 7.4 | 1.3 | 9 | 1.4 | 84 | 0.09 | 0.05 | 5.3 |
| **4GH2 DARK** | | | | | | | | | | | | | | | | | | | |
| Min | 0.08 | 0.21 | 0.1 | 1.3 | 2.4 | 1.5 | 7.2 | 1.4 | 9.5 | 49 | 1.3 | 4.8 | 0.82 | 1.8 | 0.31 | 48 | 3.7 | 0.6 | 71 |
| Max | 2.7 | 10 | 1.8 | 9.8 | 7.8 | 7.1 | 15 | 4.1 | 27 | 174 | 6.1 | 20 | 3 | 22 | 3.7 | 267 | 1.6 | 0.22 | 19 |
| **Mean(8)** | 0.48 | 2.1 | 0.52 | 4.1 | 4 | 3.2 | 11 | 2.9 | 23 | 151 | 5.1 | 16 | 2.3 | 16 | 2.7 | 114 | 1.3 | 0.17 | 22 |
| S.D. | 0.9 | 3.3 | 0.6 | 3.1 | 1.7 | 1.9 | 2.6 | 0.85 | 5.7 | 42 | 1.6 | 4.8 | 0.74 | 7 | 1.2 | 90 | 0.16 | 0.1 | 1.2 |
| **4GH2 RIM** | | | | | | | | | | | | | | | | | | | |
| Min | 0.03 | 0.05 | 0.06 | 0.43 | 1.1 | 1.6 | 6.8 | 1.6 | 21 | 98 | 3.2 | 6.7 | 0.6 | 3.8 | 0.38 | 185 | 1.9 | 3.4 | 3.4 |
| Max | 1.2 | 1.7 | 0.58 | 5.4 | 11 | 4.2 | 26 | 6.2 | 50 | 285 | 9.4 | 33 | 5.1 | 34 | 5.9 | 440 | 0.56 | 0.47 | 2.2 |
| **Mean(12)** | 0.19 | 0.43 | 0.25 | 2.8 | 5.6 | 2.6 | 16 | 3.7 | 28 | 178 | 5.8 | 18 | 2.5 | 17 | 2.6 | 283 | 0.5 | 0.92 | 0.55 |
| S.D. | 0.33 | 0.46 | 0.18 | 2.2 | 4.1 | 0.83 | 8.5 | 1.4 | 8.7 | 67 | 2.2 | 8.6 | 1.5 | 9.9 | 1.8 | 90 | 0.18 | 0.12 | 1.5 |
| **4GH2 RETROGRADE 3-APATITE EMULSION** | | | | | | | | | | | | | | | | | | | |
| Min | 0.09 | 0.19 | 0.02 | 0.72 | 1.9 | 1.4 | 8 | 1.8 | 9 | 53 | 2 | 4.7 | 0.56 | 4.1 | 0.83 | 49 | 142 | 102 | 94 |
| Max | 634 | 980 | 85 | 275 | 51 | 5.1 | 32 | 8 | 57 | 344 | 12 | 32 | 4.4 | 37 | 6.8 | 2322 | 9.3 | 9.3 | 10 |
| **Mean(35)** | 46 | 86 | 9.7 | 38 | 12 | 2.7 | 17 | 3.4 | 25 | 170 | 5.8 | 19 | 2.7 | 19 | 3 | 444 | 24 | 22 | 15 |
| S.D. | 107 | 165 | 14 | 45 | 8.1 | 0.82 | 6.4 | 1.4 | 9.4 | 59 | 1.9 | 6.7 | 0.9 | 7.2 | 1.3 | 350 | 0.13 | 0.01 | 2.7 |
| **5GH1 UNDIFFERENTIATED** | | | | | | | | | | | | | | | | | | | |
| Min | 23 | 61 | 5.2 | 10 | 0.37 | 1.6 | 0.11 | 0.05 | 0.26 | 1 | 0.04 | 0.17 | 0.02 | 0.21 | 0.02 | 109 | 0.72 | 3.1 | 45 |
| Max | 100 | 679 | 142 | 668 | 88 | 23 | 32 | 2.6 | 12 | 42 | 1.6 | 3.6 | 0.66 | 4.9 | 0.68 | 1765 | 0.39 | 0.66 | 14 |
| **Mean(13)** | 51 | 246 | 40 | 152 | 19 | 9.3 | 7.7 | 0.65 | 3 | 12 | 0.49 | 1.3 | 0.22 | 1.4 | 0.18 | 544 | 0.15 | 0.84 | 12 |
| S.D. | 25 | 185 | 40 | 189 | 27 | 7.2 | 11 | 0.84 | 3.5 | 12 | 0.5 | 1.3 | 0.22 | 1.4 | 0.2 | 488 | 0.17 | 0.06 | 7.2 |
| **5GH1 BRIGHT** | | | | | | | | | | | | | | | | | | | |
| Min | 0.3 | 2.5 | 0.94 | 8.7 | 1.0 | 1.9 | 0.37 | 0.04 | 0.48 | 2.2 | 0.13 | 0.34 | 0.07 | 0.36 | 0.05 | 110 | 7.7 | 5.6 | 71 |
| Max | 38 | 137 | 20 | 56 | 8.3 | 6.4 | 20 | 4.6 | 37 | 246 | 8.7 | 26 | 4.0 | 30 | 4.4 | 404 | 0.87 | 1.2 | 40 |
| **Mean(28)** | 22 | 91 | 13 | 43 | 4.5 | 3.8 | 2.7 | 0.43 | 3.1 | 18 | 0.72 | 2.3 | 0.37 | 2.7 | 0.39 | 207 | 1.4 | 1.2 | 15 |
| S.D. | 11 | 31 | 3.6 | 12 | 2.2 | 1.6 | 3.5 | 0.83 | 6.7 | 45 | 1.6 | 4.7 | 0.72 | 5.3 | 0.8 | 52 | 0.02 | 0.01 | 0.09 |

# Trace elements in garnet from Groundhog, S.A.

**Table 6**: Summary of LA-ICP-MS trace element data for garnet (ppm) (continued)

| | La | Ce | Pr | Nd | Sm | Eu | Gd | Tb | Dy | Y | Ho | Er | Tm | Yb | Lu | ΣREY | Pb | Th | U |
|---|---|---|---|---|---|---|---|---|---|---|---|---|---|---|---|---|---|---|---|
| **5GH1 BRECCIATED UNDIFFERENTIATED** | | | | | | | | | | | | | | | | | | | |
| Min | 0.02 | 0.15 | 0.07 | 0.14 | 0.06 | 0.02 | 0.04 | 0.01 | 0.03 | 0.01 | 0.01 | 0.03 | 0.01 | 0.01 | 0.01 | 9.0 | 57 | 19 | 79 |
| Max | 118 | 390 | 40 | 151 | 21 | 11 | 29 | 6.6 | 52 | 362 | 12 | 45 | 7.1 | 53 | 9.3 | 688 | 1.5 | 1.5 | 15 |
| **Mean(122)** | 18 | 60 | 7.4 | 26 | 5.2 | 2.4 | 7.1 | 1.5 | 11 | 77 | 2.7 | 9.0 | 1.4 | 10 | 1.6 | 241 | 6.5 | 3.1 | 20 |
| S.D. | 20 | 70 | 9 | 31 | 4.9 | 1.9 | | 2.0 | 16 | 113 | 3.8 | 13 | 2.0 | 15 | 2.4 | 165 | 0.64 | 0.04 | 6.2 |
| **5GH2 BRIGHT** | | | | | | | | | | | | | | | | | | | |
| Min | 0.91 | 3.2 | 0.18 | 0.12 | 0.16 | 0.21 | 0.17 | 0.02 | 0.11 | 0.05 | 0.06 | 0.23 | 0.03 | 0.34 | 0.06 | 8.0 | 4.6 | 0.89 | 53 |
| Max | 4.1 | 18 | 2.7 | 9.8 | 3.7 | 6.0 | 2.1 | 0.51 | 2.1 | 8.7 | 0.47 | 0.58 | 0.5 | 0.74 | 0.3 | 43 | 1.7 | 0.3 | 26 |
| **Mean(12)** | 2.2 | 8.4 | 1.1 | 3.9 | 0.91 | 2.1 | 0.71 | 0.18 | 0.68 | 2.6 | 0.18 | 0.36 | 0.12 | 0.47 | 0.13 | 24 | 1.0 | 0.25 | 16 |
| S.D. | 0.96 | 3.9 | 0.74 | 3.4 | 0.95 | 1.6 | 0.61 | 0.17 | 0.71 | 3.3 | 0.14 | 0.15 | 0.13 | 0.12 | 0.08 | 12 | 2.0 | 0.18 | 9.0 |
| **5GH2 DARK** | | | | | | | | | | | | | | | | | | | |
| Min | 0.04 | 0.58 | 0.28 | 4.2 | 5.7 | 4.4 | 9.7 | 3.1 | 19 | 101 | 3.9 | 8.7 | 0.54 | 4.8 | 0.77 | 172 | <0.01 | <0.01 | <0.01 |
| Max | 0.22 | 1.5 | 0.8 | 7.6 | 9.0 | 6.5 | 21 | 3.9 | 27 | 126 | 5.5 | 12 | 1.5 | 8.8 | 1.2 | 227 | 5.2 | 2.0 | 25 |
| **Mean(8)** | 0.13 | 1.1 | 0.47 | 5.2 | 7.7 | 5 | 17 | 3.5 | 23 | 115 | 4.4 | 10 | 1.1 | 6.8 | 0.98 | 201 | 3.4 | 0.89 | 17 |
| S.D. | 0.06 | 0.27 | 0.16 | 1.1 | 1.3 | 0.62 | 4.1 | 0.28 | 2.8 | 11 | 0.64 | 1.1 | 0.32 | 1.3 | 0.16 | 19 | 1.2 | 0.66 | 5.2 |
| **5GH2 RIM** | | | | | | | | | | | | | | | | | | | |
| Min | 0.07 | 0.17 | 0.07 | 1.7 | 1.8 | 0.64 | 7.1 | 1.4 | 9.0 | 42 | 1.5 | 4.3 | 0.45 | 2.7 | 0.72 | 82 | 1.1 | 0.06 | 0.87 |
| Max | 23 | 63 | 9.2 | 38 | 12 | 7.2 | 26 | 5.0 | 40 | 239 | 8.5 | 26 | 4.2 | 34 | 4.2 | 403 | 56 | 8.7 | 27 |
| **Mean(28)** | 1.6 | 3.9 | 0.74 | 5.7 | 6.1 | 2.9 | 14 | 3.0 | 24 | 146 | 4.8 | 15 | 2.2 | 17 | 2.4 | 250 | 8.5 | 0.7 | 4.3 |
| S.D. | 4.8 | 13 | 1.7 | 6.6 | 2.8 | 1.3 | 5.1 | 0.84 | 7.9 | 49 | 1.7 | 5.8 | 1.0 | 7.4 | 1.1 | 81 | 11 | 1.6 | 6.2 |
| **6GH1 UNDIFFERENTIATED** | | | | | | | | | | | | | | | | | | | |
| Min | 1.2 | 3.1 | 0.04 | 0.05 | 0.02 | 0.01 | 0.02 | <0.00 | 0.01 | <0.00 | <0.00 | 0.01 | <0.00 | 0.01 | <0.00 | 5.0 | 0.04 | <0 | 0.58 |
| Max | 5.3 | 14 | 1.5 | 3.6 | 0.15 | 0.5 | 0.11 | 3.0 | 0.12 | 0.58 | 0.05 | 11 | 0.02 | 0.11 | 0.02 | 21 | 0.63 | 0.02 | 6.5 |
| **Mean(26)** | 2.7 | 6.9 | 0.48 | 0.69 | 0.06 | 0.15 | 0.06 | 0.12 | 0.05 | 0.08 | 0.01 | 0.46 | 0.01 | 0.04 | 0.01 | 11 | 0.27 | 0.01 | 2.3 |
| S.D. | 1.1 | 3.3 | 0.41 | 0.82 | 0.03 | 0.15 | 0.03 | 0.58 | 0.03 | 0.12 | 0.01 | 2.2 | 0.00 | 0.03 | <0.00 | 5.0 | 0.15 | <0 | 1.7 |
| **6GH1 BRECCIATED UNDIFFERENTIATED** | | | | | | | | | | | | | | | | | | | |
| Min | <0.00 | 0.07 | 0.04 | 0.08 | 0.04 | 0.04 | <0.00 | <0.00 | 0.02 | <0.00 | <0.00 | 0.01 | <0.00 | 0.01 | <0.00 | 5.0 | 0.03 | <0 | 0.45 |
| Max | 15.1 | 40 | 4.6 | 13 | 5.5 | 2.9 | 10 | 2.0 | 14 | 72 | 2.6 | 6.3 | 0.81 | 4.9 | 0.74 | 116 | 2.4 | 0.64 | 19 |
| **Mean(52)** | 3.1 | 8.1 | 0.8 | 2.8 | 1.5 | 1.3 | 3.8 | 0.71 | 4.6 | 22 | 0.8 | 1.9 | 0.23 | 1.5 | 0.2 | 53 | 0.34 | 0.05 | 3.7 |
| S.D. | 3.78 | 9.3 | 1.0 | 2.9 | 1.3 | 0.88 | 3.7 | 0.74 | 4.8 | 25 | 0.89 | 2.2 | 0.26 | 1.6 | 0.23 | 34 | 0.58 | 0.1 | 3.2 |
| **6GH2 BRIGHT** | | | | | | | | | | | | | | | | | | | |
| Min | 0.08 | 1.0 | 0.56 | 1.1 | 0.02 | 0.29 | 0.05 | 0.00 | 0.01 | 0.01 | 0.00 | 0.00 | 0.00 | 0.00 | 0.00 | 12 | 0.01 | <0 | 6.7 |
| Max | 7.9 | 35 | 6.2 | 33 | 11 | 7.4 | 14 | 1.8 | 7.2 | 21 | 0.83 | 1.2 | 0.3 | 1.9 | 0.4 | 83 | 2.3 | 1.7 | 116 |
| **Mean(67)** | 3.5 | 19 | 3.7 | 16 | 1.8 | 3.5 | 0.67 | 0.08 | 0.31 | 1 | 0.04 | 0.1 | 0.02 | 0.11 | 0.03 | 50 | 0.18 | 0.24 | 55 |
| S.D. | 1.5 | 6.4 | 1.3 | 7.1 | 1.6 | 2.1 | 1.7 | 0.23 | 0.95 | 3.1 | 0.12 | 0.23 | 0.05 | 0.25 | 0.07 | 16 | 0.43 | 0.34 | 27 |
| **6GH2 BRECCIATED BRIGHT** | | | | | | | | | | | | | | | | | | | |
| Min | 0.51 | 3.2 | 0.83 | 2.2 | 0.18 | 0.34 | 0.07 | <0.00 | 0.03 | 0.05 | 0.01 | 0.02 | 0.01 | 0.04 | 0.01 | 21 | 0.14 | 0.01 | 10 |
| Max | 6.5 | 31 | 5.6 | 23 | 4.8 | 1.4 | 5.9 | 0.86 | 5.2 | 26 | 1.0 | 2.2 | 0.37 | 2.4 | 0.35 | 73 | 16 | 1.2 | 52 |
| **Mean(7)** | 4.6 | 20 | 3.1 | 12 | 2.2 | 0.94 | 1.3 | 0.16 | 0.88 | 4.3 | 0.17 | 0.37 | 0.06 | 0.4 | 0.06 | 51 | 3.0 | 0.47 | 32 |
| S.D. | 2.0 | 9.4 | 1.7 | 6.9 | 1.6 | 0.38 | 2.1 | 0.31 | 1.9 | 9.5 | 0.38 | 0.82 | 0.14 | 0.88 | 0.13 | 16 | 5.8 | 0.5 | 17 |
| **6GH2 BRECCIATED DARK** | | | | | | | | | | | | | | | | | | | |
| Min | 0.13 | 0.88 | 0.24 | 2.7 | 2.3 | 1.4 | 3.5 | 0.59 | 4.2 | 20 | 0.77 | 2.0 | 0.18 | 2.2 | 0.29 | 47 | 11 | 0.44 | 6.7 |
| Max | 4.8 | 21 | 3.6 | 20 | 9.4 | 4.3 | 9.5 | 1.3 | 9.6 | 60 | 2.2 | 7.0 | 0.91 | 7.4 | 1.2 | 140 | 41 | 3.6 | 31 |
| **Mean(5)** | 2.3 | 8.5 | 1.5 | 9.5 | 5.5 | 2.1 | 6.7 | 0.95 | 6.6 | 38 | 1.4 | 4.2 | 0.57 | 4.4 | 0.68 | 93 | 25 | 1.7 | 14 |
| S.D. | 1.9 | 8.0 | 1.2 | 6.9 | 2.9 | 1.2 | 2.5 | 0.27 | 2.3 | 17 | 0.64 | 2.0 | 0.27 | 2.0 | 0.35 | 35 | 13 | 1.2 | 10 |
| **6GH2 BRECCIATED UNDIFFERENTIATED** | | | | | | | | | | | | | | | | | | | |
| Min | 0.12 | 0.54 | 0.22 | 2.4 | 1.5 | 0.67 | 1.2 | 0.05 | 0.54 | 2.0 | 0.09 | 0.27 | 0.04 | 0.37 | 0.04 | 37 | 9.5 | 0.21 | 6.5 |
| Max | 725 | 1388 | 127 | 398 | 25 | 5.0 | 12 | 1.7 | 9.0 | 45 | 1.5 | 4.6 | 0.63 | 4.6 | 0.65 | 2692 | 58 | 363 | 105 |
| **Mean(19)** | 41 | 84 | 8.3 | 30 | 5.4 | 2.5 | 4.6 | 0.67 | 4.3 | 23 | 0.84 | 2.5 | 0.34 | 2.4 | 0.33 | 210 | 26 | 23 | 25 |
| S.D. | 166 | 316 | 29 | 89 | 5.2 | 1.2 | 2.9 | 0.44 | 2.4 | 13 | 0.47 | 1.4 | 0.19 | 1.4 | 0.21 | 602 | 16 | 83 | 25 |
| **6GH2 DARK** | | | | | | | | | | | | | | | | | | | |
| Min | 0.02 | 0.46 | 0.19 | 2.6 | 0.09 | 1.1 | 0.05 | 0.01 | 0.03 | 0.01 | <0.00 | 0.02 | 0.01 | 0.04 | 0.01 | 19 | 0.01 | 0.01 | 2.6 |
| Max | 5.6 | 21 | 3.4 | 21 | 15 | 7.1 | 36 | 6.8 | 54 | 400 | 14 | 48 | 8.4 | 63 | 10 | 654 | 6.3 | 0.72 | 64 |
| **Mean(34)** | 0.37 | 2.3 | 0.73 | 7.7 | 9.3 | 4.5 | 17 | 2.7 | 15 | 78 | 2.8 | 7.5 | 1.1 | 7.1 | 1.0 | 157 | 0.39 | 0.2 | 10 |
| S.D. | 1.1 | 4.3 | 0.65 | 2.9 | 3.2 | 1.2 | 9.3 | 1.9 | 13 | 86 | 3.0 | 9.8 | 1.6 | 12 | 1.9 | 134 | 1.2 | 0.2 | 13 |
| **6GH2 RIM** | | | | | | | | | | | | | | | | | | | |
| Min | 0.01 | 0.2 | 0.15 | 2.4 | 1.3 | 0.45 | 1.9 | 0.33 | 2.1 | 6.8 | 0.29 | 0.64 | 0.07 | 0.32 | 0.04 | 31 | 0.02 | 0.01 | 1.4 |
| Max | 15 | 36 | 4.5 | 21 | 14 | 7.2 | 29 | 6.3 | 43 | 301 | 10 | 38 | 6.5 | 48 | 7.8 | 493 | 238 | 6.3 | 18 |
| **Mean(61)** | 1.1 | 3.3 | 0.79 | 7.0 | 7.5 | 3.5 | 14 | 2.6 | 17 | 99 | 3.5 | 10 | 1.4 | 10 | 1.5 | 183 | 9.3 | 0.45 | 6.5 |
| S.D. | 2.8 | 6.6 | 0.83 | 3.9 | 3.4 | 1.5 | 8.5 | 1.9 | 14 | 93 | 3.2 | 10 | 1.5 | 11 | 1.7 | 142 | 31 | 0.88 | 4.2 |
| **7GH1 UNDIFFERENTIATED** | | | | | | | | | | | | | | | | | | | |
| Min | 0.03 | 0.23 | 0.11 | 1.2 | 3.5 | 1.1 | 7.6 | 1.8 | 10 | 49 | 1.7 | 4.2 | 0.78 | 4.5 | 0.59 | 89 | 0.08 | 0.09 | 0.9 |
| Max | 0.5 | 1.2 | 0.52 | 8.0 | 10 | 4.1 | 27 | 5.8 | 41 | 286 | 9.1 | 31 | 4.1 | 29 | 5.1 | 443 | 5.5 | 0.4 | 2.5 |
| **Mean(16)** | 0.13 | 0.6 | 0.31 | 4.1 | 6.9 | 2.8 | 19 | 4.2 | 30 | 197 | 6.7 | 20 | 2.8 | 20 | 3.1 | 318 | 0.74 | 0.19 | 1.7 |
| S.D. | 0.11 | 0.31 | 0.14 | 2.1 | 2.6 | 0.71 | 5.8 | 1.1 | 8.5 | 58 | 2.0 | 6.7 | 0.88 | 6.2 | 1.1 | 87 | 1.3 | 0.08 | 0.45 |

## Trace elements in garnet from Groundhog, S.A.

**Table 6**: Summary of LA-ICP-MS trace element data for garnet (ppm) (continued)

| | La | Ce | Pr | Nd | Sm | Eu | Gd | Tb | Dy | Y | Ho | Er | Tm | Yb | Lu | ΣREY | Pb | Th | U |
|---|---|---|---|---|---|---|---|---|---|---|---|---|---|---|---|---|---|---|---|
| **7GH1 BRIGHT** | | | | | | | | | | | | | | | | | | | |
| Min | 1.6 | 16 | 2.7 | 6.11 | 0.26 | 0.89 | 0.12 | 0.02 | 0.16 | 0.07 | <0.00 | 0.06 | 0.02 | 0.1 | 0.03 | 48 | 0.06 | 0.04 | 16 |
| Max | 10 | 47 | 9.1 | 43 | 11 | 8.9 | 6.7 | 0.63 | 2.5 | 10 | 0.49 | 0.95 | 0.19 | 0.65 | 0.6 | 120 | 8.0 | 3.1 | 70 |
| **Mean(25)** | 6.4 | 29 | 5.1 | 23 | 4.0 | 3.5 | 2.1 | 0.22 | 0.92 | 3.1 | 0.17 | 0.35 | 0.08 | 0.36 | 0.14 | 78 | 1.1 | 0.69 | 40 |
| S.D. | 2.6 | 7.2 | 1.5 | 13 | 3.8 | 2.0 | 2.2 | 0.2 | 0.72 | 3.0 | 0.14 | 0.21 | 0.04 | 0.15 | 0.16 | 21 | 2.0 | 0.74 | 15 |
| **7GH1 DARK** | | | | | | | | | | | | | | | | | | | |
| Min | 0.16 | 4.7 | 1.3 | 11 | 5.6 | 1.7 | 4.8 | 0.65 | 3.3 | 24 | 0.88 | 2.3 | 0.34 | 1.9 | 0.18 | 79 | 0.76 | 0.32 | 13 |
| Max | 21 | 52 | 7.8 | 41 | 17 | 3.9 | 26 | 4.7 | 22 | 125 | 4.6 | 12 | 1.2 | 7.7 | 1.3 | 344 | 42 | 11 | 35 |
| **Mean(12)** | 2.9 | 13 | 3.0 | 20 | 8.9 | 2.7 | 10 | 1.7 | 10 | 56 | 2 | 5.5 | 0.65 | 4.2 | 0.55 | 141 | 13 | 4.4 | 23 |
| S.D. | 5.6 | 13 | 1.7 | 7.8 | 3.7 | 0.77 | 6.5 | 1.2 | 5.1 | 29 | 1.1 | 3.0 | 0.29 | 1.8 | 0.34 | 72 | 13 | 3.3 | 7.2 |

### Other trace elements

Garnet can be an important repository for a wide range of other trace elements. As with REY, there are marked differences in the absolute concentrations of other trace elements in garnet from different sub-categories, and also a number of interesting and genetically interpretable correlations between element pairs. Punt Hill garnets are particularly rich in W, U, As and Sn (Table A-4, Appendix C). Type-I prograde garnet, whether brecciated or not, is characteristically enriched in W (100-1500 ppm), U, As and Sn (50-200 ppm, 50-5500 ppm, and 10-300 ppm, respectively). Aluminium-rich Type-2 (undifferentiated) garnet contains P (130-2500 ppm) and As (100-834 ppm), but lower W concentrations (362-598 ppm) compared to the Fe-rich core. Retrograde garnet displays relative enrichment in a range of incompatible elements. Of note is the strong enrichment of Cr (100-500 ppm), Ti (2000-5000 ppm) and V (150-600 ppm) in the outermost rim garnet relative to the core. Matrix garnet shows strong concentrations of Ti (3000-5300 ppm), V (96-270 ppm), Cr (101-201 ppm) and As (1430-8500 ppm).

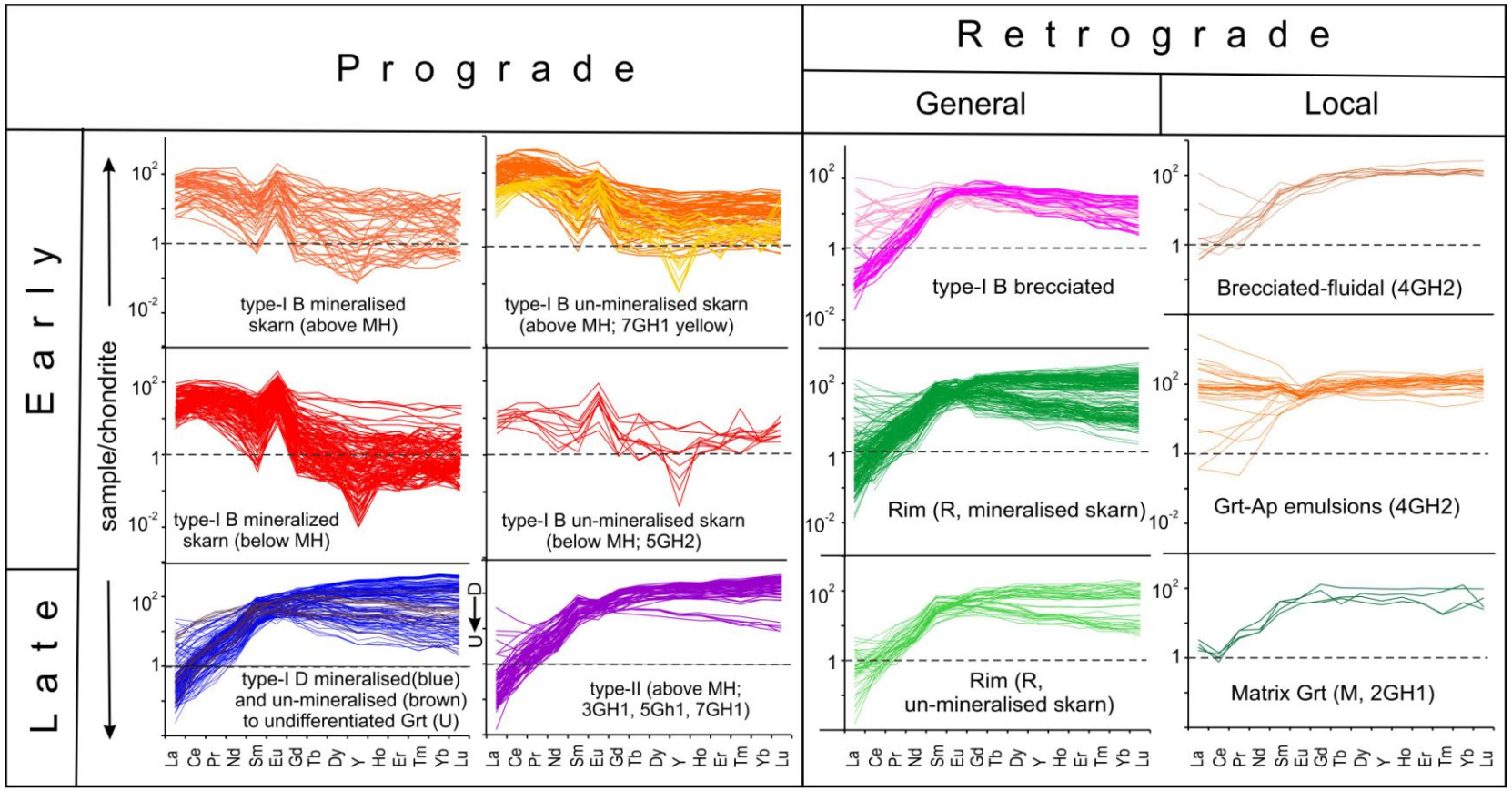


**Figure 6: Chondrite-normalised REY fractionation trends for garnet from above and below the marker horizon, and from mineralised and non-mineralised skarn. Categories of garnet are split into prograde and retrograde, with sub-categories, early to late prograde and general to local retrograde. Early prograde type-I garnet shows distinct LREE-enrichment, with positive Eu- and negative Y-anomalies. Late prograde, type-II garnet shows MREE-HREE-enrichment and LREE-depletion. Retrograde categories, including brecciated type-I, display a hybrid trend between early prograde and late prograde trends, showing slight LREE-enrichment trending up to MREE-HREE enrichment. All other trends, with the exception of the garnet containing apatite emulsions, show LREE-depletion and relative MREE-HREE enrichment. The garnet-apatite emulsions show flattish-trends with negative Eu-anomalies. (See text for further explanation)**

**Trace elements in garnet from Groundhog, S.A.**

Correlation patterns and key inter-element trends that allow discrimination between categories are shown as a series of binary plots. Figure 7a shows the strong correlation between W and As, and difference between W-As-enriched prograde garnet (Type-I and -II) and the W-As-poor retrograde garnet. Within this trend, however, a sub-pattern of type-I B, brecciated garnet is recognised, in which lower concentrations are seen for both elements (Figure 7b) in samples from drill hole GHDD2 (furthest NNE and closest to the presumed trap). A second cluster on the same diagram shows a marked decrease in As in one sample from immediately above the MH (drill hole at the junction of the two profiles). The presence of arsenopyrite and Ni-Co arsenides in samples from the MH suggests that downwards-directed fluid flow may have remobilised As from garnet.

The strong correlations between Sc and Cr (Figure 7c), Hf and Zr (Figure 7d), and V and Nb (Figure 7e) are readily interpretable in terms of the similar ionic charge and geochemical affinity of each element pair (tri-, quadri- and pentavalent, respectively). Strong positive correlations are observed between Y and V (Figure 7f), Y and Nb (Figure 7g), and between Zr and V (Figure 7h). All these elements attain their highest concentrations in the retrograde garnet rims.

Other binary plots show discrimination among garnet categories from the prograde and retrograde stages of skarn evolution. This is seen particularly well in the U vs. W (Figure 7i) and Y vs. Ce plots (Figure 7j) but also in the plots of Y vs. Cr (Figure 7k) and V vs. Sc (Figure 7l).

## Trace elements in garnet from Groundhog, S.A.

Overall the binary plots show that, besides minor elements such as Ti and Mn that correlate with Al-rich compositions, there are ranges of trace elements that can be used to discriminate individual garnet categories. Prograde and retrograde stages are characterised by specific ranges of elements, i.e. W, As, Sn, U, Ce, and Cr, V, Y, Nb, Sc, Hf, Zr, respectively. Overall, the HFSE are clearly higher in retrograde garnet whereas granitophile elements such as W, U, Sn, As are prominent in prograde garnet. Interestingly, Cr, a siderophile element that is typical for retrograde garnet, particularly in the rim, is also seen in type-I D garnet (Figure 7c, k). The overlap between type-I B and type-II garnets on the plots further emphasises that these categories belong to the same stage of skarn evolution. On the other hand, the overlap between type-I D and retrograde categories indicates that oscillatory zonation in garnet may attract, besides REE, also a preferential partitioning of HFSE.

## LA-ICP-MS element maps

LA-ICP-MS element maps (Figures 8-11) allow a visual expression of compositional zoning at the grain-scale. All the maps are from mineralised skarn and were generated to better understand how trace elements can constrain the range of garnet categories proposed on the basis of petrographic observation. Mapped areas cover portions of coarse-grained garnet (type-I) in which an oscillatory-zoned core (B) is surrounded by thin, darker zones (D), and an outermost rim (R) on Figures 8-10. The map shown as Figure 8 shows relationships between type-I and rim, where the latter consists of small garnet grains (see petrography, above). In Figure 9, the core garnet is replaced by chlorite prior to rim formation, and in Figure 10, the rim is bracketed by sulphide deposition, i.e. a thin chalcopyrite-galena band, and the chalcopyrite-sphalerite-galena assemblage outside the garnet. Galena within the darker zoned garnet is shown to be a

carrier of Ag and Se; sphalerite adjacent to chalcopyrite carries In. Nickel concentration correlates with replacement of garnet by chlorite and/or talc (Figure 9).

The effects of superimposed, fluid-assisted brecciation, resulting in redistribution of trace elements, are shown in Figure 11. Evidence of shearing and intense brecciation (Figure 11) is shown particularly well by Ti, and by the enrichment in Mn within areas that have been most strongly brecciated, and within crosscutting microfractures. This map also highlights the decoupling between LREE and HREE during fluidisation. Contrasting with this general trend, the map in Figure 10 shows Mn enrichment within the type-I B core.

All maps show the fine oscillatory zonation of trace elements as a feature of all garnet categories. The character of the type-I B cores, richer in Fe relative to Al-richer type-I D and R, is clearly underlined by distribution of minor elements such as Mn and Ti (e.g. in Figures 8 & 10). However, Mn shows enrichment in D relatively to R in Figure 11, whereas in Figure 9, Mn is slightly enriched in R. The B cores are always higher in W and As, but these elements can be also seen in the D in Figure 9.

The rim (R) in all cases is strongly highlighted by enrichment in Cr and incompatible/HFSE (Nb, Sc, V, Ga) and may display marked oscillatory zoning. Particularly strong enrichment of a range of tri-, quadri- and pentavalent ions (Ti, Cr, Ga, Sc, HREE Cr, V, Ga, Zr) is seen particularly well especially on Figure 11. Thorium is also elevated within the thin, oscillatory-zoned parts of the mapped grains (Figure 11).

**Trace elements in garnet from Groundhog, S.A.**

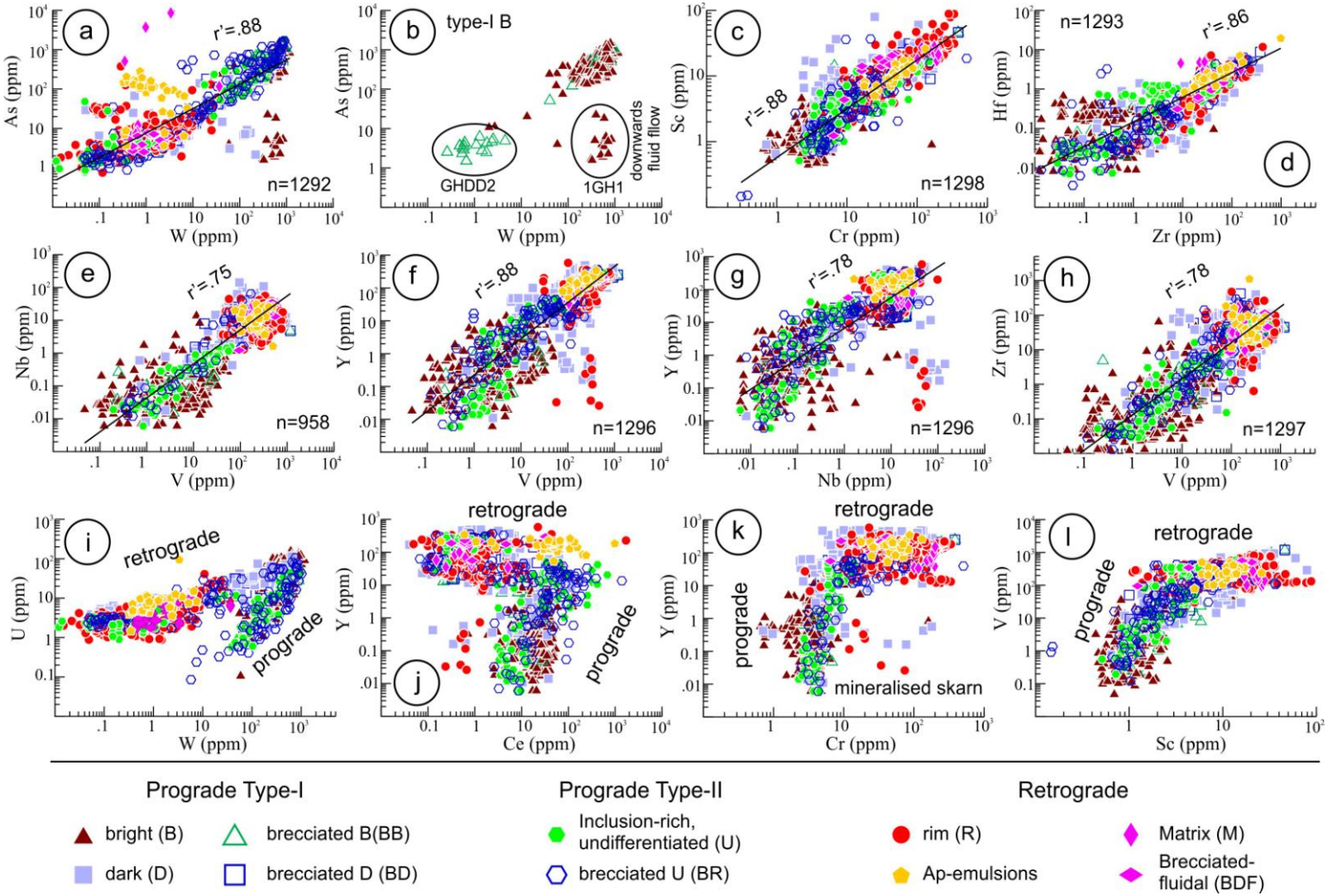


**Figure 7: Binary plots for garnet. (a) As vs. W, (b) Sc vs. Cr, (c) Hf vs. Zr, (d) Nb vs. Y, (e) Y vs. V, (f) Nb vs. V, (g) Zr vs. V, (h) U v. W, (i) Y vs. Ce, (j) Y vs. Cr, and (k) V vs. Sc. Two distinct trends can be seen: the first represents a strong correlation between two elements across the dataset; the second shows a distinct split of the population between prograde and retrograde garnet categories**

Similarly, U (and $^{206}Pb$) can show variable patterns in the B category relative to R, i.e. concentration towards the edges of the cores (Figures 8-10) but is evenly distributed in Figure 11 (R is not clearly present). Also notable on Figure 11 is the enrichment in P in type-I B garnet. This could supply P for nucleation of apatite inclusions during the retrograde stage.

Interestingly, although the distribution of REY is predictable from the REY trends as presented above, a redistribution of LREE during brecciation, e.g. Ce, on Figure 8, or La on Figure 11, is shown. A similar redistribution-via-brecciation pattern is shown by Sn on Figure 8, but not on Figure 11. Enhanced Sb is also noted within type-I B garnet on Figure 9. Strikingly, sector zoning of As and In, an element not generally reported in garnet, is observed in type-I B garnet (Figure 11). Such sector zoning does not correlate with Sn, U, or W.

These maps illustrate formation of one of the main categories of retrograde garnet (the rim) in mineralised skarn, which also has implications for ore mineral deposition. The rim can form either from in-situ brecciation followed by recrystallization of type-I garnet (Figure 8), by brecciation via fluidisation (Figure 11), or as a distinct overgrowth at the end of the retrograde stage concluded by main sulphide deposition (Figures 9 and 10). The difference between the latter two (from the same drill hole, closest to the presumed trap) is that, in Figure 9, replacement by chlorite is seen instead of sulphide deposition, whereas in Figure 10, the rim brackets the first and main stages of sulphide deposition. Chromium enrichment is a proxy for rim formation in all cases whereas As tracks the intensity of the retrograde overprint.

**Trace elements in garnet from Groundhog, S.A.**

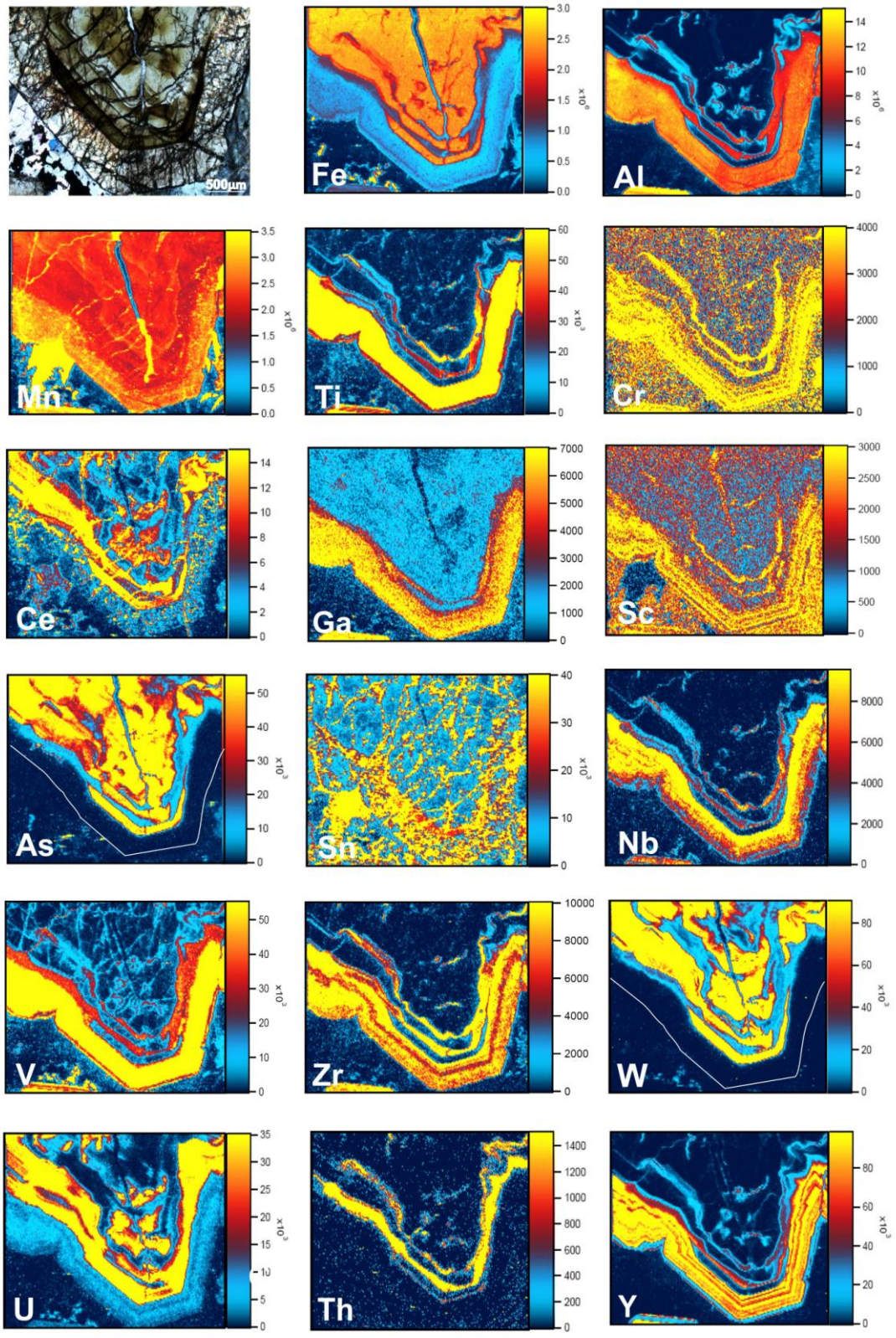


**Figure 8: LA-ICP-MS mineral element map of a coarse-grained garnet from thin section sample GH1-3_808.5 with optical image of the same grain (top left). The grain shows oscillatory zoning between darker zones within the bright core and the outermost rim. (Element analysis in *counts per second*)**

**Trace elements in garnet from Groundhog, S.A.**

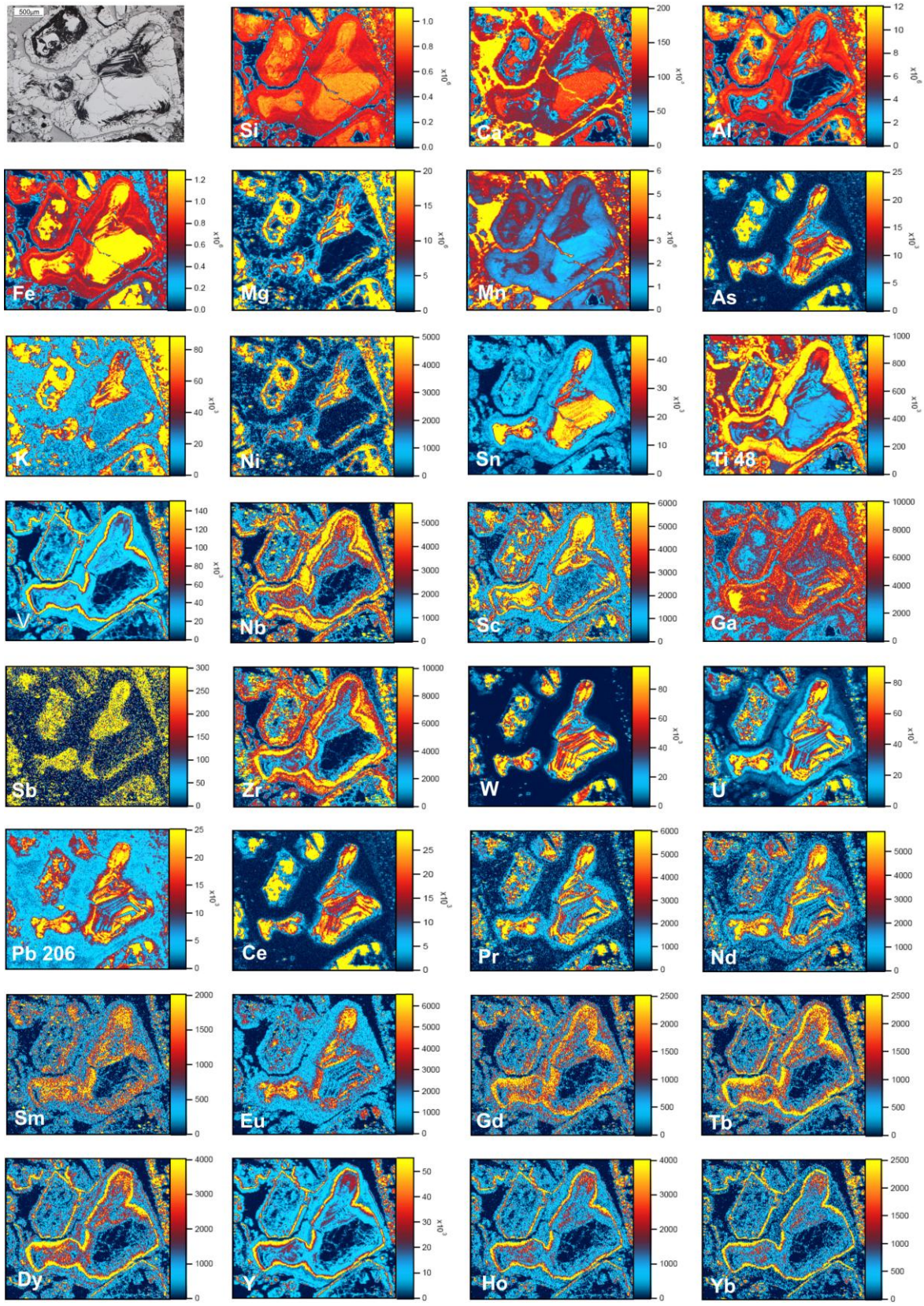


**Figure 9: LA-ICP-MS mineral element map of a coarse-grained garnet from polished block sample GH2_945.7 with optical image of the same grain (top left). The grain shows a core and dark zones with oscillatory zoning and an outermost rim. (Element analysis in *counts per second*)**

**Trace elements in garnet from Groundhog, S.A.**

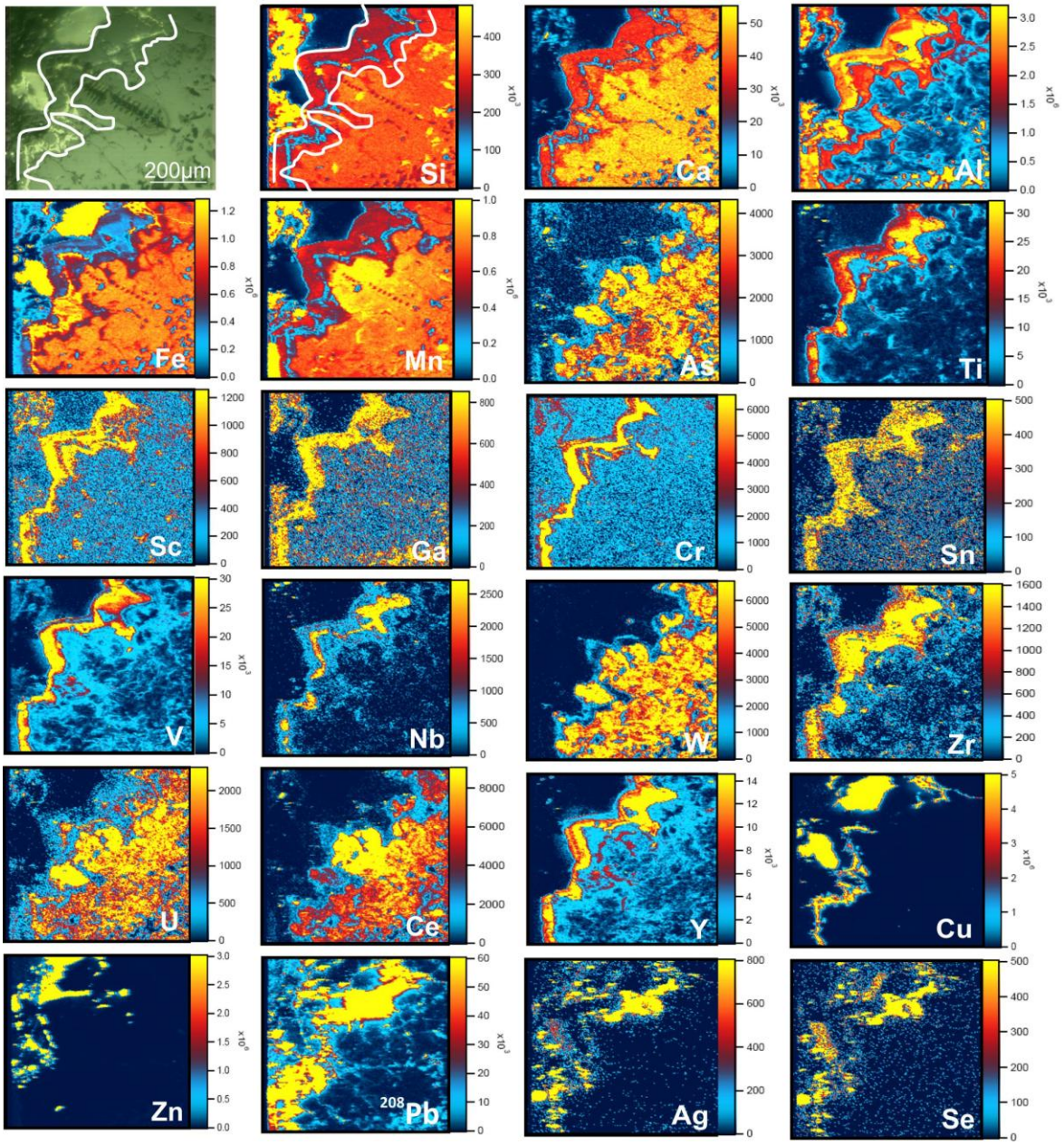


**Figure 10: LA-ICP-MS mineral element map of a coarse-grained garnet from polished block sample GH2_908.6 with optical image of the same grain (top left). The grain shows a core with darker zoning replaced by sulphides (galena and chalcopyrite) enclosed by an outermost rim. Suphides (Chalcopyrite and sphalerite) are also interstitial to the garnet. (Element analysis in *counts per second*)**

**Trace elements in garnet from Groundhog, S.A.**

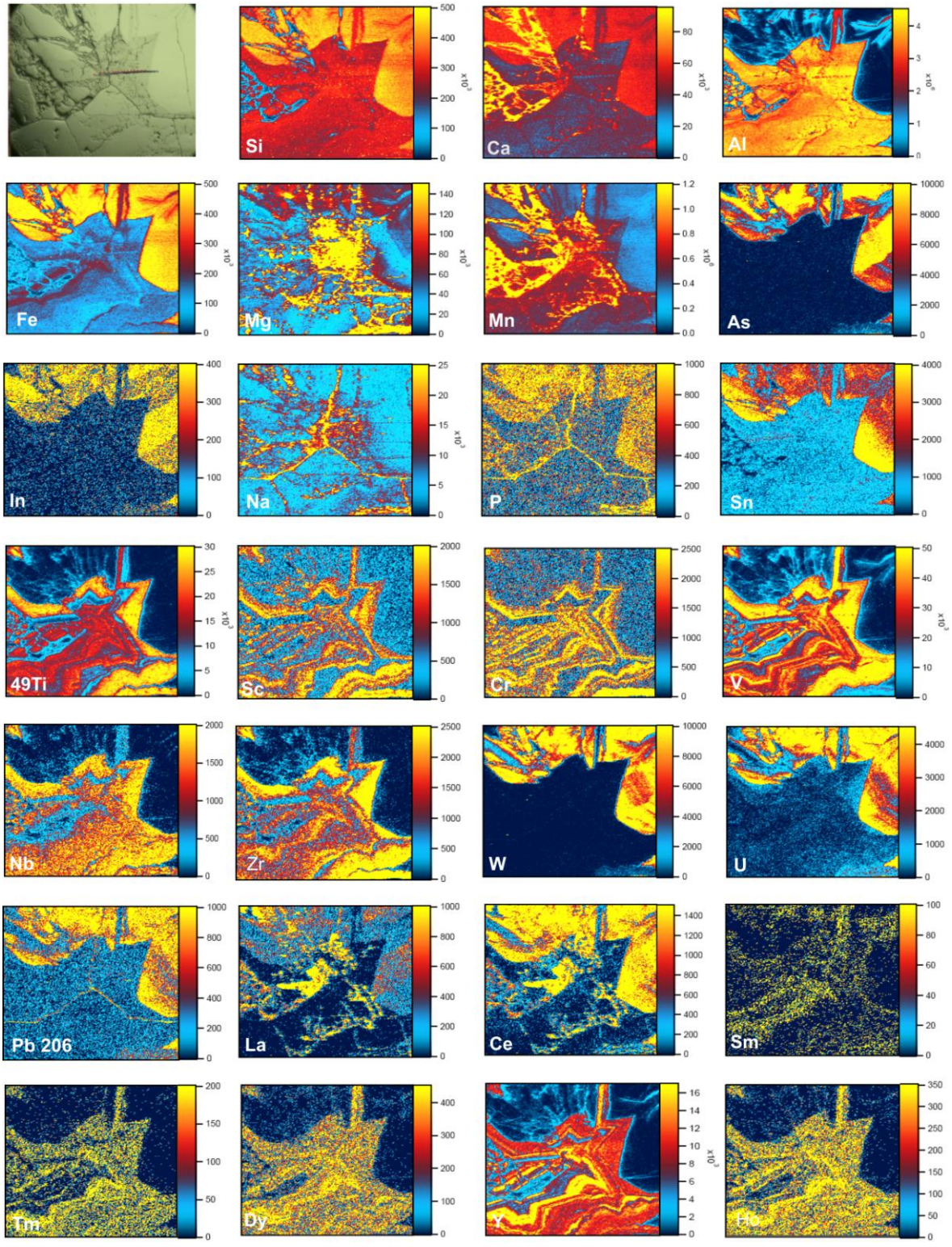


**Figure 11: LA-ICP-MS mineral element map of a brecciated garnet from polished block sample GH4_874 with optical image of the same grain (top left). The grain shows a bright core with an intensely brecciated darker zone. (Element analysis in *counts per second*)**

**Trace elements in garnet from Groundhog, S.A.**

### LA-ICP-MS analysis of accessory minerals

***Carbonates*** can incorporate concentrations of REY. Two types of calcite were analysed: coarse-grained matrix calcite; and calcite within crosscutting veins. Both types contain low ΣREY concentrations (10-100 ppm) and inconsistent REY fractionation trends. There is weak LREE enrichment and a consistent weak positive Y-anomaly.

***Fluorite*** can also incorporate REY. Two types of fluorite were analysed: an early-formed fluorite within the marker horizon; and a late, coarse-grained fluorite from GHDD3. The former is LREE-enriched (ΣREY 60-4587 ppm. REY fractionation trends are relatively flat with a slight downwards slope and negative Eu-anomaly. Late fluorite in GHDD3 contains very low concentrations of ΣREY (1–10 ppm) and features a positive Y-anomaly.

LA-ICP-MS spot analyses of ***apatite*** in 5 samples confirm REE-enrichment (ΣREY from 60 to 3500 ppm. The highest ΣREY concentrations are found within apatite in highly altered and retrogressed garnet skarn from drill hole GHDD6. REY fractionation trends range from relatively flat to sloping downwards, with a consistent negative Eu-anomaly.

## DISCUSSION

### Incorporation of trace elements and substitution mechanisms in garnet

Garnet is defined as $X_3Y_2Z_3O_{12}$, where X is a divalent cation ($Ca^{2+}$, $Mg^{2+}$, $Mn^{2+}$, $Fe^{2+}$ etc.) in eight-fold, dodecahedral coordination, Y is the trivalent cation site ($Fe^{3+}$, $Al^{3+}$ or

$Cr^{3+}$) in octahedral coordination and Z is Si in tetrahedral coordination. At least four mechanisms have been invoked to explain incorporation of trace elements into the garnet crystal structure: surface adsorption; substitution mechanisms; and interstitial solid solution (filling of voids between ions in the crystal). Kinetic effects control the first two of these during mineral growth; the remaining two are constrained by crystal chemistry (Gaspar *et al.* 2008).

Incorporation of $(Y,REE)^{3+}$ by replacement of $X^{2+}$ cations involves coupled substitution to maintain charge balance (Gaspar *et al.* 2008). Four separate substitution mechanisms are proposed: (i) YAG (yttrogarnet)-type substitution involving charge balance by substitution of a trivalent cation into the Z (Si) site (Jaffe 1951); (ii) incorporation of a monovalent cation (essentially $Na^{+}$) into the X site (Enami *et al.* 1995); (iii) charge compensation via vacancies in the dodecahedral site; and (iv) charge balance is achieved by substitution of divalent cations ($Mg^{2+}$, $Fe^{2+}$) into the Y site (menzerite-type substitution; Grew *et al.* 2010; Carlson 2012).

On the basis of analysis and numerical modelling, Smith *et al.* (2004) and Gaspar *et al.* (2008) argued that Fe- and Al-zoning in garnet supports strong partitioning between LREE to HREE via an intracrystalline effect, i.e. where Fe and Al-rich zones are preferentially enriched in LREE and HREE, respectively, and where the main substitution is YAG-type. In their study of the Hillside skarn, Ismail *et al.* (in press) acknowledged the role of YAG-type substitution during retrograde crystallization but argued that the alternative, 'menzerite-type' coupled substitution mechanism for REY-incorporation involving $Fe^{2+}$ or other divalent ions (Grew *et al.* 2010, Carlson 2012),

could explain the anomalously high Y+(H)REE incorporation in garnetite at Hillside. If correct, Ismail *et al.* (in press) believed this may hint at the importance of redox processes in governing REE partitioning into garnet. Although absolute ΣREY concentrations in garnet at Groundhog are not as high as at Hillside, and there is also less evidence for control by redox processes (oxidised, hematite stable throughout and no magnetite present), a case can nevertheless be made for similar REE incorporation processes.

This study has highlighted that garnet can also incorporate a very wide range of elements (Table A-4, Figures 8-11), including several rarely reported (e.g. Sn; Mulholland 1984, Ray *et al.* 2000) and others probably never reported elsewhere (Sb, Mo, In). Although certain general assumptions can be made about the chemical state and structural site of certain elements (e.g. $Sc^{3+}$ and $Ga^{3+}$ accompany $Al^{3+}$ into the Y site), a detailed assessment of garnet chemistry and how other elements (V, Nb, Zr, U and W) are incorporated, is beyond the scope of this paper.

## REY-patterns and other trace elements in garnet: prograde-retrograde stages

Skarn garnets commonly display wide compositional variation on the scale of an individual deposit (Meinert 1992), and may also be compositionally zoned at the grain-scale (oscillatory and sector zoning, growth zoning; e.g. Ciobanu & Cook 2004). The emergence of techniques such as LA-ICP-MS to accurately analyze patterns of trace element enrichment at low concentrations in garnet has enabled an understanding that these discrete patterns can be correlated with individual stages of skarn evolution. These trace element distributions, particularly of REY, have proven useful for tracking track

fluid source, protolith type and fluid-rock interaction (Smith *et al.* 2004; Gaspar *et al.* 2008, Ismail *et al.* in press).

Each category of garnet within sampled skarn intervals in drill holes GHDD1-GHDD7 displays distinct trace element patterns and also quantifiable changes in those patterns in separate growth zones (Figure 12). Early-formed garnet cores belonging to the prograde stage of skarn evolution are Fe-rich (marked B on Figure 3a, b, c), and also evident on the LA-ICP-MS element maps (Figures 8-10). They display a distinct signature marked by enrichment in W, U, As and LREE (Figures 8-10). As the skarn evolved, a shift took place, resulting in a change towards garnet richer in Al (Figure 12), and marked by the development of oscillatory growth zoning within the early-formed cores, well shown by the element maps (Figures 8-10). Coincident with the relative Al-enrichment is a marked partitioning of MREE-HREE (Figure 6), and also incompatible elements, into the garnet lattice. The defining geochemical signature of this dark type-I garnet is Zr, V, Sc, Th and MREE-HREE. This is shown by the REY fractionation plots for type II-retrograde garnet (Figure 6), and is seen on all four element maps (Figures 8-10). A first cycle of brecciation of this type-I garnet resulted in the obliteration of the characteristic signature, notably depleting concentrations of W and As, and causing remobilization of U and LREE (especially Ce and La; see plot B in Figure 7). During the late prograde stage, and following successive cycles of brecciation, a weakly-zoned garnet formed between and around the brecciated type-I garnet cores, and also as smaller euhedral grains with poikilitic inclusions (type-II garnet; Figure 3d) This garnet, which is comparable with type-I dark garnet, is also Al-rich. It is also richer in elements such as

Zr, V, Sc, and MREE-HREE, indicated within plot L in Figure 7, showing a clear splitting trend between the prograde and retrograde stage.

Transformation from the prograde stage to a retrograde overprint results in a marked increase in ΣREY, and a shift from relative enrichment in LREE in early-prograde garnet, to a MREE-HREE enrichment in the retrograde garnet, as shown in REY fractionation trends (Figure 6) and illustrated in Figure 12). The retrograde stage of skarn evolution saw formation of an outermost rim around the type-I early-prograde cores (Figure 3b). This is also Al-rich, strongly enriched in HREE, as well as Cr and some incompatible elements; lending this latest garnet generation a pronounced Cr-HREE signature (Figure 7c, k; Figures 8-10). Evidence for further cycles of recrystallization and brecciation of garnet can be seen throughout the retrograde stage of skarn evolution (Figures 11 & 12). These may be highly localized, such as the fluid-assisted brecciation seen in samples from drill hole GHDD4 (Figure 11). The development of apatite emulsions in garnet (Figure 3f) and crystallization of fine-grained matrix garnet can also be linked to mineral reactions, often local in character, during the retrograde stage (Figure 12). All these latest garnets display similar incorporation of Cr and HREE (Figures 8-10). Deposition of sulphides took place during the retrograde stage. Most sulphides occur interstitial to garnet (i.e. in the matrix); with the exception of the first generation of sulphides which are enclosed by the outermost garnet rim (Figure 10).

Chemical zoning in garnet (oscillatory zoning) generally reflects a primary growth texture that expresses feedback within a dynamic system between the mineral surface

and its environment (Shore & Fowler 1996). Factors which govern growth include mechanisms such as pressure and temperature changes of the fluid, surface adsorption, mineral diffusion and growth rate. Smith *et al.* (2004) indicate oscillatory zoning formed as a result of enrichment-depletion cycles in garnet components in solution during growth. This is reflected within the type-I garnet at Groundhog formed during the early prograde stage (Figure 3b).

Evidence for remobilization of trace elements within garnet grains is seen on the LA-ICP-MS element maps (Figures 8-11). LREE and some incompatible elements, notably Th and U, are extremely mobile and are ready removed and reincorporated within individual garnet grains. Uranium, and to some extent also Th, also show remobilization throughout all stages of garnet development from andradite rich zones to more-grossular zones grading out to the outermost rim (Figure 8). The most mobile LREE show patterns of migration from the core to late, crosscutting fracture zones. Tin, an element whose presence within garnet is poorly documented and even less well constrained in terms of mode of incorporation, also, displays extensive remobilization (e.g. Figures 8, 10 &11), from the core (type-I) to the outermost rim and late-stage fractures.

The variation in textures seen in samples from the same intervals (relative to the marker horizon) and from prograde to retrograde stages, suggests considerable temporal and local fluctuation in fluid/rock ratios throughout the skarn lifespan. Considering the oscillatory zoning that is marked during early prograde but becomes very weak or is lacking altogether during the retrograde stage, inferences can be made that garnet growth took place in closed- and opened systems, respectively. The substantial

remobilization and recrystallization during the retrograde stage, together with the presence of fluidal and apatite emulsion textures strongly support the idea that fluid pressure played an important role during the retrograde stage. The intensity of fluid-assisted retrogression of garnet also correlates with presence of mineralization, as well as replacement of garnet by sulphides. At least two generations of sulphide deposition can be assumed based on relationships with garnet growth cycles as seen from rims that are bracketed by sulphides.

## Comparison with other garnet skarn

There are few published studies concerning trace element distributions within skarn garnets. Despite this, data from three deposits, all with some similarities to the Punt Hill system, can be compared and contrasted against that presented here. Garnets in the Crown Jewel skarn, Washington State, USA (Gaspar *et al.* 2008) display prograde Fe-rich garnet cores which show characteristic LREE-enrichment and positive Eu-anomalies, closely resembling the data reported here. Smith *et al.* (2004) also report oscillatory-zoned skarn garnet from Beinn an Dubhaich, Scotland, which shows a strong positive Eu-anomaly analogous to that observed within trends of type I-B garnet at Groundhog.

In contrast to the Groundhog case, Ismail *et al.* (in press) report that ΣREY is highest during the prograde stage of skarn evolution at Hillside, and decreases markedly during the retrograde overprint. At Hillside, prograde garnet, Fe-rich displays HREE-enrichment, with upwards-sloping REY fractionation trends, similar to Al-rich garnets at Groundhog. Therefore, although Fe/Al compositional variation is an important factor

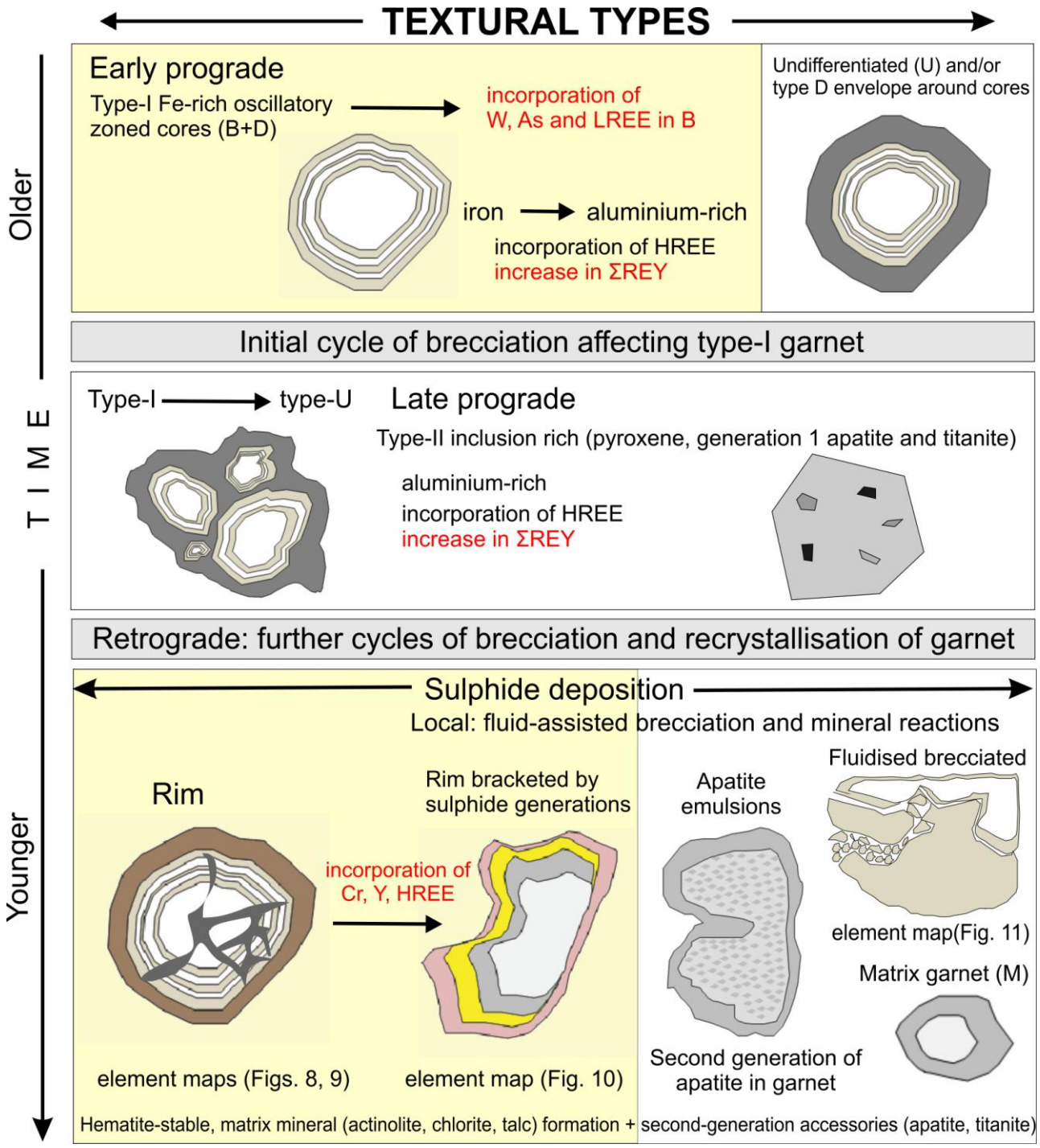


**Figure 12: Schematic diagram representing the overall textural types of garnet formed through space and time during evolution of the Punt Hill skarn system. Textures of garnet begin with early-prograde type I garnet, which undergoes an initial cycle of brecciation, progressing through to late prograde where type II garnet forms around type I as well as forming new grains rich in inclusions. The retrograde stage of skarn evolution is characterized by sulphide deposition and the formation of a rim around type I garnet. Locally, fluid-assisted brecciation and mineral reactions are formed during the late retrograde stage, including, rim bracketed by sulphides, emulsions of micron-sized apatite, fluidized brecciation and nucleation of matrix garnet**

for REY-fractionation patterns in garnet, this is not the only control. Different substitution mechanisms, i.e. YAG- and menzerite-types, respectively, for garnet with similar composition may also explain differences between Groundhog and Hillside garnets (see above). Skarn garnets from Groundhog also differ to those of Hillside in that there is a significant increase in ΣREY from the prograde to retrograde stage.

Moreover, there is a marked W- (up to hundreds ppm) and As-signature for prograde garnet at Groundhog whereas at Hillside there is a marked Sn-signature (up to hundreds ppm) throughout the prograde and retrograde garnets, even though with mild enrichment in the retrograde stage.

Differences between Hillside and Groundhog skarn garnets in terms of REY-partitioning and other trace element signatures could also be interpreted as variation in regional and local skarn setting within the Olympic Province. For example, the transition from W-rich to Sn-rich signatures can be related to variation in depth or geotectonic context of magma generation during Hiltaba magmatism. Skarn proximity to contacts with Hiltaba Suite granites at Hillside (unknown at Groundhog) also correlates with the dominant ore type, i.e. Cu- and base metals, respectively. This would imply that the fluid source at Groundhog is distal relative to proximal at Hillside.

A common feature, however, is that no zonation trends can be defined based on major garnet composition or trace elements distributions in either area. At Groundhog, a limiting factor is the intensity of retrogression which has obliterated any pre-existing zonation patterns. Secondly, the Punt Hill system may show zonation patterns in garnet

that are larger in scale than the Groundhog orefield alone. This would imply that the fluid-mineral reactions leading to skarn formation are driven by large fluid-flow patterns controlled by regional structures rather than being tied to local fluid sources or intrusive contacts. Whichever the answer, the high REY budget, together with the presence of elements such as W, Sn, As, suggests a granitic affiliation for the skarn fluid. In contrast, Cr identified here in the rim garnet implies an affiliation with mafic magmatism or alternatively, the presence of rocks that are rich in this element and which provided a source for hydrothermal fluids along structures focusing such fluids. Uranium-enrichment together with high REY concentration in garnet skarn at Groundhog, although not unique to IOCG systems (the skarn at Beinn an Dubhaich, Scotland, Smith *et al.* 2004, is an example), is nevertheless a signature that typifies such deposits. Considering that skarn formation and associated mineralization at Punt Hill is constrained to the same 1.6 Ga magmatic event (Reid *et al.* 2011) and this event corresponds to formation of IOCG systems throughout the Olympic Province, the Groundhog base metal skarn can definitively be considered within this deposit class.

## Vector modelling using trace elements in garnets

The use of compositional variation in garnet to track orefield skarn zonation relative to fluid sources is a consecrated exploration tool (e.g. Meinert 2002). The hypothesis followed in this study was that garnet along the same intervals (relative to a marker horizon) can track fluid flow along the two main structural orientations in the orefield. Although compositional patterns are highly variable depending on the local context, and the superimposed retrogression can obliterate such compositional patterns, the present study has identified several correlations between key textures, trace elements and mineralization (Figure 2 & 13). These are:

1. a positive correlation with Cr and rim garnet;
2. an inverse correlation with As and W in prograde type-I B garnet; and
3. subtle ΣREY variation in late prograde type-II garnet and type-I D, and rim garnets.

These correlations have been tested as spatial vectors within the orefield. A range of diagrams, including plan views, sliced cross-sections and oblique, and, were generated using *Leapfrog Geo* geological modeling software (Figure 13). The plots were obtained using mean concentrations for garnet categories and the compositional shell contours were constrained within the skarn intervals between the GRV and Donington granite. Supported by spot analyses and element maps, the plan view diagram in Figure 13a defines a spatial trend for the same skarn horizon in which W-enrichment is associated with early prograde (type-I) garnet cores. The highest W concentrations are seen in drill holes in which the least retrogression and evidence of overprinting events is observed, preserving the early-formed garnet. The preserved prograde stage of skarn evolution is best depicted in drill holes located on the NW-trending structure including GHDD4, GHDD7 and GHDD5, in which W concentrations range from 200-400 ppm. Samples from GHDD1, at the node of two structures, display high W concentrations despite showing retrogression and mineralization overprint. The area around GHDD1 may represent a fluid pathway for redistribution of remobilized W from more ‘prograde’ drill cores in the NW-SE section.

**Trace elements in garnet from Groundhog, S.A.**

Samples from the NNE-trending drill holes, including GHDD3, GHDD1, GHDD6 and GHDD2, reflect significant amount of retrogression and overprinting events of mineralization, with the exception of drill hole GHDD3 which is non-mineralized. ΣREY concentrations plotted for type-II garnet (Figure 13b) show a split between 'prograde', non-mineralized drill cores and the heavily retrogressed drill cores that contain a significant amount of mineralization. Late, type-II prograde garnet depicts the boundary between mineralized and non-mineralized drill cores; the latter contain greater ΣREY. REY are remobilized from this type of garnet and subsequently redistributed into garnet rims formed during the retrograde stage of skarn evolution.

The plan view in Figure 13c shows the overlap between ΣREY in dark zones (D) within type-I early-prograde garnet (blue and green contour shells), and rim garnet formed during late retrograde stage (yellow-red contoured shells). Retrograde rim garnet composition represents a positive vector showing highest REE concentrations (230-350 ppm) in mineralized, retrogressed drill holes along the NNE-section (defining the target zone). Drill hole GHDD5 also contains significant ΣREY concentrations despite being relatively distal and relatively non-mineralized. The high ΣREY concentrations within this drill hole relative to GHDD7 and GHDD3 may be interpreted as resulting from higher remobilization and reworking of type-II garnet towards mineralization. Co-crystallization of a second generation of REE-bearing accessory minerals such as apatite and titanite within the matrix also explains depletion of ΣREY within retrograde garnet.

The distribution of two most important distinct trace elements, As and Cr, which are clearly defined as key geochemical signatures for early-formed prograde (type-I B, and late-retrograde garnet (R), respectively, are shown on Figure 13d and e. Contour lines

along the NNW-trending profile (Figure 13b) show highest Cr concentrations within drill hole GHDD2, closest to the target zone. This has an inverse correlation with As concentrations along the same profile. The spatial vectors are consistent with spot analyses and element maps in which As is highest in early prograde type-I garnet. Highest concentrations of As are seen from non-mineralized, less-retrogressed drill holes along the NNW-trending structure. The plan view (Figure 13c) shows strong depletion in As in drill core GHDD4 where emulsion textures in garnet indicate strong fluid-pressure assisting garnet retrogression.

The results here clearly show that the NNW-trending structures have more efficiency in driving ore fluids during the retrograde stage. The Cr vs. As vectors along the NNW-SSE structures point towards the 'target area' as defined based on ore concentrations at Groundhog (Swain 2013). In contrast, the W and ΣREY-vectors show that fluid flow along the NW-SE structures may have relevance for tracking regional zonation trends within the Punt Hill area.

Characterisation of mineral chemistry at Punt Hill, and the identification of predictable patterns in garnet that can be correlated with geological events, has potential benefits beyond the specific geological setting at Groundhog. It can assist in developing an empirical framework for regional-scale alteration patterns associated with IOCG-skarn mineralization and ore systems within the Olympic Province and beyond.

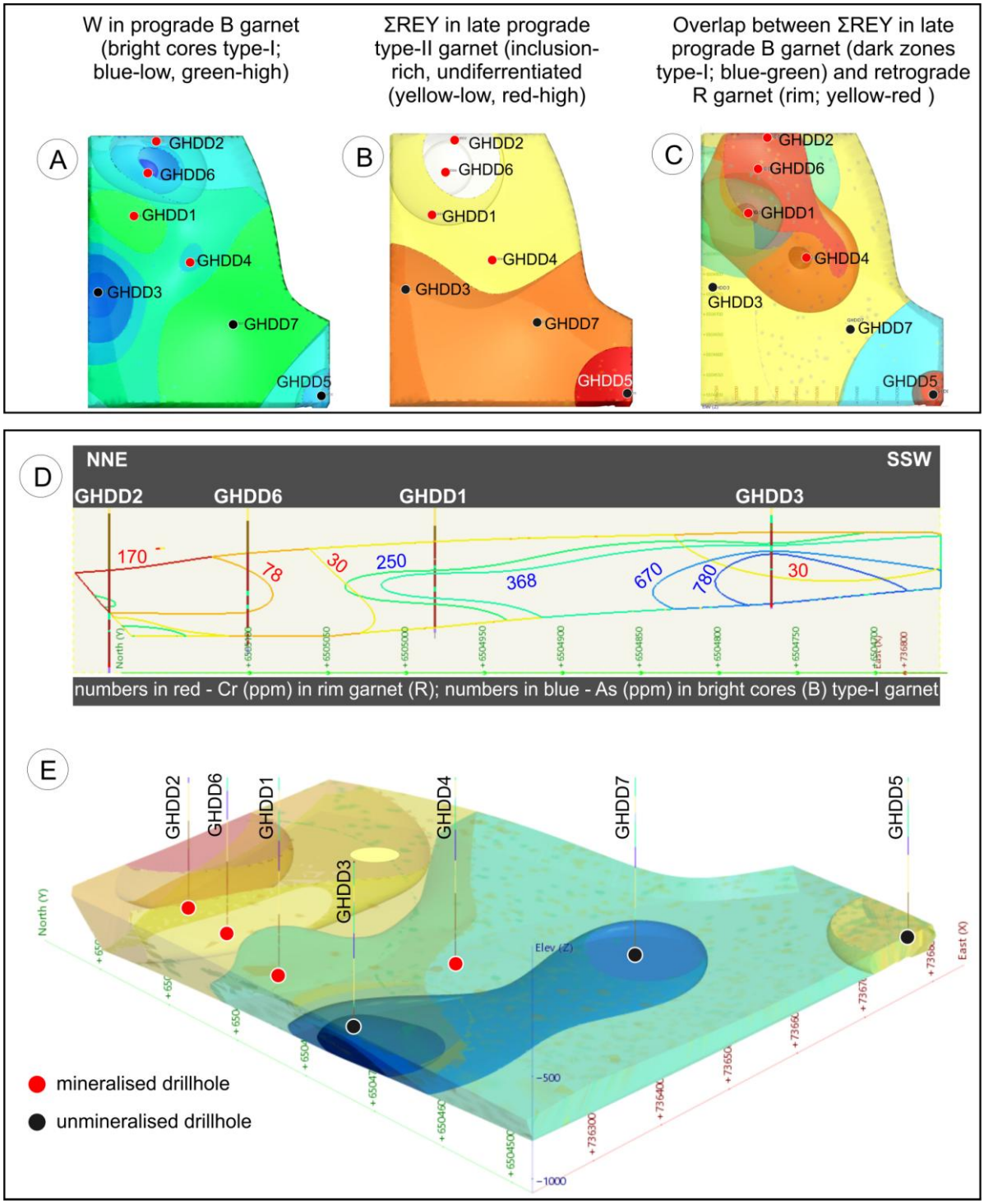


**Figure 13: (A) Contoured plan-view of the Groundhog prospect, showing W concentration in the bright cores of type-I garnet. The highest W concentrations are shown as the darkest green shell, followed by a lighter green shell, at 400 ppm and 300 ppm, respectively. The lowest W concentrations are shown in light blue shells at 200 ppm to dark blue shells at 100 ppm. (B) Contoured plan-viewof the same area, showing ΣREY concentration in late type-II garnet. White contour shells show 100-200 ppm ΣREY, yellow 200 ppm, orange 300 ppm ΣREY, and the highest concentrations (in drill hole GHDD5 at 400 ppm ΣREY). (C) Contoured plan-view showing the overlap between ΣREY in dark zones within type-I early-prograde garnet (blue and green contour shells), and rim garnet formed during late retrograde stage (yellow to red contour shells). Prograde type I-D garnet shows the lowest REE concentrations (80-150 ppm, blue contour shells) with highest concentrations ranging up to 200-350 ppm (green contour shells). (D) cross-section, and (E) and oblique plan view showing Cr contour shells (yellow, 81-95 ppm), increasing to red shells (230- 350 ppm). The NNE-section reflects lowest As concentrations (250-360 ppm; green contour shells). The highest As concentrations (dark blue contour shells, 780 ppm) are from non-mineralised, less-retrogressed drill holes along the NNW structure (SE section)**

## CONCLUSIONS

The Groundhog prospect contains distinct textural categories of garnet, reflecting the overall evolution of the skarn system in time and space. Correlation of these textures with discrete REY and other trace element signatures has been used for ore vectoring. Several conclusions can be made:

- Fe-rich prograde garnet (andradite) is oscillatory-zoned, with high contents of W and As, relatively low ΣREY, and low HREE/LREE ratio. In contrast, retrograde garnet is Al-rich (up to 50% grossular), ΣREY concentrations an order of magnitude higher, high HREE/LREE, and high concentrations of incompatible and high field strength elements. A marked enrichment in Cr typifies the garnet rim. Signatures and textures of retrograde garnet clearly track sulphide deposition.
- Acquisition of additional mineral-chemical data will assist in explaining the range of trace element substitutions observed in garnet, particularly the interplay between, and relative roles of YAG- and 'menzerite'-type coupled' substitutions.
- Although there is no discernible orefield-scale zonation as such in terms of major composition, trace elements in texturally-distinct categories of garnet were used as ore vectors along the two main structural orientations which control ore at Groundhog.
- Based on Cr in rim garnet, the NNE-trending structure is interpreted to control fluid flow, with an increasing intensity of mineralization towards NNE. In contrast, vectors defined by the REY- and W-contents in prograde and

retrograde garnets indicate the NW-SE structures as driving skarn-forming fluids on a more regional scale. This has potential for defining metallogenic patterns in the Punt Hill area, linking Groundhog to other prospects.

- Groundhog is recognised as an IOCG system with skarn alteration. It may, however, lie distal to fluid sources, and is also strongly oxidised. Skarn formation and mineralization would appear to be fluid-driven along structures that may be linked to a deep magmatic fluid source.
- Outcomes here indicate that trace element distributions in garnet can be used as spatial vectors for exploration provided that the data is interpreted in the contexts of textures and of temporal (prograde-to-retrograde) evolution of the system. The pilot project here can be tested throughout the Punt Hill area, particularly with reference to the possible existence of a large, structurally-controlled system.
- Comparison between garnet chemistry at Groundhog and Hillside points to a possible N-S zonation within the Olympic Province, from W- to Sn-enriched. Such results can form a basis for defining specific settings for magma generation within the Olympic Province and beyond.

## ACKNOWLEDGMENTS

First and foremost, I acknowledge the financial support given by the DET CRC. Secondly I extend my thanks to Monax Mining Limited for use of their drill hole data and for core to create my samples. In particular my thanks go to Greg Swain for providing me with the opportunity to work on the Punt Hill project and for his constant guidance and support throughout the year. I thank Benjamin Wade, Aoife Mc Fadden and Ken Neubauer at Adelaide Microscopy for their patience and training assistance throughout my analytical work. Similarly thanks are extended to Katie Howard for advice, Adrian Fabris at DMITRE for geochemical data, Benjamin Vanderhoek for his time, opinion and assistance with the *Leapfrog Geo* program and Tyler Bastian for reviewing, inspiring and motivating throughout the year.

I finally extend my thanks to my wonderful supervisors Nigel Cook and Cristiana Ciobanu for their assistance, inspiration, motivating, constant support and guidance throughout the year.

## REFERENCES

ALLEN, S.R., MCPHIE, J., FERRIS, G. & SIMPSON, C. 2008. Evolution and architecture of a large felsic igneous province in western Laurentia: The 1.6 Ga Gawler Range Volcanics, South Australia. *Journal of Volcanology and Geothermal Research* **172**, 132–147.

BASTRAKOV, E.N., SKIRROW, R.G. & DAVIDSON, G.J. 2007. Fluid evolution and origins of iron oxide Cu-Au prospects in the Olympic Dam District, Gawler craton, South Australia. *Economic Geology* **102**, 1415–1440.

BAU, M. & DULSKI, P. 1995. Comparative study of yttrium and rare-earth element behaviours in fluorine-rich hydrothermal fluids. *Contributions to Mineralogy and Petrology* **119**, 213–223.

CARLSON, W.D. 2012. Rates and mechanism of Y, REE, and Cr diffusion in garnet. *American Mineralogist* **97**, 1598–1618.

CIOBANU, C.L. AND COOK, N.J. 2004. Skarn textures and a case study: the Ocna de Fier-Dognecea orefield, Banat, Romania. *Ore Geology Reviews* **24**, 315–370.

CONOR, C., RAYMOND, O., BAKER, T., TEALE, G., SAY, P. & LOWE, G. 2010. Alteration and Mineralisation in the Moonta-Wallaroo Cu-Au Mining Field Region, Olympic Domain, South Australia. *In:* Porter T.M. ed. *Hydrothermal Iron Oxide Copper-Gold*

*and Related Deposits: A Global Perspective*. PGC Publishing, Adelaide, **3 & 4**, 1–24.

COOK, N.J., CIOBANU, C.L., DANYUSHEVSKY, L.V. & GILBERT, S. 2011. Minor and trace elements in bornite and associated Cu–(Fe)-sulfides:A LA-ICP-MS study Bornite mineral chemistry. *Geochimica et Cosmochimica Acta* **75**, 6473–6496.

ENAMI, M., CONG, B., YOSHIDA, H. & KAWABE, I. 1995. A mechanism for Na incorporation in garnet: an example from garnet in orthogneiss from the Su-Lu terrane, eastern China. *American Mineralogist* **80**, 475–482.

FERRIS, G.M., SCHWARZ, M.P. & HEITHERSAY, P. 2001. The Geological Framework, Distribution and Controls of IOCG mineralisation in the Gawler Craton, SA- Part 1: geological and tectonic framework. *In:* Porter T.M. ed. *Hydrothermal IOCG and related deposits: A Global Perspective*. PGC Publishing, Adelaide, **2**, 9–31.

FREEMAN, H. & TOMKINSON, M. 2011.Geological Setting of Iron Oxide Related Mineralisation in the Southern Mount Woods Domain, South Australia. *In:* Porter T.M. ed. *Hydrothermal Iron Oxide Copper-Gold and Related Deposits: A Global Perspective*. PGC Publishing, Adelaide, **3 & 4**, 171–190.

GASPAR, M., KNAACK, C., MEINERT, L.D. & MORETTI, R. 2008. REE in skarn systems: a LA-ICP-MS study of garnets from the Crown Jewel gold deposit. *Geochimica et Cosmochimica Acta* **72**, 185–205.

GREW, E.S., MARSH, J.H., YATES, M.G., LAZIC, B., ARMBRUSTER, T., LOCOCK, A., BELL, S.W., DYAR, M.D., BERNHARDT, H.J. & MEDENBACH, O. 2010. Menzerite-(Y), a new species, $\{(Y, REE)\ (Ca, Fe^{2+})_2\}[(Mg, Fe^{2+})(Fe^{3+}, Al)](Si_3)O_{12}$, from a felsic granulite, Parry Sound, Ontario, and a new garnet end-member, $Y_2Ca\}[Mg_2](Si_3)O_{12}$. *Canadian Mineralogist* **48**, 1171–1193.

GROVES, D.I., BIERLEIN, F.P., MEINERT, L.D. & HITZMAN, M.W. 2010. Iron Oxide Copper-Gold (IOCG) Deposits through Earth History: Implications for Origin, Lithospheric Setting, and Distinction from Other Epigenetic Iron Oxide Deposits. *Economic Geology* **105**, 641–654.

HAND, M., REID, A. & JAGODZINKI, L. 2007. Tectonic framework and evolution of the Gawler Craton, SA. *Economic Geology* **102**, 1377–1395.

HAYNES, D.W. 2000. Iron-oxide copper-gold deposits: Their position in the ore deposit spectrum and modes of origin. *In:* Porter, T.M. ed. *Hydrothermal iron oxide copper-*

*gold and related deposits a global perspectives*. Australian Mineral Foundation, Adelaide, 71–90.

HAYWARD, N. & SKIRROW, R.G. 2010. Geodynamic setting and controls on iron oxide Cu-Au (±U) ore in the Gawler Craton, South Australia. *In:* Porter, T.M. ed. *Hydrothermal Iron Oxide Copper-Gold & Related Deposits: A Global Perspective*. PGC Publishing, Adelaide, **3**, 1–27.

HITZMAN, M.W. 2000. Iron oxide-Cu-Au deposit: What, where, when, and why. *In:* Porter, T.M. ed. *Hydrothermal iron oxide copper-gold and related deposits a global perspective*. Australian Mineral Foundation, Adelaide, 9–26.

HITZMAN, M.W., ORESKES, N. & EINAUDI, M.T. 1992. Geological characteristics and tectonic setting of Proterozoic iron oxide (Cu-U-Au-REE) deposits. *Precambrian Research* **58**, 241–287.

ISMAIL, R., CIOBANU, C.L., COOK, N.J., GILES, D., SCHMIDT-MUMM, A., WADE, B. in press. Rare earths and other trace elements in minerals from skarn assemblages, Hillside iron oxide–copper–gold deposit, Yorke Peninsula, South Australia. *Lithos* doi.org/10.1016/j.lithos.2013.07.023.

JAFFE, H.W. 1951. The role of yttrium and other minor elements in the garnet group. *American Mineralogist* **36**, 133–155.

MCDONOUGH, W.F. & SUN, S.-S. 1995. The composition of the Earth. *Chemical Geology* **120**, 223–253.

MEINERT, L.D. 1992. Skarns and skarn deposits. *Geosciences Canada Reprint Series* **6**, 117–134.

PARKER, A.J. 1990. Gawler Craton and Stuart Shelf- regional geology and mineralisation. *In:* Hughes, F.E. ed. *Geology of the Mineral Deposits of Australia and Papua New Guinea.* The Australasian Institute of Mining and Metallurgy, Melbourne, 999–1008.

PARKER, A.J. 1990. Precambrian provinces of South Australia - tectonic setting. *In:* Hughes, F.E. ed. *Geology of the Mineral Deposits of Australia and Papua New Guinea.* The Australasian Institute of Mining and Metallurgy, Melbourne, 985-990.

PORTER, T.M. ed. 2000. Hydrothermal iron-oxide-copper-gold and related deposits. A global perspective. Australian Mineral Foundation, Adelaide, 349

PORTER, T.M. ed. 2002. Hydrothermal iron-oxide-copper-gold and related deposits: A global perspective. PGC Publishing, Adelaide, **2**, 367.

PORTER, T.M. ed. 2010. The Carrapateena Iron Oxide Copper Gold Deposit. In: Porter, T.M. ed. Hydrothermal iron-oxide-copper-gold and related deposits: A global perspective. *Advances in the understanding of IOCG Deposits*. PGC Publishing, Adelaide, **3–4**.

REID, A. J. & HAND, M. 2012. Mesoarchean to Mesoproterozoic evolution of the southern Gawler Craton, South Australia. Episodes **35**, 216–225.

REID, A. J., SWAIN, G. S. MASON, D., & MAAS, R. 2011. Nature and timing of Cu-Au-Zn-Pb mineralisation at Punt Hill, eastern Gawler Craton. *MESA Journal* **60**, 7–17.

SHORE, M., FOLWER, A.D., 1996. Oscillatory zoning in minerals: a common phenomenon. *Canadian Mineralogist* **34**, 1111–1126.

SKIRROW, R. 2008. Hematite-group" IOCG±U ore systems: tectonic settings, hydrothermal characteristics, and Cu-Au and U mineralising processes. *In:* Corriveau, L. & Mumin, A.H. eds. *Exploring for Iron Oxide Copper-gold Deposits: Canada and Global Analogues* Geological Association of Canada, Short Course Notes **20**, 39–57.

SKIRROW, R.G., BASTRAKOV, E.N., BAROVICH, K., FRASER, G.L., CREASER, R., FANNING, M.C., RAYMOND, O.L. & DAVIDSON, G.J. 2007. Timing of iron oxide Cu-Au-(U) hydrothermal activity and Nd isotope constraints on metal sources in the Gawler craton, South Australia. *Economic Geology* **102**, 1441–1470.

SKIRROW, R.G., RAYMOND, O.L., BASTRAKOV, E., DAVIDSON, G. & HEITHERSAY, P. 2002. The geological framework distribution and controls of Fe oxide Cu-Au mineralisation in the Gawler craton, SA. Part II. Alteration and mineralisation. *In*: Porter, T.M. ed. *Hydrothermal IOCG and related deposits: A global perspective*, Australian Mineral Foundation, Adelaide, **2**, 33–47.

SMITH, M.P., HENDERSON, P., JEFFRIES, T.E.R., LONG, J. & WILLIAMS, C.T. 2004. The rare earth elements and uranium in garnets from the Beinnan Dubhaich Aureole, Skye, Scotland, UK: constraints on processes in a dynamic hydrothermal system. *Journal of Petrology* **45**, 457–484.

SWAIN, G. 2013. Punt Hill Project 'Achievements & Challenges. Unpublished presentation, Australian Institute of Geoscientists, Adelaide Branch, June 2013.

VERKOUTEREN, J.R. & WYLIE, A.G. 2000. The tremolite-actinolite-ferro–actinolite series: Systematic relationships among cell parameters, composition, optical properties, and habit, and evidence of discontinuities. *American Mineralogist* **85**, 1239–1254.

YARDLEY, B.W.D., BANKS, D.A. & BARNICOAT, A.C. 2000. The chemistry of crustal brines: Tracking their origins. *In:* Porter, T.M. ed. *Hydrothermal iron-oxide-copper-gold and related deposits: A global perspective*, **1**, PGC Publishing, Adelaide, 61–70.

# APPENDIX A: METHODOLOGY

## Sample Suite

A total of 31 samples were collected from the Groundhog drill holes 1-7 (Table A-1). These samples are representative of calc-silicate skarn, metasediments and Gawler Range Volcanics from drill holes 9SAR and Groundhog 1-7, which intersects mineralization. Drill hole GH1 and GH6 show intersections of mineralization and massive calc-silicate skarn. The samples were set in epoxy resin and prepared as one-inch polished blocks and polished thin sections by Pontifex and Associates for mineralogical and petrographic analysis.

The polished blocks and thin sections were examined under a Nikon LV100 polarizing microscope (in transmitted/reflected light mode) and using a FEI Quanta 450 scanning electron microscope (SEM) with energy dispersive X-ray spectrometry and back-scattered electron (BSE) imaging capabilities (Adelaide Microscopy, University of Adelaide). BSE imaging was used to characterise mineral parageneses, assemblages, document significant textures, mineralogical relationships, as well as to identify inclusions of REE and incompatible distributions within iron oxides, calc-silicates and accessory minerals.

## Electron Microprobe Microanalysis

Calc-silicates which vary in composition (e.g. garnet) and accessory minerals in selected representative samples were analysed by Electron Probe Microanalyser (EPMA) to obtain quantitative major and minor element compositional data. The instrument used was a Cameca SX-Five electron probe microanalyser (Adelaide Microscopy, University of Adelaide) operated at an accelerating voltage of 20 kV and a

beam current of 20 nA. Standards, X-ray lines, count times and typical minimum detection limits (mdl) were as tabulated below (Table A- 1).

**Table A- 1: Electron Microprobe standards, X-ray lines, count times and typical minimum detection limits**

| Element | Standard | X-ray line | Count time (s) unknown/background | Average mdl (ppm) |
|---|---|---|---|---|
| Na | Albite | Na Kα | 20/10 | 120 |
| K | Sanadine | K Kα | 20/10 | 130 |
| Ca | Wollastonite | Ca Kα | 20/10 | 120 |
| Mn | Rhodonite | Mn Kα | 20/10 | 300 |
| Mg | Almandine | Mg Kα | 20/10 | 220 |
| Fe | Almandine | Fe Kα | 20/10 | 350 |
| Al | Almandine | Al Kα | 20/10 | 250 |
| Si | Almandine | Si Kα | 20/10 | 300 |
| Cr | Chromite | Cr Kα | 20/10 | 400 |
| Ti | Rutile | Ti Kα | 20/10 | 150 |
| F | Synthetic $CaF_2$ | F Kα | 30/15 | 300 |
| Cl | Tugtupite | Cl Kα | 30/15 | 200 |
| P | Apatite | P Kα | 20/10 | 200 |
| S | Marcasite | S Kα | 30/15 | 170 |
| As | GaAs | As Lα | 20/10 | 600 |
| Nb | Nb metal | Nb Lα | 20/10 | 360 |
| V | V metal | V Lα | 20/10 | 400 |
| Sr | Celestite | Sr Lα | 20/10 | 600 |
| Sc | Sc metal | Sc Kα | 20/10 | 180 |
| Zr | Synthetic zircon | Zr Lα | 20/10 | 325 |
| Hf | Zircon | Hf Lα | 20/10 | 740 |
| Ta | Ta metal | Ta Lα | 20/10 | 1025 |
| W | W metal | W Lα | 20/10 | 750 |
| Pb | Synthetic Pb-silicate | Pb Mß | 20/10 | 375 |
| Th | Huttonite | Th Mα | 20/10 | 1500 |
| U | $UO_2$ | U Mß | 20/10 | 360 |

## Laser-Ablation Inductively-Coupled Mass Spectrometry

Laser-Ablation Inductively-Coupled Mass Spectrometry (LA-ICP-MS) was used on selected samples to provide trace element concentrations in calc-silicate and accessory minerals (Figure 14**Error! Reference source not found.**).

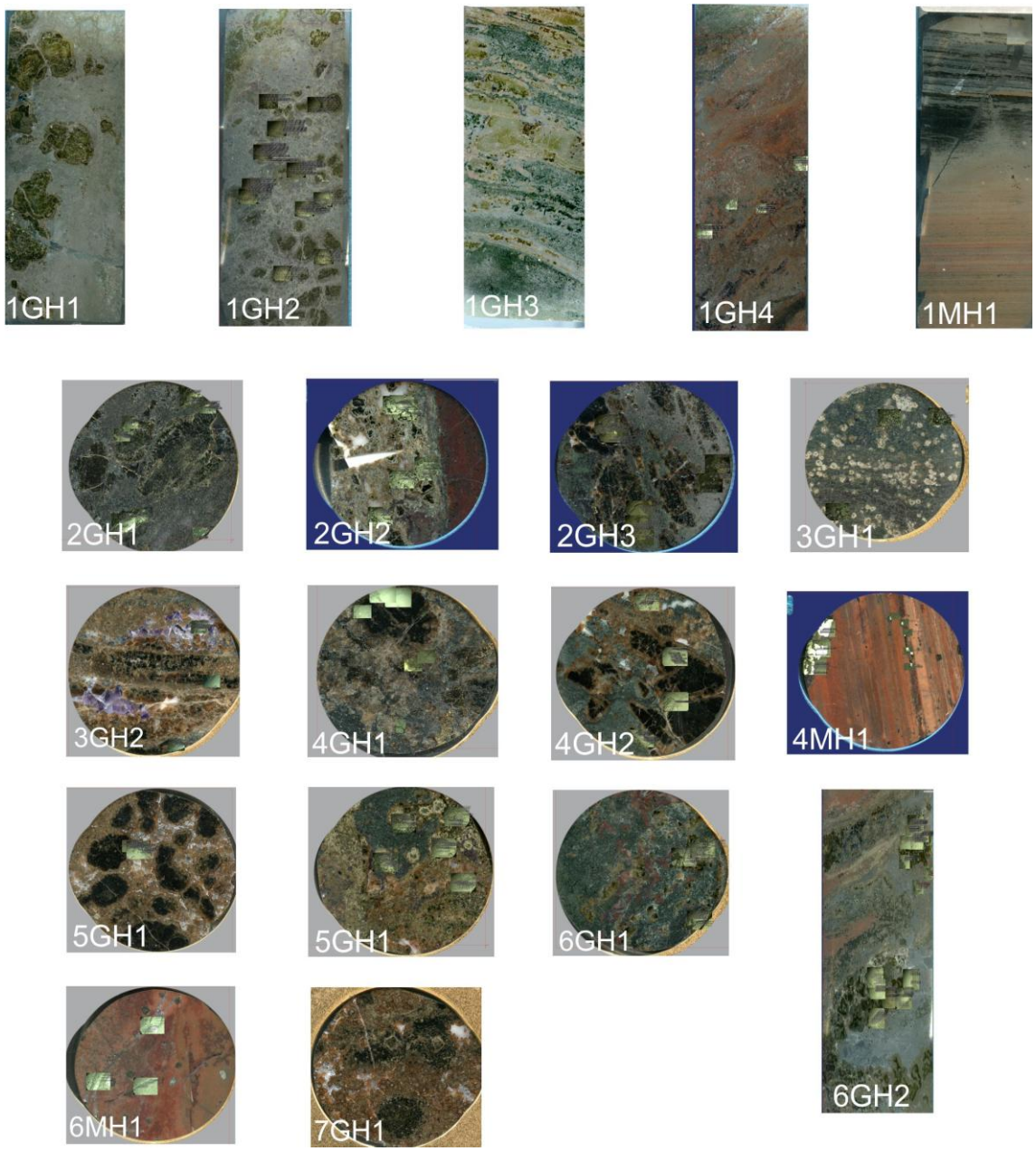


**Figure 14: All LA-ICP-MS samples from drillcores GHDD1, GHDD2, GHDD3, GHDD4, GHDD5, GHDD6 and GHDD7. Samples include skarn and marker horizon intervals**

LA-ICP-MS spot analysis was used to measure concentrations of REE and other trace elements. Spot analysis was performed on a Resonetics M-50-LR 193-nm Excimer laser microprobe coupled to an Agilent 7700cx Quadrupole ICP-MS, and housed at Adelaide Microscopy, University of Adelaide. The latter, new-generation laser system offers

excellent spatial resolution coupled with sub-ppm level sensitivity. In both cases, data reduction was performed using Glitter software (Van Achterbergh *et al.* 2001).

Spot analysis was made with a uniform spot size diameter of 12 µm. Both laser systems were operated at pulse rates of 5 Hz and power levels of 75-80% power level; laser energy was typically 6-9 J/cm$^{-2}$, giving an ablation rate of approx. 1.5µm/s$^{-1}$. The following basic set of isotopes were monitored: $^{23}$Na, $^{24}$Mg, $^{27}$Al, $^{29}$Si, $^{31}$P, $^{43}$Ca, $^{45}$Sc, $^{47}$Ti, $^{48}$Ti (or $^{49}$Ti), $^{51}$V, $^{53}$Cr, $^{55}$Mn, $^{57}$Fe, $^{58}$Fe, $^{59}$Co, $^{60}$Ni, $^{65}$Cu, $^{66}$Zn, $^{69}$Ga, $^{75}$As, $^{89}$Y, $^{90}$Zr, $^{93}$Nb, $^{95}$Mo, $^{118}$Sn, $^{139}$La, $^{140}$Ce, $^{141}$Pr, $^{146}$Nd, $^{147}$Sm, $^{153}$Eu, $^{157}$Gd, $^{159}$Tb, $^{163}$Dy, $^{165}$Ho, $^{166}$Er, $^{169}$Tm, $^{172}$Yb, $^{175}$Lu, $^{181}$Ta, $^{182}$W, $^{206}$Pb, $^{207}$Pb, $^{208}$Pb, $^{232}$Th and $^{238}$U. Analytical runs for feldspar also include a number of additional isotopes (e.g. $^{85}$Rb, $^{88}$Sr, $^{133}$Cs, $^{137}$Ba and $^{178}$Hf). Multiple isotopes of Fe and Ti were measured to test for data consistency. Analysis time for each spot analysis was a uniform 90 s, comprising a 30-s measurement of background (laser-off), and 60-s analysis of the unknown (laser-on). Standard reference materials were NIST-610 using coefficients given by Pearce *et al.* (1997) and Hawaiian basalt glass BHVO-1 (e.g. Flanagan 1976). Standards were run after each 10-15 unknowns; detection limits were calculated for each element in each spot analysis. Internal calibration was achieved using concentration values of Al (feldspar) or Ca (calcite, garnet, pyroxenes, amphiboles, titanite and apatite) obtained from electron probe microanalysis.

Data was chondrite-normalized using values given by Table A- 2 (values of McDonough & Sun 1995).

**Table A- 2: Chondrite values for rare earth elements (McDonough & Sun 1995)**

| | |
|---|---|
| $La_N$ | 0.237 |
| $Ce_N$ | 0.613 |
| $Pr_N$ | 0.093 |
| $Nd_N$ | 0.457 |
| $Sm_N$ | 0.148 |
| $Eu_N$ | 0.056 |
| $Gd_N$ | 0.199 |
| $Tb_N$ | 0.036 |
| $Dy_N$ | 0.246 |
| $Y_N$ | 1.57 |
| $Ho_N$ | 0.055 |
| $Er_N$ | 0.16 |
| $Tm_N$ | 0.025 |
| $Yb_N$ | 0.161 |
| $Lu_N$ | 0.0246 |

## LA-ICP-MS element mapping

LA-ICP-MS element mapping of an approximately 4 $mm^2$-sized area of sample GH101 was focussed on areas of zonation to obtain a visual image of trace element distribution within grains. LA-ICP-MS mapping was conducted using a Resonetics M-50-LR 193-nm Excimer laser microprobe coupled to an Agilent 7700cx Quadrupole ICP mass spectrometer. The M-50 instrument utilizes a two-volume small volume ablation cell (Laurin Technic Pty designed for excellent trace element sensitivity (e.g. Müller *et al.* 2009). Ablation was performed in an atmosphere of UHP He (0.7 l/min), and upon exiting the cell the aerosol cell is mixed with Ar (0.93 l/min) immediately after the ablation cell, after which the mix is passed through a pulse-homogenizing device or "squid" prior to direct introduction into the torch. The ICPMS was optimized daily to maximize sensitivity on isotopes of the mass range of interest, while keeping production of molecular oxide species (i.e. $^{232}Th^{16}O/^{232}Th$) and doubly charged ion species (i.e. $^{140}Ce^{2+}/^{140}Ce^{+}$) as low as possible, and usually <0.2%.

Imaging was performed by ablating sets of parallel line rasters in a grid across the sample. A beam size of 12 μm and a scan speed of 24 μm/s were chosen which resulted

in the desired sensitivity of elements of interest, and adequate spatial resolution for the study. The spacing between the lines was kept at a constant 12 μm to match the size of the laser beam used. The effect of reposition during mapping was minimized by pre-ablating each line prior to its main data collection run. A laser repetition of 10 Hz was selected at a constant energy output of 100mJ, resulting in an energy density of ~6 J/cm$^2$ at the target. Using these beam conditions depth of ablation during mapping was around 5-10 μm. A set of 21 elements were analyzed with dwell time for all masses set to 0.003 s, resulting in a total sweep time was ~0.07 s. A 30 second background acquisition was acquired at the start of every raster, and to allow for cell wash-out, gas stabilization, and computing processing, a delay of 15 s was used after each line. Identical rasters were done on USGS reference glasses NIST-610, BCR-2G and BHVO-2G (http://georem.mpch-mainz.gwdg.de/) at the start and end of a mapping run.

Element maps were compiled and processed using the program Iolite developed by the Melbourne Isotope Group at Melbourne University (e.g. Woodhead *et al.* 2007). Iolite is an open source software package for processing ICP-MS data, and is an add-in for the data analysis program Igor developed by WaveMetrics. A typical mapping run was analyzed over a 6-7 hour session, in which significant instrument drift could occur. To correct for this, standards were analyzed immediately before and after the run to assess drift and if present, was corrected for by applying a linear fit between the two sets of standards. Following this, for each raster and every element, the average background was subtracted from its corresponding raster, and the rasters were compiled into a 2-D image displaying combined background/drift corrected intensity for each element.

**Trace elements in garnet from Groundhog, S.A.**

## Whole rock geochemistry

Detailed geochemical data for drill core investigated in this project was supplied by Monax Mining Limited and DMITRE. Geochemical analysis has been undertaken periodically between 2007 and 2013 by Intertek Genalysis Laboratory Services, Adelaide.

The production of a homogeneous sub-sample, representative of the material submitted to the laboratory was undertaken using pulveriser vessels with quartz washes between samples, reducing the potential for contamination. Routine analysis of standards, blanks and duplicates were performed, with results reported to be within range of acceptable error. A combination of different analytical methodologies was used and is detailed in Table A- 3 below.

**Table A- 3: Whole rock geochemistry (DMITRE 2013)**

| Company | Element/s | Method |
|---|---|---|
| Monax | Au | 50g Lead collection fire assay. Analysed by Flame Atomic Absorption Spectrometry |
| Monax | Ag, Fe, S, Al, K, Sb, As, La, Sc, Ba, Li, Sn, Bi, Mg, Sr, Ca, Mn, Te, Cd, Mo, Ti, Ce, Na, Tl, Co, Ni, V, Cr, P, W, Cu, Pb, Zn | Multi-acid digest including Hydrofluoric, Nitric, Perchloric and Hydrochloric acids in Teflon Tubes. Analysed by Inductively Coupled Plasma Optical (Atomic) Emission Spectrometry |
| Monax | Ce, La, Th, U | Lithium metaborate/tetraborate fusion Analysed by Inductively Coupled Plasma Mass Spectrometry |
| DMITRE | Au, Pt, Pd | 25g Lead collection fire assay. Analysed by Inductively Coupled Plasma Mass Spectrometry |
| DMITRE | Cu, Ni, S, Li, Pb, Zn | Multi-acid digest including Hydrofluoric, Nitric, Perchloric and Hydrochloric acids in Teflon Tubes. Analysed by Inductively Coupled Plasma Optical (Atomic) Emission Spectrometry |
| DMITRE | Ag, As. Bi, Cd, Co, Cs, Ge, In, Mo, Nb, Re, Sb, Se, Te, Tl | Multi-acid digest including Hydrofluoric, Nitric, Perchloric and Hydrochloric acids in Teflon Tubes. Analysed by Inductively Coupled Plasma Mass Spectrometry |
| DMITRE | F | Carbonate Fusion |
| DMITRE | $Al_2O_3$, CaO, $Fe_2O_3$, $K_2O$, MgO, MnO, $Na_2O$, $P_2O_5$, $SiO_2$, $TiO_2$, V | Lithium metaborate/tetraborate fusion Analysed by Inductively Coupled Plasma Optical (Atomic) Emission Spectrometry |
| DMITRE | Ba, Be, Ce, Dy, Er, Eu, Ga, Hf, Ho, La, Lu, Nd, Pr, Rb, Sc, Sm, Sn, Sr, Ta, Tb, Th, Tm, U, W, Y, Yb, Zr | Lithium metaborate/tetraborate fusion Analysed by Inductively Coupled Plasma Mass Spectrometry |

## References

COOK, N.J., CIOBANU, C.L., MERIA, D., SILCOCK, D., WADE, B., 2013. Arsenopyrite-pyrite association in an orogenic gold ore: tracing mineralization history from textures and trace elements. *Economic Geology* **108**, 1273-1283.

MCDONOUGH, W.F. & SUN, S.-S. 1995. The composition of the Earth. *Chemical Geology* **120**, 223–253.

MULLER, W., SHELLEY, M., MILLER, P. & BROUDE, S. 2009 Initial performance metrics of a new custom-designed ArF excimer LA-ICPMS system coupled to a two-volume laser-ablation cell, *Journal of Analytical Atomic Spectrometry*, **24**, 209–214.

PEARCE N.J.G., PERKINS W.T., WESTGATE J.A., GORTON M.P., JACKSON S.E., NEAL C.R. & CHENERY S.P. 1997 A compilation of new and published major and trace element data for NIST SRM 610 and NIST SRM 612 glass reference material, *Geostandards Newsletter*, **21**, 115–144.

VAN ACHTERBERGH, E., RYAN, C.G., JACKSON, S.E. & GRIFFIN, W.L. 2001 LA-ICP-MS in the Earth Sciences - Appendix 3, data reduction software for LA-ICP-MS, in Sylvester, P.J., ed., *Mineralogical Association of Canada Short Course* **29**, 239-243.

WOODHEAD, J.D., HELLSTROM, J., HERGT, J.M., GREIG, A. & MAAS, R. 2007 Isotopic and elemental imaging of geological materials by laser ablation inductively coupled plasma-mass spectrometry, *Geostandards and Geoanalytical Research*, **31**, 331–343.

## APPENDIX B: PETROGRAPHY (THIN SECTIONS FROM GHDD1 AND GHDD6)

### Sample ID: (GHDD1 729.4-729.5 m)

*Gawler Range Volcanics*

| ***Composition*** | ***Percentage*** | ***Alteration*** |
|---|---|---|
| K- feldspar | 40 | Altered relic grains |
| Infill clay material | 40 | Highly altered |
| Hematite | 10 | altered |
| Quartz | 5 | Infill and veinlets |
| Sericite | 5 | Highly altered |

The sample showed non-layering, heavy alteration and cross cutting veinlets. Weak porphyritic textures are preserved in select lithic fragments. Small crystals of K-feldspar approximately 1mm, in size were observed and are heavily altered. K-feldspar is fine grained and observed within the matrix to having a broken/ mosaic like texture. Feldspar is a dominant mineral observed throughout the section and comprises around 40% of the sample as crystals and broken up mosaic like textures within the matrix. Fine grained, heavily altered clays infill and form the matrix together with the mosaic K-feldspar, comprising approximately 40% of the sample. Areas of replacement of hematite and sericite are disseminated throughout the matrix and appear significantly altered, comprising approximately 15% of the sample. A late stage quartz veinlet crosscutting through the sample contains minor quartz comprising around 5% of the sample.

### Sample ID: (GHDD1 730.3-760.4 m)

*Quartz-K-feldspar-chlorite veined metasediment*

| ***Composition*** | ***Percentage*** | ***Alteration*** |
|---|---|---|
| K- feldspar | 55 | Retrogressive alteration |
| Chlorite | 15 | Retrogressive alteration |
| Hematite | 5 | Retrogressive alteration |
| Quartz | 5 | infill |
| Calcite | 20 | Retrogressive infill |

The sample shows a large vein running through the middle of the section with alteration surrounding it. It is fine grained, heavily altered, with the least altered minerals located towards the edges of the sample, distal to the vein. The dominant mineral is K-feldspar which is altered and shows small grains approximately 0.5mm, intertwined with each other. Small amphibole grains are replaced by retrogressive chloritic and haematitic alteration, comprising approximately 20% and 10% of the sample respectively. The intensity of choritic and haematitic alteration increases closer to the vein. Calcite is present within small veinlets and proximal to the large vein. The large vein is coarse-grained and comprises dominantly of quartz, making up 5% of the sample. K-feldspar

crystals and quartz occupy the dominant space of the vein with lesser chlorite and hematite alteration. Hematite is also concentrated into small bands.

**Sample ID: (GHDD1 805.8-805.9 m)**
*Talc-garnet-actinolite skarn*

| *Composition* | *Percentage* | *Alteration* |
|---|---|---|
| Garnet | 20 | Metasomatic |
| Actinolite | 10 | Metasomatic |
| Talc | 45 | Retrogressive |
| Quartz | 5 | Metasomatic |
| Calcite | 5 | Metasomatic |
| Ore Minerals | 15 | Retrogressive |

| *Mineralization* | *Relative to abundance* | *Relative to sample* |
|---|---|---|
| Chalcocite | 40 | 5 |
| Bornite | 10 | 2 |
| Chalcopyrite | 10 | 1 |
| Wittichenite | 5 | 1 |
| Sphalerite | 20 | 2 |
| Galena | 5 | 1 |
| Hematite | 10 | 2 |

The sample is relatively fine grained, inequigranular with porphyroblastic garnets showing metasomatic alteration with a retrogressive overprint. Stubby, tabular talc (relic forsterite or pyroxene) intergrown with quartz, dominantly comprises the matrix along with lesser actinolite. Garnets are coarse (approximately 1cm in size) and porphyroblastic comprising 20% of the sample. They are brown to yellow in colour, anisotropic and display features of oscillatory growth zoning between grossular and andradite end members. Darker areas of the garnet are andradite-rich and lighter areas are more grossular-rich. There is another generation of overgrowth garnet which is unzoned and rims grossular-andradite core. Unzoned garnet is brecciated and fractured, also present within the sample, showing poikiloblastic inclusions of talc, quartz and accessories. Accessory inclusions are small (approximately 2 microns in length) and consist of titanite and apatite grains. Quartz is intergrown with the talc, as poikiloblastic grains scattered throughout the matrix and minor late veinlets crosscutting garnets. Similarly, calcite is within the matrix, infilling between grains and as veinlets cross cutting garnet.
The sample contains mineralization dominantly as copper sulphides with lesser base metal sulphides and iron oxides disseminated throughout the sample. Mineralization is concentrated within late cross cutting veinlets. Chalcocite is the dominant ore mineral found within the sample. It shows an irregular patchy texture and contains inclusions of wittichenite, chalcopyrite and bornite. It is mostly found within crosscutting quartz and calcite veins or within vuggy infilled areas. Chalcocite also shows rare intergrowths with bornite as symplectites. Bornite is found disseminated in the matrix but is more commonly found as inclusions within chalcocite. Wittichenite is bright white in colour and seen in sparse amounts as micron long inclusions within chalcocite. It contains a rim of alteration around the irregularly shaped inclusions. Sphalerite is the second most dominant ore mineral throughout the sample. It is found as larger grains (approximately 500 microns in length) and contains inclusions of galena. Hematite is less commonly

found within the sample, appearing disseminated throughout the matrix of the sample and as rare inclusions within the garnet grains.

**Sample ID: (GHDD1 808.9-809.0 m)**
*'Marker horizon' K-feldspar-hematite rock*

| ***Composition*** | ***Percentage*** | ***Alteration*** |
|---|---|---|
| Calcite | 50 | Infill and Metasomatic |
| K-feldspar | 20 | Metasomatic |
| Hematite | 20 | Retrogressive |
| Actinolite | 5 | Retrogressive |
| Garnet | 10 | Metasomatic |
| Quartz | 5 | Metasomatic |

The sample shows a lighter banded, calcite- rich half and a darker banded half, which is K-feldspar, hematite-rich. Green banded areas within the light half sample are composed of fine-grained anhedral K-feldspar crystals and actinolite. A rare case of a coarse garnet porphyroblast is seen scattered in the matrix, containing a brecciated and fractured texture. Minor quartz and calcite infill is between garnet. The remaining matrix of the light half of the sample consists of approximately 50% calcite which is fine grained. Hematite needles irregularly scatter through the veinlets. The darker half of the sample is rich in hematite and K-feldspar. K-feldspar is approximately 20% of the sample with most of it within the dark half as patches of fine-grained anhedral crystals. Hematite makes up approximately 20% of the total sample, with most dominant in the dark half of the sample. Patches of rhodonite were observed using SEM techniques and were difficult to distinguish in the thin section, however, they were concentrated within the darker band of the sample. Accessory minerals found throughout the sample consisted dominantly of zircon and lesser apatite.

**Sample ID: (GHDD1 839.7-839.8 m)**
*'Marker horizon' K-feldspar rock*

| ***Composition*** | ***Percentage*** | ***Alteration*** |
|---|---|---|
| Garnet | 60 | Metasomatic |
| Calcite | 30 | Retrogressive |
| Ore minerals | 10 | Retrogressive |

| ***Mineralization*** | ***Relative to abundance*** |
|---|---|
| Chalcocite | 5 |
| Hematite | 5 |
| Chalcopyrite | 20 |
| Pyrite | 5 |
| Sphalerite | 60 |
| Galena | 5 |

The sample has undergone metasomatic alteration and overprinting. It dominantly comprises of coarse-grained garnet porphyroblasts approximately 1mm in size, making up 60% of the total sample. Garnet shows the typical andradite and grossular oscillatory zoning with overgrowths of later generation garnets. Poikilitic inclusions are present within the grains, concentrated towards the centre of the grains. These inclusions are very small, approximately 3-4 microns in length and are difficult to distinguish, appearing as accessory phases- titanite and apatite and pyroxenes. Medium grained

calcite is abundant throughout, comprising approximately 30% of the sample. It is seen occurring as a later infill between grains of garnet and fine-grained replacement (pseudomorphism) of other grains seen enclosed within garnet.
Chalcocite, elongated, light-bluish coloured grains (approximately 500 microns in length) are scattered throughout the sample, making up approximately 10% abundance of the total sulphides. Bornite was absent in the sample. Medium-coarse chalcopyrite was seen in close proximity to the calcite infill near the grains of garnet. Sphalerite is adjacent to chalcopyrite, between grains of garnet. Inclusions of galena are present within the sphalerite. Late stage formed hematite as bladed growths are scattered throughout the matrix.

**Sample ID: (GHDD1 853.9-854.0 m)**
*Mineralised garnet-calcite skarn*

| ***Composition*** | ***Percentage*** | ***Alteration*** |
|---|---|---|
| Garnet | 40 | Metasomatic |
| Calcite | 20 | Retrogressive/infill |
| K-feldspar | 5 | Metasomatic |
| Ore minerals | 35 | Retrogressive |

| ***Mineralization*** | ***Relative to abundance*** |
|---|---|
| Chalcocite | 5 |
| Hematite | 10 |
| Chalcopyrite | 40 |
| Sphalerite | 30 |
| Galena | 5 |
| Wittichenite | 5 |
| Bornite | 5 |

This sample is heavily altered (metasomatically), showing overprinting and abundant mineralization. Garnet is the dominant mineral with abundant ore minerals. Garnets appear porphyroblastic, coarse-grained with some showing a euhedral crystal shape. There is strong oscillatory zoning present between the andradite and grossular end members. Garnet contains inclusions of sulphides and also accessories such as apatite. K-feldspar is a lesser component of the sample, making up approximately 5% as patches of anhedral fine-grained crystals. Calcite is abundant within the sample comprising approximately 20% as infilling aggregates between grains of garnet, in particular grains, which are brecciated and fractured. It is also represented pseudomorphing relic grains of elongated blocky-like crystals.
Significant mineralization is present within the sample, with the dominant sulphide, chalcopyrite comprising approximately 40%. Chalcopyrite is coarse-grained and infills around grains of garnet. Course-grained sphalerite is the second dominant sulphide present within the sample, making up approximately 30% of the sample, infilling between garnet grains. It is also seen as islands within chalcopyrite. Galena is present as infill adjacent to garnet grains and also present as inclusions within the sphalerite. Garnet grains also contain inclusions of sulphides, approximately 3-5 microns in length, including chalcopyrite, chalcocite and bornite. Bornite contains inclusions of a bright white coloured mineral known as wittichenite. Fine-grained bornite and chalcocite are also present within the garnet grains as inclusions within the infilled quartz and calcite vuggy areas.

**Trace elements in garnet from Groundhog, S.A.**

**Sample ID: (GHDD1 857.8-857.9 m)**
*Mineralised-calcite-chlorite skarn*

| *Composition* | *Percentage* | *Alteration* |
|---|---|---|
| Calcite | 70 | Retrogressive |
| Chlorite | 25 | Retrogressive |
| Ore minerals | 10 | Retrogressive |

| *Mineralization* | *Relative to abundance* |
|---|---|
| Chalcocite | 8 |
| Hematite | 10 |
| Chalcopyrite | 10 |
| Silver | 2 |
| Bornite | 70 |

This sample is extremely fine-grained, with a significant retrogressive overprint. It predominantly comprises of calcite, making up approximately 65% of the sample. Calcite alteration is fine-grained and pseudomorphs earlier-formed minerals (pyroxenes). Retrograde stage chloritic alteration is abundant throughout the sample bundled together in radial growths.
The dominant sulphide present within the sample is bornite, which is coarse-grained and irregular. Bornite contains inclusions of bright white hematite, which is stubby-like in nature and scattered irregularly through the grains. A later generation of hematite is also observed throughout the calcite matrix which appears disoriented and needle-like in nature. Less dominant sulphides within the sample are coarse chalcocite and irregular chalcopyrite disseminated throughout the matrix. Very few grains of native silver are spotted near bornite.

**Sample ID: (GHDD1 857.8-857.9 m)**
*'Marker horizon' K-feldspar-chlorite metasediment*

| *Composition* | *Percentage* | *Alteration* |
|---|---|---|
| K-feldspar | 60 | Metasomatic |
| Chlorite | 10 | Retrogressive |
| Quartz | 5 | Metasomatic |
| Calcite | 10 | Metasomatic |
| Fluorite | 5 | overprint |
| Ore minerals | 10 | overprint |

| *Mineralization* | *Relative to abundance* |
|---|---|
| Chalcocite | 5 |
| Bornite | 15 |
| Chalcopyrite | 20 |
| Pyrite | 5 |
| Galena | 10 |
| Sphalerite | 35 |
| Hematite | 10 |

This sample is representative of the marker horizon band, consisting of a fine-grained, laminated sedimentary texture. It shows fracturing and overprinting. The dominant mineral within the sample is K-feldspar, comprising approximately 60% of the matrix. K-feldspar is fine-grained and forms a regular banding pattern. Chlorite forms as fine-

grained aggregates clumped together within bands, dominating the darker green banded areas within the sample, making up approximately 10%. Quartz is a minor component (5%) scattered through bands with the feldspar. Fluorite cross-cuts the fabric and contains remobilised sulphides. Sulphides within the fluorite are dominantly sphalerite and chalcopyrite; however, brighter white sulphides present are likely to be a part of the tetrahedrite-tennantite series. Less dominant sulphides are chalcopyrite, bornite, chalcocite and hematite. Hematite is also present within the darker bands as brown flakes disseminated throughout.

**Sample ID: (GHDD1 847.8-847.09 m)**
*Mineralized-hematite skarn*

| ***Composition*** | ***Percentage*** | ***Alteration*** |
|---|---|---|
| Garnet | 60 | Metasomatic |
| Calcite | 30 | Retrogressive |
| Actinolite | 5 | Retrogressive/metasomatic |
| Ore minerals | 5 | Retrogressive |

Two types of garnet present-

1. Grossular-andradite oscillatory zoned cores (porphyroblastic) with a late stage outer growth rim which is unzoned (30% of the total sample)
2. Unzoned/undifferentiated garnet which forms small euhedral crystals (30% of the total sample)

Calcite is the second dominant mineral, forming fine-grained anhedral grains, cementing between garnet grains and in between brecciated and fractured areas. Late-formed actinolite is present around grains of garnet.
No sulphides/mineralization are present within the sample, however, minor dissemination of hematite is present throughout the sample.

**Sample ID: (GHDD1 889.9-890.0 m)**
*Mineralised garnet-carbonate skarn*

| ***Composition*** | ***Percentage*** | ***Alteration*** |
|---|---|---|
| Calcite | 30 | Recrystallisation |
| Quartz | 10 | Recrystallisation |
| Garnet | 40 | Metasomatic |
| Chlorite | 5 | Retrogressive |
| Ore minerals | 15 | Metasomatic |

| ***Mineralization*** | ***Relative to abundance*** |
|---|---|
| Chalcopyrite | 50 |
| Pyrite | 5 |
| Galena | 5 |
| Sphalerite | 30 |
| Hematite | 10 |

This sample is a microgranular calc-sillicate sedimentary rock comprising of coarse replacement within bands. The matrix of the rock comprises of small, fine-grained anhedral calcite grains, scattered throughout, approximately <0.5mm in size. The matrix is uniform and likely a representative of the original host rock. Two types of garnets are present in the sample

**Trace elements in garnet from Groundhog, S.A.**

1. A coarse porphyroblastic euhedal type of garnet, which is approximately 3mm in size and isotropic in nature.
2. The other type of garnet is approximately 0.2mm in size, unzoned and rims the andradite-grossular porphyroblasts suggesting a later formed generation.

Garnets show evidence of brecciation and fracturing, dominantly in the outer rim of unzoned garnet. Small euhedral crystals and aggregates of the unzoned garnet are seen scattered throughout the matrix in close proximity to the porphyroblastic zoned garnet cores. They are likely to have formed during the same generation as the outer rim of garnet, which is similarly brecciated, and also unzoned. Minor chlorite is present in the sample showing partial replacement within garnet.
The dominant sulphide present is chalcopyrite, showing typical triangular textures suggesting it infilled between earlier formed grains. Chalcopyrite also forms islands within quartz, sphalerite and hematite. Small inclusions of pyrite are present within chalcopyrite and are blocky in nature. The second dominant mineral is sphalerite, which also depicts diagnostic infilling textures between garnet and chalcopyrite. Galena consists as inclusions within sphalerite and between garnet grains. Hematite appears as larger crystals which have a texture that is ragged. Larger aggregates are brecciated and fractured.
Paragenesis:
1) Host/ primary rock- calc-sillicate formation with abundant calcite and some minor silica
2) Recrystallization of the primary host as a result of diagenesis resulting in fine-grained massive and regular calcite + quartz.
3) Garnet and sulphide alteration due to metasomatism- infiltration of a fluid rich in sulphur + metals caused precipitation of sulphides and zoned garnets nucleating from triple points on the carbonates.

**Sample ID: (GHDD1 952-952.1 m)**
*Mineralised- actinolite- clinopyroxene skarn*

| *Composition* | *Mineralization* | *Percentage* | *Relative to abundance* | *Alteration* |
|---|---|---|---|---|
| Actinolite | Chalcopyrite | 50 | 50 | Metasomatic |
| Clinopyroxene | Pyrite | 5 | 5 | Metasomatic |
| K-feldspar | Galena | 10 | 5 | Metasomatic |
| Fluorite | Hematite | 5 | 30 | Metasomatic |
| Quartz | | 5 | | Metasomatic |
| Chlorite | | 5 | | Metasomatic |
| Apatite | | 5 | | Metasomatic |
| Ore Minerals | | 10 | | Metasomatic |
| Titanite | | 5 | | Metasomatic |

The sample is irregular in nature, showing metasomatic replacement textures with little preservation of original minerals and textures. The most dominant mineral within this sample is amphibole (actinolite) comprising 50% of the total and is relatively coarse grained (5 mm in length approximately). K-feldspar is the second dominant present as subhedral crystals approximately 1mm in size. It is concentrated within coarse-grained aggregates and intergrown with amphiboles, sulphides and iron-oxides. Lesser

clinopyroxene is present as small elongated, euhedral prisms approximately 3 mm in size. Trace amounts of isotropic fluorite are present as anhedral grains intergrown with sulphides and amphiboles. Chlorite is present as very fine-grained flakes scattered throughout the matrix comprising around 5%. Very little quartz is present throughout the sample and is only observed intergrown with later formed sulphides. Accessory phase minerals present within the sample consist of apatite and titanite, intergrown within amphiboles and K-feldspar.
Sulphides present within the sample form intergrown aggregates. Chalcopyrite is the most dominant sulphide, comprising 50% of the opaques within the sample, it is coarse-grained and ragged-in nsture, forming in patches of approximately 6 mm. Hematite is the second common opaque mineral intergrown with galena in chalcopyrite. Lesser fine-grained pyrite is seen within chalcopyrite and comprises approximately 5% of opaque minerals within the sample.

**Sample ID: (GHDD1 958.30-958.3 m)**
*Biotite-talc-actinolite rock*

| ***Composition*** | ***Percentage*** | ***Alteration*** |
|---|---|---|
| Biotite | 60 | Metasomatic |
| Talc | 20 | Retrogressive |
| Actinolite | 5 | Metasomatic |
| Fluorite | 5 | Metasomatic |
| Calcite | 5 | Metasomatic |
| Apatite | 5 | Metasomatic |
| Ore minerals | 5 | Retrogressive |

The sample is fine-grained, showing metasomatic alteration with a retrogressive overprint. Biotite is the dominant mineral within the sample comprising up to 60%. It forms fine-grained flakes, which are approximately 10 microns in size and disoriented. Small pyroxene grains approximately 0.3 mm in length are present concentrated as small aggregates. A significant portion of the pyroxene has been altered to fine-grained talc, which is abundant throughout the sample. Grains of calcite are present between pyroxenes and show significant alteration. Less dominant minerals present are fluorite, actinolite and apatite, which are disseminated throughout the sample.
Hematite is the only opaque mineral disseminated throughout the sample and appears retrogressed.

**Sample ID: (GHDD6 923.2-923.3 m)**
*Mineralized-garnet- feldspar-calcite skarn*

| ***Composition*** | ***Percentage*** | ***Alteration*** |
|---|---|---|
| Garnet | 30 | Alteration |
| K-feldspar | 15 | Alteration |
| Calcite | 15 | Alteration |
| Actinolite | 10 | Alteration |
| Chlorite | 10 | Alteration |
| Titanite | 5 | Alteration |
| Ore minerals | 15 | Infill |

**Trace elements in garnet from Groundhog, S.A.**

| *Mineralization* | *Relative to abundance* |
|---|---|
| Chalcopyrite | 60 |
| Pyrite | 5 |
| Galena | 5 |
| Sphalerite | 20 |
| Hematite | 10 |

The sample contains two types of banding :

1. K-feldspar-chloritic rich (retrogressive) with a sulphide overprint
2. Garnet-calcite rich with a later retrogressive chlorite and sulphide overprint.

The pink feldspathic bands are fine-grained comprising of K-feldspar aggregates that form an altered mosaic texture. Chlorite is present as aggregates scattered throughout the pinkish bands. Alteration garnets are formed near the edge of the feldspathic bands, which are isotropic, small and relatively fine-grained in nature. Accessory minerals present are small-scattered grains of titanite within the feldspathic bands. The garnet-calcite bands are coarse-grained and show larger, anisotropic subhedral grains of garnet that are zoned. Relic cavities are infilled with calcite grains and smaller inclusions of fine-grained unzoned garnets. Aggregates of fine-grained chlorite and actinolite are present scattered throughout garnet bands.

Sulphides are present within both bands as overprinting and infilling textures. The dominant sulphide present within the sample is chalcopyrite which is coarse-grained and contains inclusions of sphalerite, pyrite and galena. Chalcopyrite is also present as aggregates within feldspathic bands. Hematite occurs as minor flakes and coarser aggregates within both bands.

**Trace elements in garnet from Groundhog, S.A.**

## APPENDIX C: SUMMARY LA-ICP-MS RESULTS

**Table A- 4** :Summary of LA-ICP-MS trace element data for garnet (ppm)

| | Mg | Al | P | Sc | Ti | V | Cr | Mn | Co | Ni | Cu | Zn | Ga | As | Rb | Sr | Zr | Nb | Mo | Sn | Sb | Cs | Hf | Ta | W |
|---|---|---|---|---|---|---|---|---|---|---|---|---|---|---|---|---|---|---|---|---|---|---|---|---|---|
| **1GH1 BRIGHT** | | | | | | | | | | | | | | | | | | | | | | | | | |
| Min | 80 | 13 | 10 | 0.57 | 3.1 | 0.3 | 0.73 | 3677 | 17 | 0.95 | 0.38 | 0.2 | 1.3 | 1.6 | 423 | 0.14 | 0.01 | 0.03 | 0.02 | 0.57 | 3.1 | 0.08 | <0 | 0.01 | 846 |
| Max | 592 | 5436 | 79 | 1.6 | 428 | 12 | 4.4 | 4370 | 1581 | 1.4 | 77 | 1.5 | 7.2 | 18 | 1261 | 0.19 | 7.8 | 14 | 1.5 | 2.7 | 92 | 0.1 | 0.22 | 0.12 | 523 |
| **Mean(11)** | 292 | 658 | 39 | 0.99 | 46 | 2.8 | 1.4 | 3965 | 1352 | 1.2 | 7.5 | 0.51 | 4 | 4.3 | 904 | 0.17 | 0.99 | 1.3 | 0.17 | 1.2 | 14 | 0.09 | 0.07 | 0.03 | 221 |
| S.D. | 189 | 1597 | 19 | 0.29 | 127 | 3.2 | 1.2 | 237 | 444 | 0.12 | 23 | 0.44 | 1.9 | 4.8 | 306 | 0.02 | 2.3 | 4.1 | 0.43 | 0.59 | 26 | <0 | 0.06 | 0.04 | 0.05 |
| **1GH1 DARK** | | | | | | | | | | | | | | | | | | | | | | | | | |
| Min | 148 | 138 | 7.5 | 0.65 | 9.6 | 0.75 | 0.97 | 4032 | 866 | 0.76 | 0.4 | 0.3 | 1.4 | 2.2 | 1.9 | 0.15 | 0.26 | 0.1 | 0.05 | 0.14 | 2.9 | 0.09 | 0.06 | 0.02 | 218 |
| Max | 1049 | 59506 | 476 | 9 | 4111 | 304 | 24 | 10739 | 1570 | 27 | 0.85 | 7.9 | 10 | 29 | 649 | 0.19 | 350 | 142 | 46 | 1.8 | 70 | 0.13 | 3.4 | 2.8 | 94 |
| **Mean (8)** | 533 | 41373 | 124 | 4.7 | 2318 | 123 | 11 | 6661 | 1061 | 4.3 | 0.61 | 1.5 | 4.5 | 12 | 167 | 0.18 | 138 | 53 | 17 | 0.54 | 24 | 0.1 | 1.7 | 0.91 | 81 |
| S.D. | 264 | 18671 | 174 | 2.7 | 1656 | 97 | 7.3 | 2186 | 232 | 9.1 | 0.12 | 2.6 | 2.7 | 10 | 209 | 0.02 | 107 | 46 | 14 | 0.52 | 21 | 0.01 | 1.2 | 0.9 | <0 |
| **1GH1 RIM** | | | | | | | | | | | | | | | | | | | | | | | | | |
| Min | 249 | 45085 | 5.8 | 2.5 | 527 | 57 | 4.4 | 6993 | 0.28 | 0.51 | 0.33 | 0.35 | 1.4 | 1.5 | 0.02 | <0 | 23 | 4.7 | <0 | 0.13 | 0.1 | <0 | 1.1 | 0.17 | 5.7 |
| Max | 3125 | 62895 | 30 | 14 | 4483 | 506 | 83 | 10945 | 1047 | 23 | 7.4 | 68 | 35 | 36 | 2.1 | 5.4 | 262 | 55 | 26 | 50 | 37 | 0.28 | 3.9 | 1.8 | 0.19 |
| **Mean (59)** | 479 | 53195 | 11 | 7.9 | 2939 | 285 | 34 | 8415 | 114 | 1.7 | 0.87 | 3.9 | 27 | 5.7 | 0.27 | 0.39 | 60 | 18 | 1.8 | 30 | 4 | 0.04 | 2.5 | 0.76 | 0.73 |
| STDV | 372 | 4792 | 4.2 | 3.2 | 1084 | 131 | 20 | 801 | 313 | 3.7 | 1.1 | 9.6 | 9.1 | 9.5 | 0.5 | 0.97 | 58 | 11 | 4.8 | 13 | 11 | 0.04 | 0.72 | 0.39 | 40 |
| **1GH2 BRIGHT** | | | | | | | | | | | | | | | | | | | | | | | | | |
| Min | 68 | 11 | 9.7 | 0.47 | 2.3 | 0.09 | 1.5 | 3098 | 0.53 | 0.27 | 0.09 | 0.52 | 1.5 | 241 | 0.02 | 0.09 | 0.01 | 0.01 | 0.31 | 2.2 | 0.07 | <0 | 0.01 | <0 | 1010 |
| Max | 831 | 27603 | 167 | 2.6 | 452 | 20 | 5.7 | 4525 | 2.3 | 1.9 | 10 | 12 | 32 | 1095 | 0.33 | 1.1 | 11 | 2.9 | 2.8 | 295 | 3.9 | 0.31 | 0.23 | 0.15 | 548 |
| **Mean (78)** | 294 | 1330 | 42 | 0.98 | 21 | 2.5 | 3.5 | 3608 | 1.1 | 0.55 | 0.52 | 3 | 13 | 668 | 0.06 | 0.37 | 0.55 | 0.15 | 1.2 | 83 | 0.54 | 0.02 | 0.04 | 0.01 | 246 |
| S.D. | 153 | 3622 | 25 | 0.33 | 55 | 3.2 | 1 | 246 | 0.3 | 0.23 | 1.1 | 2 | 7.3 | 244 | 0.04 | 0.19 | 1.4 | 0.4 | 0.46 | 69 | 0.6 | 0.03 | 0.03 | 0.02 | 0.06 |
| **1GH2 DARK** | | | | | | | | | | | | | | | | | | | | | | | | | |
| Min | 283 | 52 | 5.7 | 1 | 9.1 | 0.95 | 2.7 | 3666 | 0.36 | 0.41 | 0.29 | 0.45 | 1.9 | 1.5 | 0.04 | 0.01 | 0.03 | 0.01 | 0.05 | 23 | 0.08 | 0.01 | <0 | <0 | 687 |
| Max | 10099 | 72792 | 1001 | 21 | 7081 | 489 | 183 | 12276 | 10 | 12 | 1 | 87 | 36 | 592 | 5.9 | 14 | 136 | 55 | 1.4 | 241 | 2 | 2.3 | 5.6 | 2.1 | 14 |
| **Mean(104)** | 899 | 63176 | 21 | 8.8 | 4307 | 211 | 50 | 8303 | 1.1 | 1 | 0.66 | 4.7 | 25 | 14 | 0.31 | 0.63 | 66 | 29 | 0.26 | 53 | 0.21 | 0.12 | 2.7 | 0.97 | 68 |
| S.D. | 1416 | 9430 | 97 | 5.2 | 1492 | 111 | 50 | 948 | 1.7 | 1.2 | 0.14 | 13 | 4.8 | 58 | 0.89 | 2.1 | 34 | 15 | 0.16 | 33 | 0.26 | 0.31 | 1.2 | 0.48 | 0.08 |
| **1GH2 RIM** | | | | | | | | | | | | | | | | | | | | | | | | | |
| Min | 289 | 49199 | 5.7 | 3.2 | 1323 | 47 | 13 | 6903 | 0.47 | 0.63 | 0.43 | 0.61 | 21 | 1.4 | 0.05 | 0.02 | 14 | 6.8 | 0.06 | 22 | 0.07 | 0.01 | 0.58 | 0.16 | 18 |
| Max | 4278 | 68642 | 14 | 18 | 5365 | 580 | 139 | 10018 | 7.1 | 8.1 | 48 | 55 | 35 | 25 | 3 | 40 | 95 | 43 | 0.45 | 116 | 4.1 | 1.7 | 3.8 | 1.2 | 1.6 |
| **Mean(20)** | 941 | 58098 | 8.2 | 8.1 | 3329 | 232 | 35 | 8536 | 1.2 | 1.6 | 3.5 | 6 | 28 | 4.3 | 0.35 | 2.5 | 41 | 18 | 0.25 | 38 | 0.35 | 0.16 | 2 | 0.77 | 4 |
| S.D. | 1116 | 6355 | 2.3 | 4.3 | 783 | 160 | 29 | 778 | 1.5 | 1.8 | 11 | 12 | 3.4 | 5.7 | 0.69 | 9 | 17 | 7.9 | 0.11 | 20 | 0.87 | 0.4 | 0.86 | 0.32 | 374 |

## Trace elements in garnet from Groundhog, S.A.

**Table A- 4 :Summary of LA-ICP-MS trace element data for garnet (ppm) (continued)**

| | Mg | Al | P | Sc | Ti | V | Cr | Mn | Co | Ni | Cu | Zn | Ga | As | Rb | Sr | Zr | Nb | Mo | Sn | Sb | Cs | Hf | Ta | W |
|---|---|---|---|---|---|---|---|---|---|---|---|---|---|---|---|---|---|---|---|---|---|---|---|---|---|
| **1GH3 BRIGHT** | | | | | | | | | | | | | | | | | | | | | | | | | |
| Min | 9685 | 81 | 26 | 0.52 | 5.7 | 0.18 | 0.65 | 3957 | 1171 | 1.2 | 0.4 | 0.18 | 1.6 | 4.7 | 427 | 0.12 | <0 | 0.05 | 0.02 | 1.2 | 10 | 0.06 | <0 | 0.01 | 720 |
| Max | 15798 | 17516 | 51 | 0.89 | 103 | 14 | 161 | 4466 | 1417 | 2.4 | 252 | 9.5 | 15335 | 22 | 713 | 0.21 | 12 | 8.2 | 0.41 | 3.4 | 43 | 0.1 | 0.21 | 0.03 | 552 |
| **Mean(5)** | 14575 | 3732 | 42 | 0.74 | 34 | 4.2 | 33 | 4233 | 1344 | 1.6 | 51 | 2.2 | 3069 | 8.8 | 576 | 0.14 | 2.8 | 2.4 | 0.13 | 2.3 | 21 | 0.08 | 0.09 | 0.02 | 157 |
| S.D. | 2734 | 7707 | 10 | 0.15 | 40 | 5.5 | 72 | 227 | 99 | 0.47 | 112 | 4.1 | 6857 | 7.6 | 102 | 0.04 | 5.2 | 3.5 | 0.16 | 0.99 | 13 | 0.01 | 0.09 | 0.01 | 0.1 |
| **1GH3 DARK** | | | | | | | | | | | | | | | | | | | | | | | | | |
| Min | 2067 | 24852 | 7.4 | 0.86 | 28 | 12 | 0.71 | 4570 | 834 | 0.65 | 0.92 | 0.43 | 0.77 | 7.2 | 4.2 | 0.14 | 2.2 | 1.4 | 0.17 | 0.07 | 23 | 0.08 | 0.08 | 0.01 | 131 |
| Max | 7538 | 54973 | 22 | 30 | 5927 | 331 | 180 | 7840 | 1160 | 0.94 | 3 | 1.2 | 2.6 | 25 | 128 | 0.75 | 397 | 108 | 24 | 0.52 | 46 | 0.78 | 5.9 | 2.1 | 22 |
| **Mean(6)** | 3583 | 47710 | 12 | 21 | 3981 | 232 | 95 | 6848 | 909 | 0.82 | 2 | 0.68 | 1.7 | 21 | 32 | 0.42 | 216 | 63 | 16 | 0.21 | 32 | 0.23 | 3.7 | 1.4 | 53 |
| S.D. | 2096 | 11335 | 6.4 | 11 | 2153 | 116 | 67 | 1199 | 124 | 0.11 | 0.81 | 0.26 | 0.71 | 7 | 48 | 0.23 | 132 | 35 | 8.2 | 0.17 | 8.2 | 0.27 | 2.2 | 0.73 | 53 |
| **2GH1 UNDIFFERENTIATED** | | | | | | | | | | | | | | | | | | | | | | | | | |
| Min | 141 | 75 | 19 | 1 | 9 | 2 | 5.8 | 3864 | 0.37 | 2 | 0.58 | 1.7 | 1.5 | 184 | <0 | 0.17 | 0.2 | 0.08 | <0 | 6.7 | 0.31 | <0 | 0.1 | 0.09 | 598 |
| Max | 9155 | 4368 | 2438 | 5 | 342 | 62 | 14 | 6986 | 45 | 27 | 3E+05 | 17703 | 52 | 834 | 22 | 2.5 | 16 | 1.6 | 5.3 | 55 | 2.5 | 0.48 | 1.5 | 0.58 | 362 |
| **Mean(32)** | 2096 | 1673 | 138 | 2.7 | 130 | 20 | 7.9 | 5366 | 4.8 | 6.4 | 8391 | 586 | 11 | 447 | 1 | 0.91 | 3.3 | 0.64 | 2.4 | 24 | 0.96 | 0.19 | 0.87 | 0.28 | 139 |
| S.D. | 2165 | 1396 | 422 | 1.1 | 92 | 16 | 2.4 | 1020 | 7.9 | 5 | 44681 | 3124 | 10 | 197 | 3.8 | 0.6 | 3 | 0.41 | 1.4 | 12 | 0.45 | 0.1 | 0.4 | 0.13 | 120 |
| **2GH1 BRIGHT** | | | | | | | | | | | | | | | | | | | | | | | | | |
| Min | 180 | 35 | 17 | 0.69 | 9 | 0.6 | 3 | 3267 | 0.36 | 0.25 | 0.1 | 1.3 | 2 | 67 | 0.02 | 0.16 | 0.02 | 0.02 | 0.4 | 1.9 | 0.12 | 0.01 | 0.02 | 0.01 | 844 |
| Max | 7224 | 26341 | 5643 | 13 | 708 | 48 | 12 | 11010 | 8.3 | 9.6 | 4.2 | 107 | 12 | 566 | 0.6 | 4.5 | 29 | 4.5 | 4.1 | 83 | 1.5 | 3.5 | 1.1 | 0.6 | 364 |
| **Mean(41)** | 819 | 2334 | 199 | 2 | 86 | 9.5 | 5.8 | 5861 | 1.2 | 3.2 | 1.5 | 9.3 | 5.4 | 270 | 0.19 | 0.77 | 2.5 | 0.57 | 2 | 16 | 0.75 | 0.23 | 0.42 | 0.22 | 173 |
| S.D. | 1420 | 4766 | 874 | 1.8 | 118 | 10 | 1.8 | 1936 | 1.3 | 2.1 | 1.1 | 19 | 2.3 | 130 | 0.14 | 0.8 | 5.1 | 0.76 | 1.1 | 25 | 0.35 | 0.53 | 0.31 | 0.16 | 267 |
| **2GH1 DARK** | | | | | | | | | | | | | | | | | | | | | | | | | |
| Min | 873 | 3716 | 30 | 8.9 | 300 | 25 | 5.5 | 4206 | 0.97 | 0.41 | 0.2 | 3.3 | 5.5 | 288 | 0.05 | 1.1 | 5.8 | 1.3 | 0.9 | 13 | 0.6 | 0.02 | 0.42 | 0.03 | 450 |
| Max | 3912 | 6712 | 406 | 16 | 3402 | 35 | 16 | 4888 | 2.1 | 2.7 | 0.35 | 31 | 9.6 | 504 | 0.17 | 7.2 | 29 | 15 | 2.3 | 37 | 1.4 | 0.08 | 1.3 | 1.2 | 330 |
| **Mean(5)** | 2128 | 4474 | 125 | 12 | 949 | 28 | 8.7 | 4603 | 1.6 | 1.3 | 0.27 | 15 | 7.1 | 398 | 0.08 | 3 | 12 | 4.1 | 1.5 | 24 | 0.8 | 0.04 | 0.68 | 0.28 | 72 |
| S.D. | 1284 | 1292 | 158 | 2.5 | 1372 | 3.9 | 4.4 | 262 | 0.47 | 0.96 | 0.07 | 11 | 1.7 | 99 | 0.05 | 2.5 | 9.7 | 5.9 | 0.56 | 8.8 | 0.35 | 0.02 | 0.35 | 0.54 | 0.35 |
| **2GH1 MATRIX** | | | | | | | | | | | | | | | | | | | | | | | | | |
| Min | 402 | 45087 | 9 | 17 | 3144 | 96 | 101 | 7315 | 0.68 | 7.1 | 1.1 | 2.2 | 11 | 6 | 0.2 | 0.1 | 9.7 | 5 | <0 | 14 | 0.66 | 0.09 | 1.7 | 0.29 | 37 |
| Max | 17512 | 62675 | 494 | 28 | 5305 | 270 | 201 | 14035 | 35 | 5525 | 66 | 584 | 252 | 8519 | 184 | 27 | 167 | 29 | 2.3 | 82 | 169 | 34 | 6.1 | 1.8 | 4.9 |
| **Mean(9)** | 7807 | 53305 | 83 | 23 | 3637 | 155 | 168 | 9686 | 13 | 673 | 18 | 195 | 62 | 1431 | 26 | 4.4 | 46 | 16 | 0.85 | 30 | 21 | 7.8 | 4.1 | 0.84 | 12 |
| S.D. | 7653 | 5161 | 155 | 3.8 | 655 | 56 | 37 | 2450 | 11 | 1821 | 25 | 217 | 84 | 2917 | 60 | 8.7 | 48 | 6.7 | 0.68 | 21 | 55 | 12 | 1.5 | 0.51 | <0 |

## Trace elements in garnet from Groundhog, S.A.

**Table A- 4 :Summary of LA-ICP-MS trace element data for garnet (ppm) (continued)**

| | Mg | Al | P | Sc | Ti | V | Cr | Mn | Co | Ni | Cu | Zn | Ga | As | Rb | Sr | Zr | Nb | Mo | Sn | Sb | Cs | Hf | Ta | W |
|---|---|---|---|---|---|---|---|---|---|---|---|---|---|---|---|---|---|---|---|---|---|---|---|---|---|
| **2GH1 RIM** | | | | | | | | | | | | | | | | | | | | | | | | | |
| Min | 336 | 40538 | 12 | 7 | 2463 | 74 | 13 | 6057 | 0.16 | 2.8 | 0.1 | 1.7 | 17 | 5.3 | 0.1 | 0.1 | 19 | 2.4 | <0 | 16 | 0.59 | 0.07 | 1.1 | 0.11 | 25 |
| Max | 20394 | 67872 | 2848 | 36 | 5367 | 406 | 337 | 9689 | 23 | 42 | 120 | 1117 | 31 | 22 | 3.8 | 1.6 | 77 | 43 | 3.8 | 35 | 4.3 | 7.4 | 8.9 | 1.1 | 1.8 |
| **Mean(45)** | 2696 | 50655 | 84.16 | 24 | 3337 | 265 | 173 | 7353 | 3.5 | 8.5 | 11 | 71 | 26 | 7.8 | 0.59 | 0.39 | 36 | 11 | 1.4 | 26 | 1.1 | 0.84 | 3.9 | 0.47 | 3.7 |
| S.D. | 4243 | 7534 | 422 | 6.1 | 633 | 104 | 87 | 893 | 4.9 | 8.4 | 23 | 179 | 3.5 | 2.5 | 0.82 | 0.3 | 13 | 8.8 | 0.84 | 5.1 | 0.57 | 1.8 | 1.7 | 0.21 | 120 |
| **2GH2 BRIGHT** | | | | | | | | | | | | | | | | | | | | | | | | | |
| Min | 199 | 54 | 17 | 1.1 | 9 | 0.68 | 3 | 3723 | 1.1 | 0.25 | 0.13 | 1.4 | 3.3 | 191 | 0.02 | 0.29 | 0.02 | 0.02 | 0.91 | 2.3 | 0.12 | 0.01 | 0.02 | 0.01 | 741 |
| Max | 6067 | 16710 | 56 | 13 | 708 | 37 | 5.9 | 4832 | 3.2 | 5.8 | 0.47 | 60 | 12 | 566 | 0.25 | 2.4 | 18 | 2.5 | 3.7 | 83 | 0.54 | 0.07 | 0.68 | 0.14 | 337 |
| **Mean(10)** | 900 | 1943 | 30 | 3.3 | 110 | 8.8 | 3.7 | 4105 | 1.6 | 0.86 | 0.27 | 8.3 | 5.3 | 366 | 0.05 | 0.58 | 2.4 | 0.52 | 1.8 | 50 | 0.27 | 0.02 | 0.12 | 0.02 | 194 |
| S.D. | 1817 | 5190 | 13 | 3.4 | 212 | 11 | 0.84 | 395 | 0.65 | 1.7 | 0.11 | 18 | 2.7 | 138 | 0.07 | 0.63 | 5.5 | 0.71 | 0.96 | 33 | 0.14 | 0.02 | 0.2 | 0.04 | 0.26 |
| **2GH2 BRECCIATED BRIGHT** | | | | | | | | | | | | | | | | | | | | | | | | | |
| Min | 285 | 188 | 4.8 | 1.7 | 42 | 3.7 | 2.9 | 3886 | 0.4 | 0.41 | 0.27 | 0.51 | 25 | 1.5 | 0.04 | 0.01 | 0.2 | 0.14 | 0.08 | 30 | 0.08 | 0.01 | 0.03 | 0.01 | 465 |
| Max | 595 | 46126 | 38 | 12 | 4387 | 344 | 56 | 6536 | 1.3 | 1.3 | 0.6 | 3.8 | 45 | 324 | 0.07 | 0.52 | 50 | 21 | 1.8 | 286 | 0.42 | 0.03 | 2 | 1.5 | 135 |
| **Mean(10)** | 342 | 27115 | 15 | 3.9 | 2509 | 73 | 13 | 5386 | 0.78 | 0.78 | 0.4 | 1.7 | 34 | 84 | 0.05 | 0.16 | 28 | 11 | 0.67 | 132 | 0.15 | 0.02 | 1.1 | 0.82 | 197 |
| S.D. | 93 | 22902 | 11 | 2.9 | 2102 | 100 | 16 | 1268 | 0.4 | 0.27 | 0.11 | 1.1 | 7.7 | 116 | 0.01 | 0.17 | 24 | 9.4 | 0.7 | 126 | 0.1 | 0.01 | 0.93 | 0.69 | 0.55 |
| **2GH2 BRECCIATED DARK** | | | | | | | | | | | | | | | | | | | | | | | | | |
| Min | 324 | 34467 | 5.1 | 3.6 | 3137 | 72 | 11 | 6335 | 0.37 | 0.49 | 0.28 | 0.91 | 28 | 2.3 | 0.04 | 0.02 | 30 | 4.8 | 0.04 | 27 | 0.08 | 0.01 | 1.6 | 0.2 | 4.5 |
| Max | 691 | 49586 | 15 | 46 | 4756 | 1178 | 385 | 7310 | 0.8 | 1.2 | 0.54 | 4.7 | 38 | 6.1 | 0.08 | 0.15 | 59 | 21 | 0.3 | 40 | 0.12 | 0.03 | 4.5 | 1.7 | 1.8 |
| **Mean(10)** | 390 | 42691 | 8.8 | 19 | 3689 | 526 | 120 | 6823 | 0.56 | 0.84 | 0.36 | 1.6 | 33 | 3.9 | 0.06 | 0.07 | 42 | 12 | 0.16 | 34 | 0.1 | 0.02 | 2.7 | 0.83 | 1.2 |
| S.D. | 115 | 4600 | 3.7 | 13 | 557 | 362 | 115 | 305 | 0.14 | 0.25 | 0.07 | 1.2 | 3.9 | 1.3 | 0.01 | 0.04 | 11 | 5.4 | 0.1 | 4.1 | 0.01 | 0.01 | 1.1 | 0.44 | 0.07 |
| **2GH2 RIM** | | | | | | | | | | | | | | | | | | | | | | | | | |
| Min | 328 | 44162 | 4.2 | 3.2 | 729 | 65 | 13 | 6389 | 0.37 | 0.39 | 0.26 | 0.51 | 16 | 1.3 | 0.03 | 0.04 | 20 | 5.1 | 0.06 | 25 | 0.05 | 0.01 | 0.42 | 0.12 | 18 |
| Max | 7859 | 55189 | 19 | 19 | 4414 | 388 | 64 | 7734 | 2.8 | 6 | 0.72 | 59 | 27 | 28 | 0.48 | 19 | 45 | 22 | 0.42 | 72 | 0.2 | 0.18 | 2 | 1.5 | 3.4 |
| **Mean(16)** | 2260 | 49287 | 9.1 | 7.8 | 3348 | 114 | 27 | 7062 | 1.2 | 2.1 | 0.42 | 19 | 25 | 6.1 | 0.12 | 3.1 | 35 | 15 | 0.17 | 40 | 0.1 | 0.05 | 1.5 | 1.1 | 6.3 |
| S.D. | 2212 | 2479 | 3.9 | 5.1 | 1220 | 76 | 13 | 387 | 0.74 | 1.8 | 0.15 | 19 | 3.6 | 8.1 | 0.12 | 5.7 | 6.7 | 5.1 | 0.09 | 15 | 0.04 | 0.06 | 0.42 | 0.5 | 56 |
| **2GH3 BRIGHT** | | | | | | | | | | | | | | | | | | | | | | | | | |
| Min | 292 | 33 | 6.1 | 0.44 | 2.3 | 0.05 | 1.7 | 3551 | 0.46 | 0.23 | 0.21 | 0.64 | 6.2 | 75 | 0.02 | 0.09 | 0.01 | 0.01 | 0.2 | 2.2 | 0.07 | <0 | 0.02 | <0 | 836 |
| Max | 943 | 18415 | 72 | 1.6 | 346 | 35 | 17 | 4857 | 1.8 | 16 | 0.85 | 5.1 | 45 | 806 | 14 | 0.84 | 12 | 1.6 | 5.7 | 316 | 1.1 | 0.03 | 0.5 | 0.5 | 456 |
| **Mean(53)** | 618 | 2621 | 45 | 0.84 | 21 | 4.7 | 3.9 | 4112 | 1 | 0.79 | 0.42 | 2.3 | 20 | 433 | 0.4 | 0.34 | 0.94 | 0.11 | 1.8 | 130 | 0.37 | 0.01 | 0.09 | 0.06 | 192 |
| S.D. | 180 | 4231 | 15 | 0.21 | 51 | 6.2 | 2.1 | 331 | 0.42 | 2.1 | 0.13 | 1.2 | 11 | 236 | 2 | 0.17 | 2.2 | 0.28 | 1.4 | 114 | 0.23 | 0.01 | 0.1 | 0.11 | 0.26 |

## Trace elements in garnet from Groundhog, S.A.

**Table A- 4 :Summary of LA-ICP-MS trace element data for garnet (ppm) (continued)**

| | Mg | Al | P | Sc | Ti | V | Cr | Mn | Co | Ni | Cu | Zn | Ga | As | Rb | Sr | Zr | Nb | Mo | Sn | Sb | Cs | Hf | Ta | W |
|---|---|---|---|---|---|---|---|---|---|---|---|---|---|---|---|---|---|---|---|---|---|---|---|---|---|
| **2GH3 BRECCIATED BRIGHT** | | | | | | | | | | | | | | | | | | | | | | | | | |
| Min | 285 | 188 | 4.8 | 1.7 | 42 | 3.7 | 2.9 | 3886 | 0.37 | 0.41 | 0.27 | 0.51 | 25 | 1.5 | 0.04 | 0.01 | 0.2 | 0.14 | 0.04 | 27 | 0.08 | 0.01 | 0.03 | 0.01 | 465 |
| Max | 691 | 49586 | 38 | 46 | 4756 | 1178 | 385 | 7310 | 1.3 | 1.3 | 0.6 | 4.7 | 45 | 324 | 0.08 | 0.52 | 59 | 21 | 1.8 | 286 | 0.42 | 0.03 | 4.5 | 1.7 | 68 |
| **Mean(20)** | 366 | 34903 | 12 | 11 | 3099 | 299 | 66 | 6104 | 0.67 | 0.81 | 0.38 | 1.7 | 34 | 44 | 0.05 | 0.12 | 35 | 11 | 0.41 | 83 | 0.13 | 0.02 | 1.9 | 0.82 | 152 |
| S.D. | 105 | 17953 | 8.7 | 12 | 1614 | 348 | 97 | 1161 | 0.32 | 0.26 | 0.09 | 1.1 | 6 | 90 | 0.01 | 0.13 | 19 | 7.4 | 0.55 | 101 | 0.07 | 0.01 | 1.3 | 0.56 | 17 |
| **2GH3 DARK** | | | | | | | | | | | | | | | | | | | | | | | | | |
| Min | 163 | 60 | 34 | 0.83 | 12 | 0.7 | 5.4 | 7189 | 0.27 | 2 | 0.5 | 2.7 | 3.8 | 26 | 0.09 | 0.16 | 0.59 | 0.27 | 0.2 | 2.7 | 0.47 | 0.06 | 0.2 | 0.08 | 352 |
| Max | 16250 | 57254 | 7266 | 11 | 5892 | 56 | 35 | 12111 | 18 | 46 | 9.5 | 290 | 11 | 270 | 1.4 | 4.6 | 116 | 27 | 4.9 | 7.6 | 2.3 | 1 | 4.2 | 3.6 | 212 |
| **Mean(16)** | 3360 | 15520 | 1098 | 3.7 | 907 | 23 | 11 | 8936 | 4 | 10 | 3 | 57 | 6.2 | 152 | 0.43 | 1.6 | 21 | 4.4 | 1.6 | 4.7 | 1 | 0.26 | 1.2 | 0.5 | 121 |
| S.D. | 5371 | 19849 | 2399 | 3.2 | 1528 | 19 | 9 | 1502 | 6 | 14 | 2.6 | 91 | 2.2 | 80 | 0.33 | 1.5 | 34 | 6.6 | 1.1 | 1.6 | 0.44 | 0.29 | 0.95 | 0.84 | 0.04 |
| **2GH3 RIM** | | | | | | | | | | | | | | | | | | | | | | | | | |
| Min | 234 | 19932 | 4.2 | 3.1 | 729 | 43 | 13 | 6389 | 0.28 | 0.32 | 0.23 | 0.48 | 10 | 0.75 | 0.03 | 0.02 | 11 | 3.5 | 0.06 | 14 | 0.05 | 0.01 | 0.42 | 0.12 | 18 |
| Max | 21495 | 62049 | 542 | 21 | 4414 | 489 | 207 | 9241 | 8.1 | 17 | 122 | 193 | 63 | 28 | 79 | 69 | 92 | 22 | 0.53 | 72 | 0.46 | 1 | 4.9 | 1.6 | 1.8 |
| **Mean(41)** | 3897 | 45468 | 29 | 8 | 3221 | 158 | 47 | 7473 | 1.7 | 3.5 | 3.6 | 34 | 25 | 4 | 2.3 | 11 | 34 | 13 | 0.19 | 33 | 0.12 | 0.13 | 1.6 | 1 | 4.2 |
| S.D. | 4837 | 8836 | 87 | 5.4 | 1013 | 133 | 50 | 648 | 1.7 | 3.9 | 19 | 45 | 8 | 5.5 | 12 | 17 | 14 | 5.2 | 0.1 | 13 | 0.07 | 0.21 | 0.77 | 0.41 | 0.01 |
| **3GH1 UNDIFFERENTIATED** | | | | | | | | | | | | | | | | | | | | | | | | | |
| Min | 386 | 46423 | 3.6 | 3.7 | 3415 | 178 | 26 | 7318 | 0.57 | 0.46 | 0.19 | 0.52 | 25 | 0.79 | 0.04 | 0.02 | 31 | 4.5 | 0.1 | 24 | 0.06 | 0.01 | 1.9 | 0.39 | 1.3 |
| Max | 1E+05 | 1E+05 | 3625 | 17 | 4950 | 576 | 171 | 22819 | 81 | 111 | 17 | 3564 | 58 | 48 | 23 | 31 | 52 | 30 | 0.4 | 43 | 1.9 | 8.1 | 4.9 | 1.8 | 0.14 |
| **Mean(15)** | 16013 | 61331 | 254 | 11 | 4050 | 364 | 89 | 9444 | 9.4 | 12 | 2 | 375 | 31 | 5 | 2.5 | 2.8 | 40 | 16 | 0.19 | 31 | 0.23 | 0.81 | 3.4 | 0.98 | 0.31 |
| S.D. | 42484 | 18642 | 933 | 5.1 | 454 | 114 | 44 | 4038 | 23 | 32 | 4.3 | 1019 | 8.7 | 12 | 6.7 | 8 | 7.9 | 8 | 0.09 | 5.9 | 0.46 | 2.2 | 0.94 | 0.45 | 0.26 |
| **3GH1 BRECCIATED BRIGHT** | | | | | | | | | | | | | | | | | | | | | | | | | |
| Min | 285 | 188 | 4.8 | 1.7 | 42 | 3.7 | 2.9 | 3886 | 0.4 | 0.41 | 0.27 | 0.51 | 25 | 1.5 | 0.04 | 0.01 | 0.2 | 0.14 | 0.08 | 30 | 0.08 | 0.01 | 0.03 | 0.01 | 465 |
| Max | 595 | 46126 | 38 | 12 | 4387 | 344 | 56 | 6536 | 1.3 | 1.3 | 0.6 | 3.8 | 45 | 324 | 0.07 | 0.52 | 50 | 21 | 1.8 | 286 | 0.42 | 0.03 | 2 | 1.5 | 135 |
| **Mean(10)** | 342 | 27115 | 15 | 3.9 | 2509 | 73 | 13 | 5386 | 0.78 | 0.78 | 0.4 | 1.7 | 34 | 84 | 0.05 | 0.16 | 28 | 11 | 0.67 | 132 | 0.15 | 0.02 | 1.1 | 0.82 | 197 |
| S.D. | 93 | 22902 | 11 | 2.9 | 2102 | 100 | 16 | 1268 | 0.4 | 0.27 | 0.11 | 1.1 | 7.7 | 116 | 0.01 | 0.17 | 24 | 9.4 | 0.7 | 126 | 0.1 | 0.01 | 0.93 | 0.69 | 0.55 |
| **3GH1 BRECCIATED DARK** | | | | | | | | | | | | | | | | | | | | | | | | | |
| Min | 324 | 34467 | 5.1 | 3.6 | 3137 | 72 | 11 | 6335 | 0.37 | 0.49 | 0.28 | 0.91 | 28 | 2.3 | 0.04 | 0.02 | 30 | 4.8 | 0.04 | 27 | 0.08 | 0.01 | 1.6 | 0.2 | 4.5 |
| Max | 691 | 49586 | 15 | 46 | 4756 | 1178 | 385 | 7310 | 0.8 | 1.2 | 0.54 | 4.7 | 38 | 6.1 | 0.08 | 0.15 | 59 | 21 | 0.3 | 40 | 0.12 | 0.03 | 4.5 | 1.7 | 1.8 |
| **Mean(10)** | 390 | 42691 | 8.8 | 19 | 3689 | 526 | 120 | 6823 | 0.56 | 0.84 | 0.36 | 1.6 | 33 | 3.9 | 0.06 | 0.07 | 42 | 12 | 0.16 | 34 | 0.1 | 0.02 | 2.7 | 0.83 | 1.2 |
| S.D. | 115 | 4600 | 3.7 | 13 | 557 | 362 | 115 | 305 | 0.14 | 0.25 | 0.07 | 1.2 | 3.9 | 1.3 | 0.01 | 0.04 | 11 | 5.4 | 0.1 | 4.1 | 0.01 | 0.01 | 1.1 | 0.44 | 0.05 |

# Trace elements in garnet from Groundhog, S.A.

**Table A- 4 :Summary of LA-ICP-MS trace element data for garnet (ppm) (continued)**

| | Mg | Al | P | Sc | Ti | V | Cr | Mn | Co | Ni | Cu | Zn | Ga | As | Rb | Sr | Zr | Nb | Mo | Sn | Sb | Cs | Hf | Ta | W |
|---|---|---|---|---|---|---|---|---|---|---|---|---|---|---|---|---|---|---|---|---|---|---|---|---|---|
| **3GH1 BRECCIATED UNDIFFERENTIATED** | | | | | | | | | | | | | | | | | | | | | | | | | |
| Min | 434 | 57159 | 4.6 | 2.8 | 4469 | 79 | 20 | 7858 | 0.66 | 0.67 | 0.33 | 0.59 | 22 | 1.1 | 0.03 | 0.03 | 43 | 12 | 0.09 | 25 | 0.08 | 0.02 | 2.2 | 0.84 | 0.15 |
| Max | 722 | 71288 | 10 | 16 | 5083 | 367 | 153 | 10207 | 1.3 | 1.8 | 0.68 | 7.7 | 29 | 2.2 | 0.15 | 0.08 | 56 | 30 | 0.46 | 35 | 0.16 | 0.03 | 5.4 | 2.2 | 0.08 |
| **Mean(7)** | 510 | 63408 | 7.2 | 6 | 4730 | 205 | 49 | 9046 | 0.82 | 1.1 | 0.52 | 2.1 | 26 | 1.6 | 0.08 | 0.04 | 48 | 24 | 0.3 | 31 | 0.1 | 0.02 | 3 | 1.6 | 0.04 |
| S.D. | 99 | 6147 | 2.4 | 4.5 | 200 | 121 | 47 | 951 | 0.22 | 0.37 | 0.13 | 2.5 | 3 | 0.37 | 0.04 | 0.02 | 4.5 | 6 | 0.13 | 3.2 | 0.02 | <0 | 1.1 | 0.55 | 0.04 |
| **3GH1 RIM** | | | | | | | | | | | | | | | | | | | | | | | | | |
| Min | 234 | 19932 | 4.5 | 3.1 | 1398 | 43 | 15 | 6745 | 0.28 | 0.32 | 0.23 | 0.48 | 10 | 0.75 | 0.03 | 0.02 | 11 | 3.5 | 0.08 | 14 | 0.07 | 0.01 | 0.71 | 0.49 | 3.9 |
| Max | 21495 | 62049 | 542 | 21 | 4398 | 489 | 207 | 9241 | 8.1 | 17 | 122 | 193 | 63 | 8.6 | 79 | 69 | 92 | 21 | 0.53 | 46 | 0.46 | 1 | 4.9 | 1.6 | 0.74 |
| **Mean(26)** | 5112 | 43468 | 41 | 8.1 | 3163 | 184 | 59 | 7753 | 2.1 | 4.5 | 5.4 | 46 | 25 | 2.6 | 3.5 | 15 | 34 | 12 | 0.2 | 28 | 0.14 | 0.18 | 1.7 | 0.93 | 1 |
| S.D. | 5694 | 10539 | 108 | 5.6 | 864 | 151 | 59 | 642 | 2 | 4.6 | 24 | 53 | 9.7 | 1.9 | 16 | 19.48 | 17 | 5 | 0.1 | 8 | 0.08 | 0.25 | 0.9 | 0.34 | 424 |
| **3GH2 BRIGHT** | | | | | | | | | | | | | | | | | | | | | | | | | |
| Min | 364 | 111 | 42 | 0.97 | 9.2 | 2 | 3.9 | 4009 | 1.3 | 0.36 | 0.22 | 1.5 | 5.5 | 643 | 0.04 | 0.59 | 0.03 | 0.03 | 1.1 | 2 | 0.3 | 0.02 | 0.11 | 0.02 | 588 |
| Max | 899 | 8690 | 59 | 1.9 | 50 | 18 | 5.7 | 4425 | 2.2 | 1.3 | 0.63 | 6.2 | 8.7 | 1075 | 0.11 | 1.3 | 2.3 | 0.43 | 3.4 | 6.7 | 0.7 | 0.09 | 0.16 | 0.3 | 526 |
| **Mean(6)** | 711 | 1755 | 51 | 1.3 | 23 | 9.4 | 4.9 | 4192 | 1.7 | 0.64 | 0.44 | 3.3 | 6.6 | 897 | 0.07 | 0.85 | 0.59 | 0.16 | 2 | 3.8 | 0.45 | 0.04 | 0.12 | 0.11 | 71 |
| S.D. | 200 | 3406 | 6.9 | 0.37 | 18 | 7.8 | 0.74 | 160 | 0.33 | 0.36 | 0.15 | 1.8 | 1.2 | 146 | 0.03 | 0.25 | 0.83 | 0.18 | 0.9 | 2 | 0.15 | 0.03 | 0.02 | 0.12 | 10 |
| **3GH2 DARK** | | | | | | | | | | | | | | | | | | | | | | | | | |
| **(1)** | 319 | 57002 | 14 | 7.2 | 4548 | 141 | 7.9 | 7012 | 0.99 | 0.65 | 0.62 | 1 | 23 | 16 | 0.07 | 0.12 | 128 | 17 | 0.21 | 80 | 0.21 | 0.07 | 4.4 | 0.79 | 10 |
| **4GH1 BRECCIATED BRIGHT** | | | | | | | | | | | | | | | | | | | | | | | | | |
| Min | 268 | 72 | 21 | 1 | 6 | 1 | 3 | 3834 | 0.15 | 1.5 | 0.15 | 2.1 | 11 | 469 | 0.07 | 0.21 | 0.09 | 0.07 | 1.4 | 4.8 | 0.25 | 0.02 | 0.1 | 0.09 | 627 |
| Max | 1221 | 7153 | 49 | 3 | 156 | 17 | 11 | 4085 | 0.79 | 2.7 | 1.2 | 14 | 21 | 667 | 0.24 | 0.83 | 2.8 | 0.43 | 3.5 | 11 | 0.65 | 0.5 | 0.5 | 0.3 | 541 |
| **Mean(8)** | 524 | 1561 | 39 | 1.9 | 44 | 4.9 | 5.9 | 3960 | 0.34 | 1.8 | 0.72 | 4.5 | 15 | 571 | 0.11 | 0.42 | 0.7 | 0.17 | 2 | 7.6 | 0.37 | 0.12 | 0.28 | 0.15 | 109 |
| S.D. | 296 | 2382 | 9.5 | 0.64 | 52 | 5.5 | 2.4 | 90 | 0.21 | 0.39 | 0.34 | 3.7 | 3.6 | 79 | 0.06 | 0.23 | 0.89 | 0.12 | 0.7 | 1.9 | 0.12 | 0.16 | 0.16 | 0.07 | 3.9 |
| **4GH1 BRECCIATED DARK** | | | | | | | | | | | | | | | | | | | | | | | | | |
| Min | 457 | 47544 | 13 | 1 | 152 | 50 | 4 | 6382 | 0.24 | 2.5 | 0.85 | 1.8 | 4.9 | 6.6 | 0.1 | 0.39 | 0.44 | 1.9 | 0.5 | 0.86 | 0.21 | 0.08 | 0.1 | 0.13 | 21 |
| Max | 2957 | 59088 | 870 | 9 | 6140 | 182 | 154 | 9837 | 2.2 | 11 | 1.9 | 34 | 16 | 40 | 0.95 | 4.5 | 54 | 26 | 0.76 | 17 | 2 | 0.43 | 1.9 | 2.1 | 12 |
| **Mean(5)** | 1174 | 53891 | 186 | 4 | 2299 | 89 | 43 | 7826 | 0.69 | 4.4 | 1.3 | 12 | 8 | 19 | 0.3 | 1.7 | 29 | 10 | 0.62 | 5.1 | 0.88 | 0.17 | 0.92 | 0.74 | 6.6 |
| S.D. | 1037 | 5247 | 382 | 3.1 | 2435 | 53 | 63 | 1265 | 0.84 | 3.9 | 0.37 | 13 | 4.4 | 13 | 0.36 | 1.7 | 26 | 9.6 | 0.11 | 6.9 | 0.73 | 0.15 | 0.82 | 0.84 | 0.6 |
| **4GH1 RIM** | | | | | | | | | | | | | | | | | | | | | | | | | |
| Min | 391 | 51165 | 16 | 2 | 437 | 82 | 6 | 7247 | 0.19 | 3.4 | 1.9 | 16 | 3.5 | 8.7 | 0.17 | 0.16 | 3.7 | 4.2 | 0.55 | 1.3 | 0.79 | 0.06 | <0 | 0.08 | 11 |
| Max | 3276 | 65122 | 25 | 15 | 3699 | 398 | 149 | 9157 | 2.9 | 6.8 | 7 | 79 | 28 | 22 | 0.4 | 4.1 | 472 | 46 | 1.5 | 21 | 3.3 | 0.26 | 15 | 2 | 4.6 |
| **Mean(8)** | 1334 | 57325 | 20 | 7.5 | 2156 | 169.6 | 51 | 8131 | 0.99 | 5.4 | 3 | 37 | 10 | 12 | 0.31 | 1 | 83 | 14 | 0.93 | 8.4 | 1.3 | 0.18 | 3.2 | 0.67 | 4 |
| S.D. | 967.2 | 4610 | 3.3 | 5.4 | 1486 | 112 | 57 | 691 | 0.92 | 1.2 | 1.7 | 21 | 9.1 | 4.4 | 0.09 | 1.4 | 159 | 13 | 0.32 | 7.8 | 0.86 | 0.06 | 4.7 | 0.65 | 213 |

## Trace elements in garnet from Groundhog, S.A.

**Table A- 4 :Summary of LA-ICP-MS trace element data for garnet (ppm) (continued)**

| | Mg | Al | P | Sc | Ti | V | Cr | Mn | Co | Ni | Cu | Zn | Ga | As | Rb | Sr | Zr | Nb | Mo | Sn | Sb | Cs | Hf | Ta | W |
|---|---|---|---|---|---|---|---|---|---|---|---|---|---|---|---|---|---|---|---|---|---|---|---|---|---|
| **4GH2 BRIGHT** | | | | | | | | | | | | | | | | | | | | | | | | | |
| Min | 139 | 12 | 29 | 0.88 | 3.9 | 0.17 | 2.7 | 3455 | 0.73 | 0.57 | 0.41 | 0.91 | 4 | 199 | 0.03 | 0.18 | 0.04 | 0.02 | 0.41 | 13 | 0.27 | 0.02 | <0 | 0.03 | 1175 |
| Max | 565 | 26494 | 85 | 3.5 | 573 | 64 | 14 | 4493 | 2 | 1.8 | 1.1 | 5 | 32 | 1089 | 1.62 | 1.28 | 20.51 | 3.47 | 2.31 | 198.3 | 1.02 | 0.41 | 0.8 | 0.5 | 694 |
| **Mean(29)** | 404 | 5128 | 54 | 1.5 | 47 | 13 | 5.5 | 3895 | 1.2 | 0.98 | 0.73 | 2.3 | 18 | 776 | 0.15 | 0.52 | 1.3 | 0.37 | 0.98 | 117 | 0.5 | 0.09 | 0.31 | 0.11 | 225 |
| S.D. | 128 | 7701 | 14 | 0.56 | 115 | 17 | 2 | 261 | 0.27 | 0.32 | 0.19 | 1 | 8 | 252 | 0.28 | 0.29 | 3.9 | 0.82 | 0.46 | 59 | 0.19 | 0.07 | 0.16 | 0.08 | 713 |
| **4GH2 BRECCIATED BRIGHT** | | | | | | | | | | | | | | | | | | | | | | | | | |
| Min | 148 | 59 | 49 | 1.1 | 4.4 | 0.23 | 3.1 | 3950 | 1.3 | 0.94 | 0.61 | 4 | 2.5 | 983 | 0.05 | 0.57 | 0.07 | 0.02 | 0.77 | 13 | 0.47 | 0.02 | 0.09 | 0.03 | 963 |
| Max | 249 | 2530 | 69 | 5.8 | 159 | 11 | 8.1 | 4216 | 2.2 | 54 | 33 | 5.9 | 7 | 1115 | 0.67 | 3.6 | 4.8 | 0.51 | 1.6 | 15 | 0.8 | 0.14 | 0.41 | 0.13 | 828 |
| **Mean(5)** | 177 | 799 | 57 | 3.1 | 63 | 4.1 | 6 | 4061 | 1.7 | 12 | 7.1 | 4.8 | 5.2 | 1064 | 0.22 | 1.2 | 1.8 | 0.22 | 1.3 | 13 | 0.6 | 0.06 | 0.33 | 0.1 | 97 |
| S.D. | 43 | 1017 | 8 | 2.2 | 75 | 5 | 2 | 97 | 0.36 | 24 | 14 | 0.85 | 1.7 | 51 | 0.25 | 1.3 | 2.1 | 0.2 | 0.34 | 0.64 | 0.13 | 0.05 | 0.14 | 0.04 | 8 |
| **4GH2 BRECCIATED DARK** | | | | | | | | | | | | | | | | | | | | | | | | | |
| **(1)** | 782 | 38452 | 7 | 13 | 2121 | 336 | 31 | 13431 | 0.92 | 0.86 | 0.83 | 4.3 | 18 | 18 | 0.7 | 11 | 39 | 12 | 0.67 | 25 | 0.27 | 0.33 | 2.2 | 0.48 | 8 |
| **4GH2 BRECCIATED DARK FLUIDAL** | | | | | | | | | | | | | | | | | | | | | | | | | |
| Min | 205 | 35713 | 7.2 | 1.2 | 138 | 95 | 6.5 | 6660 | 0.45 | 1.1 | 0.86 | 1 | 18 | 2.5 | 0.12 | 0.08 | 8.3 | 1.2 | 0.15 | 19 | 0.23 | 0.07 | 0.37 | 0.08 | 5.6 |
| Max | 11786 | 61693 | 18 | 22 | 4963 | 552 | 48 | 12514 | 13 | 39 | 918 | 214 | 33 | 7.7 | 2.6 | 26 | 116 | 35 | 0.65 | 85 | 0.74 | 0.28 | 5 | 1.2 | 1.7 |
| **Mean(14)** | 3606 | 51763 | 11 | 13 | 2928 | 413 | 29 | 9038 | 5.1 | 13 | 67 | 70 | 25 | 4.9 | 0.43 | 4.1 | 59 | 21 | 0.36 | 44 | 0.44 | 0.11 | 2.4 | 0.69 | 1.4 |
| S.D. | 3436 | 6902 | 3.5 | 6.3 | 1374 | 136 | 14 | 1794 | 4.4 | 12 | 245 | 67 | 4 | 1.7 | 0.62 | 7.5 | 35 | 9.7 | 0.15 | 16 | 0.14 | 0.05 | 1.4 | 0.32 | 3.4 |
| **4GH2 DARK** | | | | | | | | | | | | | | | | | | | | | | | | | |
| Min | 361 | 21581 | 8 | 2 | 138 | 60 | 5.2 | 4889 | 0.34 | 1 | 0.75 | 1.7 | 15 | 6.5 | 0.12 | 0.05 | 2.7 | 1.9 | 0.15 | 33 | 0.22 | 0.06 | 0.1 | 0.1 | 478 |
| Max | 1435 | 58427 | 41 | 30 | 5093 | 564 | 61 | 7896 | 2.3 | 5.8 | 29 | 23 | 23 | 377 | 0.41 | 0.67 | 115 | 35 | 1.2 | 91 | 0.57 | 0.17 | 6.8 | 0.97 | 72 |
| **Mean(8)** | 809 | 51051 | 17 | 15 | 3259 | 382 | 25 | 6937 | 1.3 | 2.2 | 4.6 | 11 | 20 | 63 | 0.21 | 0.32 | 73 | 24 | 0.5 | 53 | 0.42 | 0.12 | 3.3 | 0.53 | 164 |
| S.D. | 446 | 12293 | 11 | 12 | 2109 | 191 | 21 | 930 | 0.74 | 1.6 | 9.7 | 9.5 | 2.6 | 128 | 0.1 | 0.24 | 45 | 13 | 0.32 | 22 | 0.12 | 0.03 | 2.6 | 0.34 | <0 |
| **4GH2 RIM** | | | | | | | | | | | | | | | | | | | | | | | | | |
| Min | 322 | 42542 | 7.4 | 6.5 | 1902 | 233 | 11 | 7322 | 0.31 | 0.79 | 0.7 | 1.1 | 20 | 2.8 | 0.12 | 0.07 | 28 | 7.2 | 0.14 | 29 | 0.2 | 0.03 | 1.2 | 0.23 | 2.3 |
| Max | 513 | 66978 | 251 | 22 | 3606 | 492 | 55 | 10119 | 1 | 1.9 | 1.3 | 3.6 | 31 | 4.9 | 0.27 | 0.74 | 65 | 33 | 0.62 | 46 | 0.51 | 0.4 | 3.7 | 1.3 | 0.82 |
| **Mean(12)** | 380 | 53572 | 30 | 11 | 2464 | 326 | 30 | 8545 | 0.66 | 1.2 | 0.89 | 1.8 | 25 | 3.4 | 0.17 | 0.26 | 42 | 19 | 0.38 | 35 | 0.37 | 0.13 | 1.8 | 0.73 | 0.6 |
| S.D. | 47 | 8995 | 70 | 4.8 | 528 | 71 | 15 | 906 | 0.25 | 0.31 | 0.21 | 0.68 | 3.3 | 0.65 | 0.04 | 0.25 | 11 | 9.5 | 0.16 | 6.1 | 0.09 | 0.09 | 0.66 | 0.31 | 0.33 |
| **4GH2 RETROGRADE 3-APATITE EMULSION** | | | | | | | | | | | | | | | | | | | | | | | | | |
| Min | 391 | 24966 | 8.4 | 5.2 | 1350 | 78 | 18 | 4794 | 0.37 | 1.3 | 0.46 | 0.74 | 5.8 | 3.6 | 0.03 | 0.09 | 12 | 1.6 | <0 | 0.54 | 0.16 | <0 | 0.43 | 0.1 | 7.6 |
| Max | 16075 | 57976 | 51748 | 26 | 5344 | 499 | 131 | 10757 | 11 | 48 | 1.4 | 149 | 95 | 281 | 35 | 103 | 1108 | 31 | 0.89 | 41 | 8.6 | 1.7 | 25 | 1.8 | 1.8 |
| **Mean(35)** | 3666 | 36693 | 27287 | 12 | 2823 | 236 | 56 | 6924 | 2.5 | 10 | 0.78 | 32 | 17 | 102 | 1.8 | 21 | 79 | 12 | 0.28 | 16 | 0.75 | 0.34 | 3.2 | 0.65 | 1.9 |
| S.D. | 4157 | 10195 | 16797 | 3.9 | 993 | 102 | 23 | 1288 | 2.7 | 13 | 0.23 | 42 | 15 | 67 | 5.9 | 18 | 183 | 7.4 | 0.19 | 7.7 | 1.5 | 0.46 | 4 | 0.5 | 18 |

## Trace elements in garnet from Groundhog, S.A.

**Table A- 4 :Summary of LA-ICP-MS trace element data for garnet (ppm) (continued)**

| | Mg | Al | P | Sc | Ti | V | Cr | Mn | Co | Ni | Cu | Zn | Ga | As | Rb | Sr | Zr | Nb | Mo | Sn | Sb | Cs | Hf | Ta | W |
|---|---|---|---|---|---|---|---|---|---|---|---|---|---|---|---|---|---|---|---|---|---|---|---|---|---|
| **5GH1 UNDIFFERENTIATED** | | | | | | | | | | | | | | | | | | | | | | | | | |
| Min | 309 | 244 | 27 | 0.95 | 12 | 1.5 | 2.9 | 3778 | 0.27 | 0.32 | 0.2 | 6 | 1.7 | 21 | 0.02 | 0.35 | 0.06 | 0.03 | 1.5 | 0.7 | 0.25 | 0.01 | 0.02 | <0 | 908 |
| Max | 12150 | 4409 | 1605 | 5.1 | 410 | 91 | 6.7 | 9785 | 15 | 56 | 0.79 | 143 | 39 | 1837 | 0.61 | 5.7 | 3.5 | 1.8 | 5.7 | 40 | 5.1 | 0.45 | 0.53 | 0.3 | 279 |
| **Mean(13)** | 2414 | 1939 | 282 | 1.9 | 76 | 22 | 4.7 | 5622 | 2.3 | 5.1 | 0.4 | 37 | 11 | 581 | 0.17 | 1.6 | 1.1 | 0.29 | 3.2 | 7.2 | 1.4 | 0.1 | 0.09 | 0.04 | 324 |
| S.D. | 3729 | 1423 | 572 | 1.2 | 106 | 31 | 1.1 | 1715 | 3.8 | 15 | 0.15 | 44 | 11 | 594 | 0.19 | 1.5 | 1.4 | 0.47 | 1.3 | 13 | 1.2 | 0.15 | 0.13 | 0.08 | 13 |
| **5GH1 BRIGHT** | | | | | | | | | | | | | | | | | | | | | | | | | |
| Min | 550 | 554 | 14 | 1.1 | 17.5 | 4 | 3.6 | 3575 | 0.44 | 0.24 | 0.2 | 2.2 | 4.4 | 20 | 0.05 | 0.4 | 0.11 | 0.1 | 0.19 | 1.7 | 0.1 | 0.01 | 0.02 | 0.01 | 803 |
| Max | 23260 | 47920 | 621 | 3.9 | 1794 | 262 | 27 | 6613 | 5.8 | 11 | 2.2 | 264 | 28 | 1435 | 1.1 | 3.7 | 59 | 15 | 2.6 | 52 | 1.9 | 4.2 | 2.4 | 0.41 | 575 |
| **Mean(28)** | 4807 | 7589 | 92 | 2.3 | 214 | 29 | 7.4 | 4646 | 1.8 | 1.8 | 0.58 | 51 | 8.8 | 655 | 0.22 | 1.7 | 6.3 | 1.1 | 1.2 | 19 | 0.51 | 0.25 | 0.24 | 0.05 | 178 |
| S.D. | 4602 | 9019 | 107 | 0.82 | 339 | 46 | 5.5 | 749 | 1.1 | 2.4 | 0.43 | 55 | 4.9 | 338 | 0.23 | 0.93 | 13 | 2.7 | 0.64 | 18 | 0.42 | 0.78 | 0.45 | 0.08 | 0.06 |
| **5GH1 BRECCIATED UNDIFFERENTIATED** | | | | | | | | | | | | | | | | | | | | | | | | | |
| Min | 50 | 54 | 3 | 0.15 | 4.3 | 0.12 | 0.31 | 372 | 0.17 | 0.03 | 0.03 | 0.72 | 0.27 | 1.3 | <0 | 0.03 | 0.03 | 0.01 | 0.1 | 0.15 | 0.07 | <0 | <0 | <0 | 1016 |
| Max | 36552 | 63653 | 1693 | 10 | 7893 | 443 | 73 | 11581 | 33 | 372 | 438 | 499 | 33 | 1676 | 12 | 27 | 140 | 44 | 3.9 | 110 | 16 | 10 | 4.8 | 2.4 | 268 |
| **Mean(122)** | 3198 | 18623 | 69 | 2.9 | 1040 | 108 | 9.3 | 5680 | 1.9 | 5.9 | 4.1 | 43 | 11 | 453 | 0.38 | 1.4 | 18 | 6.2 | 1.3 | 17 | 1.3 | 0.2 | 0.94 | 0.27 | 289 |
| S.D. | 6159 | 22836 | 187 | 2.3 | 1474 | 155 | 11 | 2291 | 3.2 | 37 | 40 | 86 | 11 | 439 | 1.5 | 2.7 | 29 | 9.8 | 0.98 | 20 | 2.9 | 0.94 | 1.3 | 0.41 | 181 |
| **5GH2 BRIGHT** | | | | | | | | | | | | | | | | | | | | | | | | | |
| Min | 130 | 15 | 18 | 0.87 | 5.7 | 0.11 | 2.6 | 3050 | 0.46 | 1.3 | 0.43 | 5.4 | 4.8 | 153 | 0.03 | 0.13 | 0.05 | 0.03 | 0.36 | 49 | 0.06 | 0.04 | 0.1 | 0.03 | 598 |
| Max | 494 | 7862 | 42 | 2.1 | 1250 | 5.8 | 7.5 | 3524 | 1.2 | 2.2 | 1.4 | 12 | 13 | 473 | 0.15 | 0.84 | 64 | 9.9 | 2.2 | 122 | 0.9 | 0.5 | 2.1 | 0.51 | 304 |
| **Mean(12)** | 303 | 1870 | 31 | 1.3 | 223 | 1.9 | 3.8 | 3306 | 0.81 | 1.7 | 0.89 | 8.2 | 8.1 | 330 | 0.09 | 0.35 | 8.1 | 1.9 | 0.97 | 101 | 0.35 | 0.17 | 0.46 | 0.16 | 151 |
| S.D. | 113 | 2470 | 7.9 | 0.31 | 390 | 1.9 | 1.4 | 159 | 0.2 | 0.26 | 0.21 | 1.9 | 2.6 | 118 | 0.04 | 0.19 | 18 | 3.3 | 0.68 | 22 | 0.2 | 0.17 | 0.54 | 0.13 | 3 |
| **5GH2 DARK** | | | | | | | | | | | | | | | | | | | | | | | | | |
| Min | 307 | 38172 | 10 | 7.4 | 722 | 55 | 26 | 5152 | 0.27 | 2.5 | 0.84 | 8.9 | 17 | 5 | 0.1 | 0.13 | 97 | 8.2 | 0.23 | 65 | 0.46 | 0.04 | 0.97 | 0.06 | 18 |
| Max | 1506 | 42741 | 22 | 13 | 2600 | 110 | 57 | 6101 | 0.78 | 3.9 | 2.1 | 84 | 133 | 140 | 0.27 | 0.45 | 123 | 14 | 0.92 | 79 | 0.77 | 0.7 | 3.9 | 1.4 | 11 |
| **Mean(8)** | 509 | 40002 | 14 | 10 | 1872 | 88 | 42 | 5648 | 0.47 | 3.1 | 1.5 | 24 | 33 | 29 | 0.16 | 0.27 | 108 | 13 | 0.6 | 70 | 0.6 | 0.17 | 3.1 | 0.67 | 5 |
| S.D. | 406 | 1449 | 3.8 | 1.9 | 680 | 21 | 11 | 373 | 0.18 | 0.51 | 0.37 | 26 | 40 | 45 | 0.05 | 0.14 | 9 | 2 | 0.21 | 5.4 | 0.11 | 0.22 | 0.96 | 0.39 | 0.91 |
| **5GH2 RIM** | | | | | | | | | | | | | | | | | | | | | | | | | |
| Min | 298 | 32584 | 10 | 2 | 907 | 30 | 8 | 4559 | 0.28 | 2.5 | 1.5 | 6.7 | 3.9 | 4.9 | 0.12 | 0.15 | 19 | 2.8 | 0.23 | 5.6 | 0.3 | 0.06 | 0.18 | 0.1 | 0.25 |
| Max | 35582 | 57655 | 27088 | 9 | 4968 | 369 | 72 | 8613 | 17 | 19 | 7 | 423 | 27 | 130 | 16 | 26 | 122 | 98 | 2.9 | 58 | 2.1 | 1.1 | 3.2 | 4.6 | 36 |
| **Mean(28)** | 3226 | 45134 | 992 | 5 | 2102 | 230 | 22 | 7454 | 2.1 | 5.7 | 3.3 | 48 | 20 | 16 | 0.94 | 1.5 | 50 | 17 | 1.1 | 26 | 0.84 | 0.24 | 1.4 | 0.81 | 5.1 |
| S.D. | 7309 | 6386 | 5114 | 2 | 989 | 106 | 16 | 771 | 3.4 | 3.3 | 1.5 | 76 | 5.7 | 25 | 3.1 | 4.8 | 29 | 18 | 0.6 | 11 | 0.38 | 0.21 | 0.79 | 0.98 | 9.7 |

# Trace elements in garnet from Groundhog, S.A.

**Table A- 4 :Summary of LA-ICP-MS trace element data for garnet (ppm) (continued)**

| | Mg | Al | P | Sc | Ti | V | Cr | Mn | Co | Ni | Cu | Zn | Ga | As | Rb | Sr | Zr | Nb | Mo | Sn | Sb | Cs | Hf | Ta | W |
|---|---|---|---|---|---|---|---|---|---|---|---|---|---|---|---|---|---|---|---|---|---|---|---|---|---|
| **6GH1 UNDIFFERENTIATED** | | | | | | | | | | | | | | | | | | | | | | | | | |
| Min | 123 | 19 | 7.9 | 0.51 | 4.4 | 0.19 | 2.1 | 3225 | 0.34 | 0.25 | 0.15 | 0.81 | 0.91 | 52 | 0.02 | 0.08 | 0.03 | 0.01 | 0.09 | 2.1 | 0.04 | <0 | 0.01 | <0 | 38 |
| Max | 435 | 428 | 27 | 1.5 | 78 | 7.9 | 5.1 | 4157 | 1.1 | 1.1 | 0.5 | 2.5 | 12 | 167 | 0.06 | 1.3 | 0.48 | 0.36 | 2 | 38 | 0.21 | 0.09 | 0.1 | 0.02 | 215 |
| **Mean(26)** | 199 | 119 | 14 | 0.94 | 22 | 2 | 3.4 | 3708 | 0.61 | 0.42 | 0.31 | 1.6 | 6 | 94 | 0.04 | 0.33 | 0.11 | 0.06 | 0.88 | 9.6 | 0.1 | 0.02 | 0.03 | 0.01 | 99 |
| S.D. | 80 | 83 | 4.3 | 0.19 | 18 | 1.9 | 0.78 | 225 | 0.16 | 0.18 | 0.08 | 0.49 | 2.2 | 30 | 0.01 | 0.32 | 0.12 | 0.07 | 0.46 | 9.5 | 0.04 | 0.02 | 0.02 | <0 | 45 |
| **6GH1 BRECCIATED UNDIFFERENTIATED** | | | | | | | | | | | | | | | | | | | | | | | | | |
| Min | 48 | 70 | 3.5 | 0.69 | 8.2 | 0.35 | 2.5 | 3307 | 0.15 | 0.18 | 0.14 | 0.38 | 1.7 | 0.88 | 0.01 | <0 | 0.01 | 0.01 | 0.05 | 1.3 | 0.06 | 0.01 | 0.01 | <0 | 0.08 |
| Max | 1188 | 61799 | 40 | 12 | 3830 | 157 | 27 | 9549 | 1.7 | 9.4 | 13 | 10 | 28 | 516 | 0.21 | 85 | 41 | 19 | 4.1 | 36 | 0.37 | 0.07 | 3.1 | 1 | 410 |
| **Mean(52)** | 374 | 27190 | 12 | 3.5 | 1665 | 53 | 9.7 | 6276 | 0.66 | 1.1 | 0.62 | 2.7 | 15 | 99 | 0.06 | 5.9 | 14 | 7 | 0.99 | 13 | 0.13 | 0.02 | 1.1 | 0.33 | 77 |
| S.D. | 260 | 28019 | 8.4 | 3 | 1668 | 54 | 6.4 | 2419 | 0.28 | 1.6 | 1.8 | 2.5 | 9.5 | 142 | 0.03 | 16 | 13 | 7.3 | 1.1 | 11 | 0.06 | 0.01 | 1.1 | 0.35 | 100 |
| **6GH2 BRIGHT** | | | | | | | | | | | | | | | | | | | | | | | | | |
| Min | 173 | 30 | 11 | 0.7 | 2.6 | 0.65 | 1.6 | 3280 | 0.43 | 0.37 | 0.19 | 0.37 | 7.7 | 11 | 0.02 | 0.06 | 0.02 | 0.01 | 0.14 | 2.4 | 0.08 | 0.01 | 0.01 | <0 | 2.1 |
| Max | 838 | 47492 | 66 | 5.3 | 389 | 137 | 10 | 6319 | 1.3 | 1.1 | 6.22 | 3.8 | 22 | 485 | 0.19 | 1 | 2.3 | 2.1 | 3.8 | 119 | 0.55 | 0.4 | 0.5 | 0.5 | 893 |
| **Mean(67)** | 544 | 3664 | 41 | 1.9 | 25 | 16 | 3.6 | 3793 | 0.78 | 0.52 | 0.43 | 1.3 | 15 | 253 | 0.05 | 0.31 | 0.4 | 0.18 | 1.2 | 34 | 0.23 | 0.02 | 0.06 | 0.04 | 438 |
| S.D. | 127 | 7635 | 11 | 1.1 | 49 | 23 | 1.3 | 450 | 0.19 | 0.15 | 0.72 | 0.58 | 3.8 | 96 | 0.02 | 0.2 | 0.57 | 0.34 | 0.92 | 24 | 0.13 | 0.05 | 0.1 | 0.12 | 184 |
| **6GH2 BRECCIATED BRIGHT** | | | | | | | | | | | | | | | | | | | | | | | | | |
| Min | 284 | 151 | 15 | 1.4 | 13 | 3.7 | 4 | 4072 | 0.95 | 0.34 | 0.17 | 2.1 | 12 | 51 | 0.04 | 0.27 | 0.09 | 0.02 | 0.57 | 2.7 | 0.15 | 0.01 | 0.02 | 0.01 | 41 |
| Max | 3681 | 57667 | 57 | 14 | 1209 | 145 | 7.7 | 7434 | 2.5 | 3.2 | 1.3 | 34 | 22 | 639 | 0.19 | 1.4 | 33 | 9.1 | 12 | 7.2 | 0.51 | 0.04 | 0.74 | 0.32 | 825 |
| **Mean(7)** | 901 | 10166 | 40 | 4.9 | 205 | 34 | 5.6 | 4646 | 1.3 | 1 | 0.44 | 7.2 | 19 | 444 | 0.08 | 0.59 | 5.5 | 1.5 | 3.9 | 5 | 0.33 | 0.02 | 0.15 | 0.17 | 487 |
| S.D. | 1229 | 21031 | 14 | 4.4 | 444 | 50 | 1.5 | 1230 | 0.55 | 1.1 | 0.38 | 12 | 3.7 | 187 | 0.05 | 0.42 | 12 | 3.4 | 3.8 | 1.4 | 0.13 | 0.01 | 0.26 | 0.15 | 248 |
| **6GH2 BRECCIATED DARK** | | | | | | | | | | | | | | | | | | | | | | | | | |
| Min | 757 | 47075 | 28 | 11 | 1254 | 153 | 59 | 7268 | 0.77 | 1.1 | 0.36 | 8.1 | 11 | 12 | 0.31 | 1.9 | 48 | 5.4 | 0.17 | 8.7 | 0.18 | 0.08 | 1.6 | 0.29 | 5.8 |
| Max | 13629 | 62241 | 1936 | 29 | 9281 | 276 | 105 | 8810 | 7.4 | 14 | 2 | 138 | 20 | 181 | 4.6 | 9.7 | 419 | 40 | 0.61 | 37 | 0.96 | 0.43 | 11 | 3.5 | 46 |
| **Mean(5)** | 5320 | 54906 | 586 | 21 | 5573 | 182 | 76 | 7808 | 2.9 | 4.9 | 1.3 | 48 | 17 | 56 | 1.7 | 5.6 | 175 | 21 | 0.37 | 18 | 0.64 | 0.19 | 5.2 | 1.9 | 17 |
| S.D. | 5681 | 6433 | 775 | 7.2 | 2989 | 53 | 18 | 590 | 2.8 | 5.5 | 0.7 | 52 | 3.7 | 73 | 1.7 | 3.6 | 148 | 13 | 0.17 | 12 | 0.32 | 0.14 | 3.7 | 1.1 | 17 |
| **6GH2 BRECCIATED UNDIFFERENTIATED** | | | | | | | | | | | | | | | | | | | | | | | | | |
| Min | 570 | 5026 | 9.7 | 5 | 185 | 95 | 8 | 4275 | 1.2 | 0.42 | 0.36 | 4 | 10 | 6.4 | 0.06 | 0.52 | 7.9 | 1.6 | 0.04 | 2 | 0.14 | 0.02 | 0.24 | 0.01 | 3 |
| Max | 11543 | 66671 | 929 | 36 | 13197 | 243 | 508 | 8478 | 5.8 | 10 | 4299 | 113 | 24 | 453 | 0.85 | 45 | 291 | 64 | 2.6 | 48 | 2.7 | 0.16 | 8.1 | 5.6 | 759 |
| **Mean(19)** | 4005 | 52530 | 105 | 15 | 3840 | 137 | 68 | 7334 | 2.7 | 3.6 | 227 | 40 | 14 | 70 | 0.34 | 4.7 | 124 | 16 | 0.48 | 16 | 0.73 | 0.04 | 3.7 | 1.3 | 90 |
| S.D. | 2418 | 16794 | 210 | 10 | 3298 | 43 | 112 | 1116 | 1.2 | 2.2 | 986 | 27 | 4.2 | 133 | 0.23 | 10 | 84 | 15 | 0.64 | 12 | 0.64 | 0.04 | 2.6 | 1.4 | 219 |

# Trace elements in garnet from Groundhog, S.A.

**Table A- 4 :Summary of LA-ICP-MS trace element data for garnet (ppm) (continued)**

| | Mg | Al | P | Sc | Ti | V | Cr | Mn | Co | Ni | Cu | Zn | Ga | As | Rb | Sr | Zr | Nb | Mo | Sn | Sb | Cs | Hf | Ta | W |
|---|---|---|---|---|---|---|---|---|---|---|---|---|---|---|---|---|---|---|---|---|---|---|---|---|---|
| **6GH2 DARK** | | | | | | | | | | | | | | | | | | | | | | | | | |
| Min | 262 | 120 | 5.5 | 1.1 | 4.6 | 2.5 | 2.4 | 3988 | 0.39 | 0.35 | 0.2 | 0.41 | 11 | 1.6 | 0.04 | 0.02 | 0.09 | 0.02 | 0.04 | 20 | 0.07 | 0.01 | 0.03 | <0 | 0.07 |
| Max | 771 | 60324 | 171 | 79 | 4922 | 929 | 113 | 10330 | 1.3 | 15 | 1 | 6.6 | 36 | 422 | 0.39 | 0.66 | 82 | 31 | 1.6 | 85 | 0.63 | 0.04 | 4 | 1.4 | 426 |
| **Mean(34)** | 390 | 41456 | 16 | 15 | 2130 | 363 | 23 | 6656 | 0.73 | 1.2 | 0.44 | 1.4 | 25 | 32 | 0.08 | 0.14 | 28 | 10 | 0.26 | 49 | 0.18 | 0.02 | 1.2 | 0.47 | 30 |
| S.D. | 111 | 11592 | 28 | 17 | 1692 | 248 | 33 | 1068 | 0.18 | 2.6 | 0.15 | 1.2 | 7.6 | 85 | 0.06 | 0.16 | 26 | 7.8 | 0.26 | 15 | 0.12 | 0.01 | 1.5 | 0.45 | 95 |
| **6GH2 RIM** | | | | | | | | | | | | | | | | | | | | | | | | | |
| Min | 161 | 17455 | 5.1 | 1.1 | 62 | 71 | 2.8 | 3651 | 0.43 | 0.39 | 0.13 | 0.43 | 7.8 | 1.5 | 0.05 | 0.03 | 0.64 | 1.3 | 0.04 | 1 | 0.07 | 0.01 | 0.03 | 0.01 | 0.02 |
| Max | 54660 | 73078 | 6262 | 88 | 5906 | 829 | 336 | 15677 | 29 | 504 | 62 | 517 | 46 | 375 | 12 | 36 | 191 | 34 | 0.58 | 89 | 0.75 | 0.76 | 7.6 | 2.2 | 12 |
| **Mean(61)** | 3477 | 51971 | 377 | 21 | 2655 | 360 | 78 | 7716 | 2.3 | 13 | 1.8 | 30 | 23 | 21 | 0.68 | 2.3 | 59 | 13 | 0.24 | 37 | 0.18 | 0.06 | 2.4 | 0.64 | 3.1 |
| S.D. | 7732 | 10996 | 1026 | 21 | 1510 | 237 | 84 | 1622 | 4.1 | 65 | 7.9 | 72 | 10 | 52 | 1.7 | 5.5 | 47 | 8.5 | 0.11 | 22 | 0.11 | 0.11 | 1.9 | 0.48 | 3.6 |
| **7GH1 UNDIFFERENTIATED** | | | | | | | | | | | | | | | | | | | | | | | | | |
| Min | 292 | 41927 | 7.9 | 1.9 | 882 | 94 | 3.4 | 7294 | 0.48 | 0.93 | 0.65 | 1.1 | 25 | 3.5 | 0.09 | 0.05 | 26 | 4.9 | 0.1 | 22 | 0.27 | 0.02 | 0.59 | 0.1 | 0.15 |
| Max | 956 | 53245 | 193 | 12 | 2351 | 408 | 17 | 9754 | 1.9 | 17 | 308 | 23 | 31 | 28 | 0.42 | 1.6 | 95 | 22 | 3.2 | 42 | 3.7 | 1.8 | 2.8 | 0.53 | 1.6 |
| **Mean(16)** | 385 | 46117 | 23 | 4.4 | 1463 | 301 | 7.4 | 8061 | 0.86 | 2.3 | 20 | 3.6 | 28 | 6 | 0.19 | 0.21 | 46 | 11 | 0.59 | 31 | 0.61 | 0.23 | 1.5 | 0.37 | 0.51 |
| S.D. | 155 | 4008 | 45 | 2.3 | 435 | 74 | 3.7 | 589 | 0.4 | 4.1 | 77 | 5.9 | 1.8 | 6 | 0.09 | 0.36 | 17 | 5 | 0.72 | 5.1 | 0.83 | 0.43 | 0.62 | 0.12 | 0.4 |
| **7GH1 BRIGHT** | | | | | | | | | | | | | | | | | | | | | | | | | |
| Min | 64 | 48 | 31 | 0.87 | 4.2 | 0.12 | 2.8 | 3392 | 0.61 | 0.53 | 0.38 | 0.99 | 2.4 | 134 | 0.08 | 0.23 | 0.03 | 0.03 | 0.35 | 1.5 | 0.21 | 0.05 | 0.16 | 0.03 | 254 |
| Max | 4728 | 15426 | 236 | 3.1 | 413 | 9.4 | 11 | 5338 | 7.9 | 6.9 | 98 | 109 | 10 | 1460 | 1.3 | 68 | 11 | 1.1 | 3 | 13 | 1.9 | 0.76 | 0.6 | 0.35 | 802 |
| **Mean(25)** | 412 | 5527 | 63 | 2 | 46 | 2.8 | 5.3 | 4344 | 1.6 | 1.3 | 4.8 | 10 | 4.9 | 778 | 0.2 | 3.5 | 0.94 | 0.22 | 1.5 | 5.8 | 0.82 | 0.11 | 0.32 | 0.11 | 607 |
| S.D. | 906 | 5567 | 38 | 0.49 | 86 | 3.2 | 1.8 | 757 | 1.4 | 1.4 | 20 | 21 | 2.2 | 418 | 0.26 | 14 | 2.2 | 0.29 | 0.71 | 4.1 | 0.49 | 0.14 | 0.12 | 0.08 | 146 |
| **7GH1 DARK** | | | | | | | | | | | | | | | | | | | | | | | | | |
| Min | 57 | 40213 | 16 | 2.4 | 421 | 6.2 | 7.8 | 5759 | 0.66 | 0.78 | 0.67 | 2 | 1.8 | 41 | 0.1 | 0.3 | 17 | 2.8 | 0.26 | 0.88 | 0.35 | 0.07 | 0.47 | 0.1 | 20 |
| Max | 10945 | 55667 | 5296 | 8.8 | 7005 | 80 | 38 | 11582 | 16 | 18 | 1.5 | 167 | 15 | 289 | 7.4 | 13 | 119 | 41 | 0.82 | 25 | 1.4 | 0.5 | 3.5 | 3.3 | 183 |
| **Mean(12)** | 3559 | 47527 | 528 | 4.3 | 2128 | 25 | 14 | 7155 | 5.7 | 6.1 | 1 | 56 | 7.1 | 142 | 0.85 | 2.6 | 52 | 10 | 0.51 | 11 | 0.82 | 0.15 | 1.5 | 0.74 | 90 |
| S.D. | 4435 | 5236 | 1505 | 2.2 | 1866 | 22 | 8.3 | 1583 | 5.8 | 6.6 | 0.25 | 64 | 4.1 | 76 | 2.1 | 3.6 | 32 | 10 | 0.17 | 7.8 | 0.35 | 0.11 | 0.96 | 0.93 | 53 |

## APPENDIX D: LA-ICP-MS ELEMENT MAP

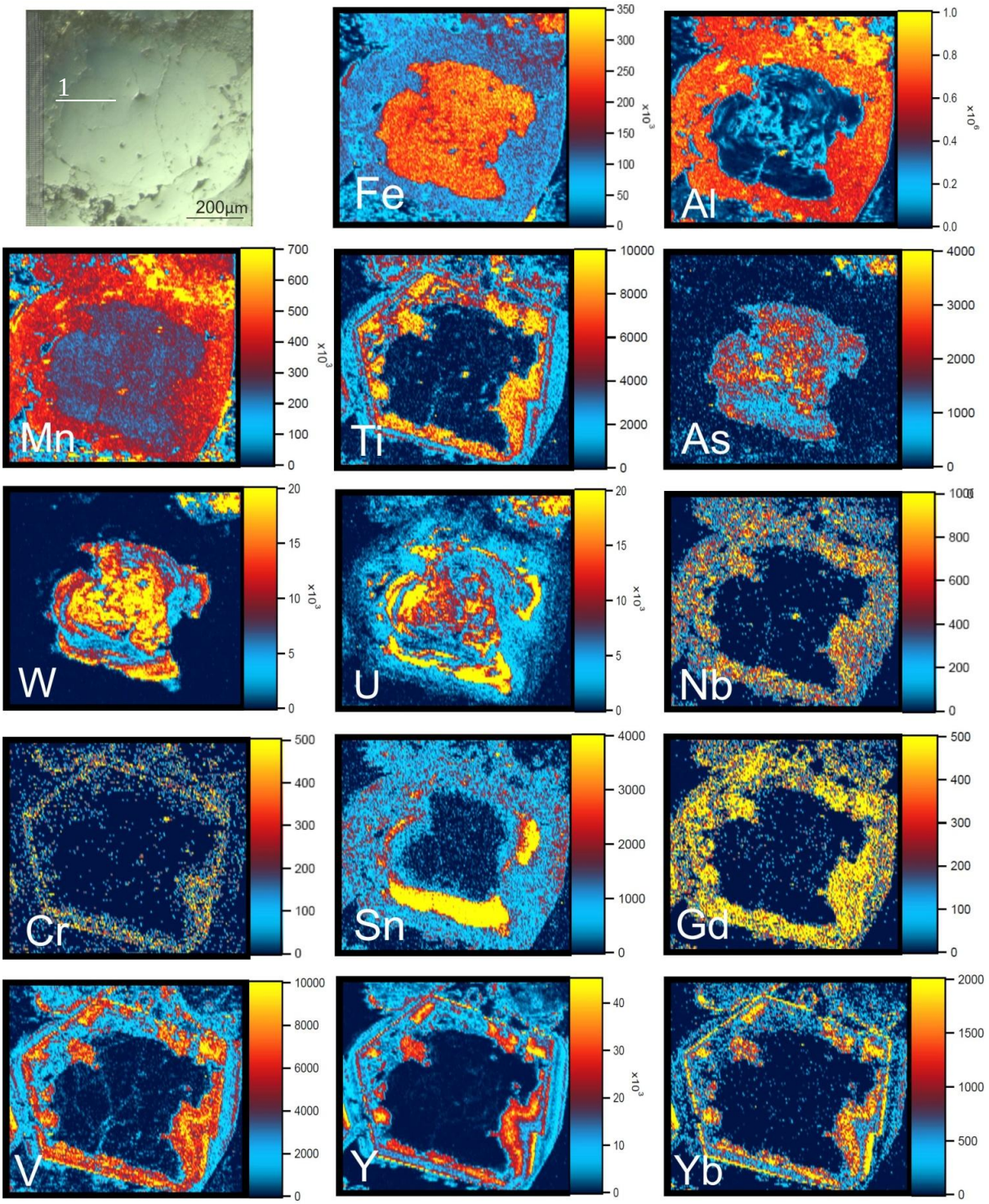


**Figure 15: LA-ICP-MS mineral element map of a course grained garnet from thin section sample GH1-932.3 with optical image of the same grain (top left). The grain shows a bright core with intermediate, darker coloured weak growth zones and an outermost rim. (*Element analysis in ppm*)**

**Trace elements in garnet from Groundhog, S.A.**

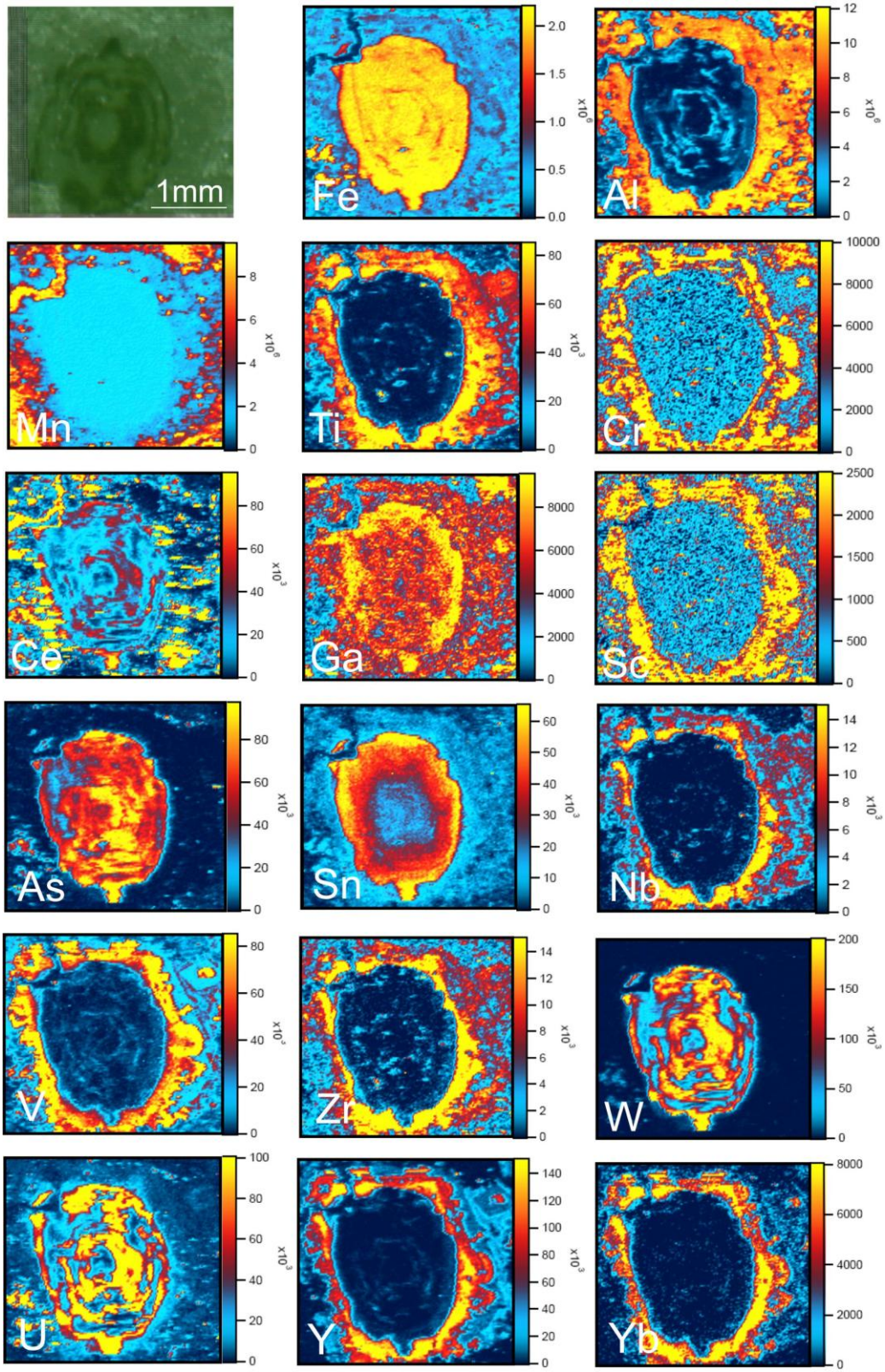


**Figure 16: LA-ICP-MS mineral element map of a course grained garnet from thin section sample GH1-847.8 with optical image of the same grain (top left). The grain shows a bright core with oscillatory zoning of intermediate, darker coloured weak growth zones and an outermost rim. (*Element analysis in counts per second*)**

**Trace elements in garnet from Groundhog, S.A.**

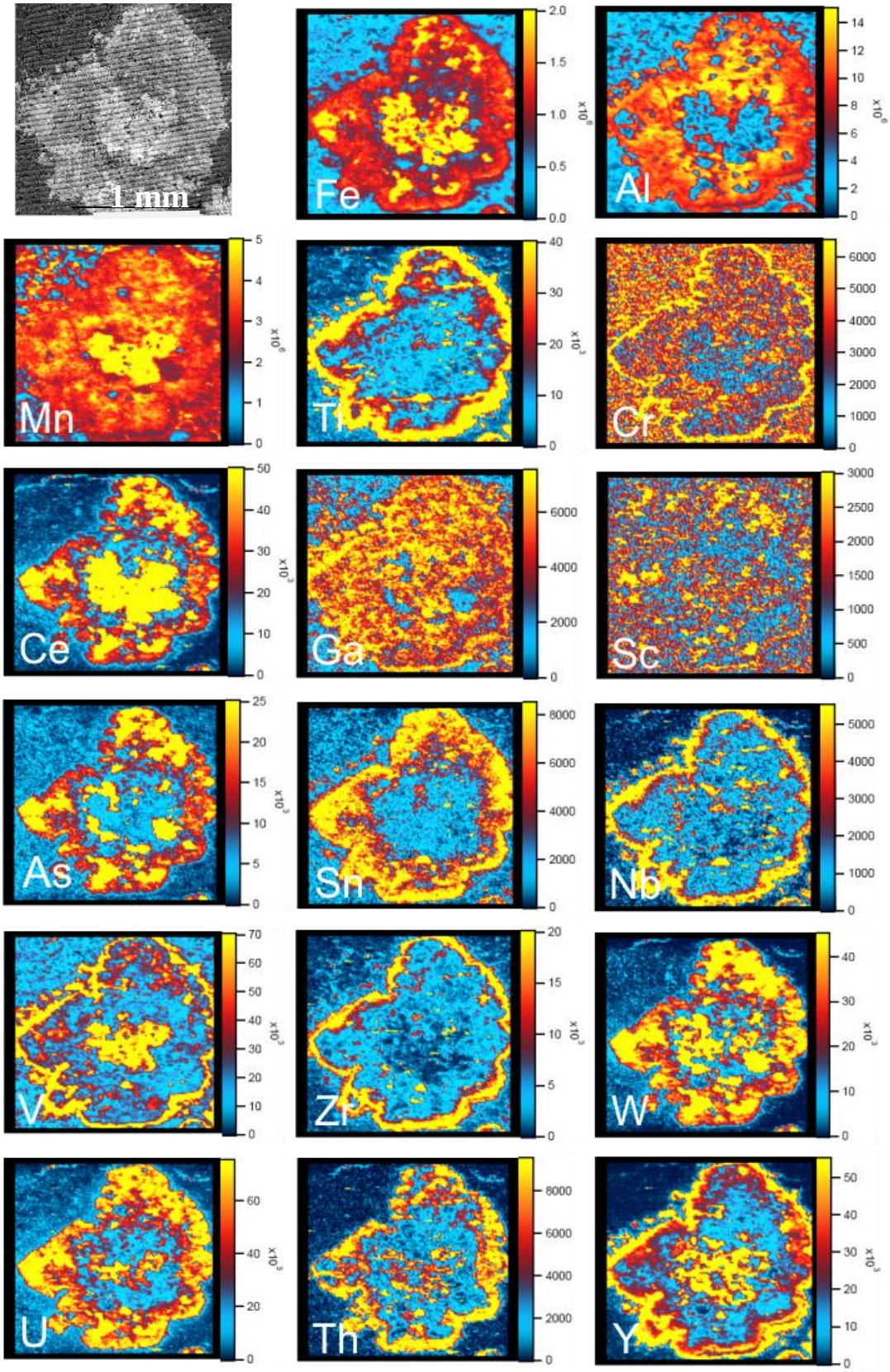


**Figure 17: LA-ICP-MS mineral element map of a course grained garnet from polished block sample GH5-845.4 with optical image of the same grain (top left). The grain shows a bright core with intermediate growth zones and an outermost rim. (*Element analysis in counts per second*)**

**Trace elements in garnet from Groundhog, S.A.**

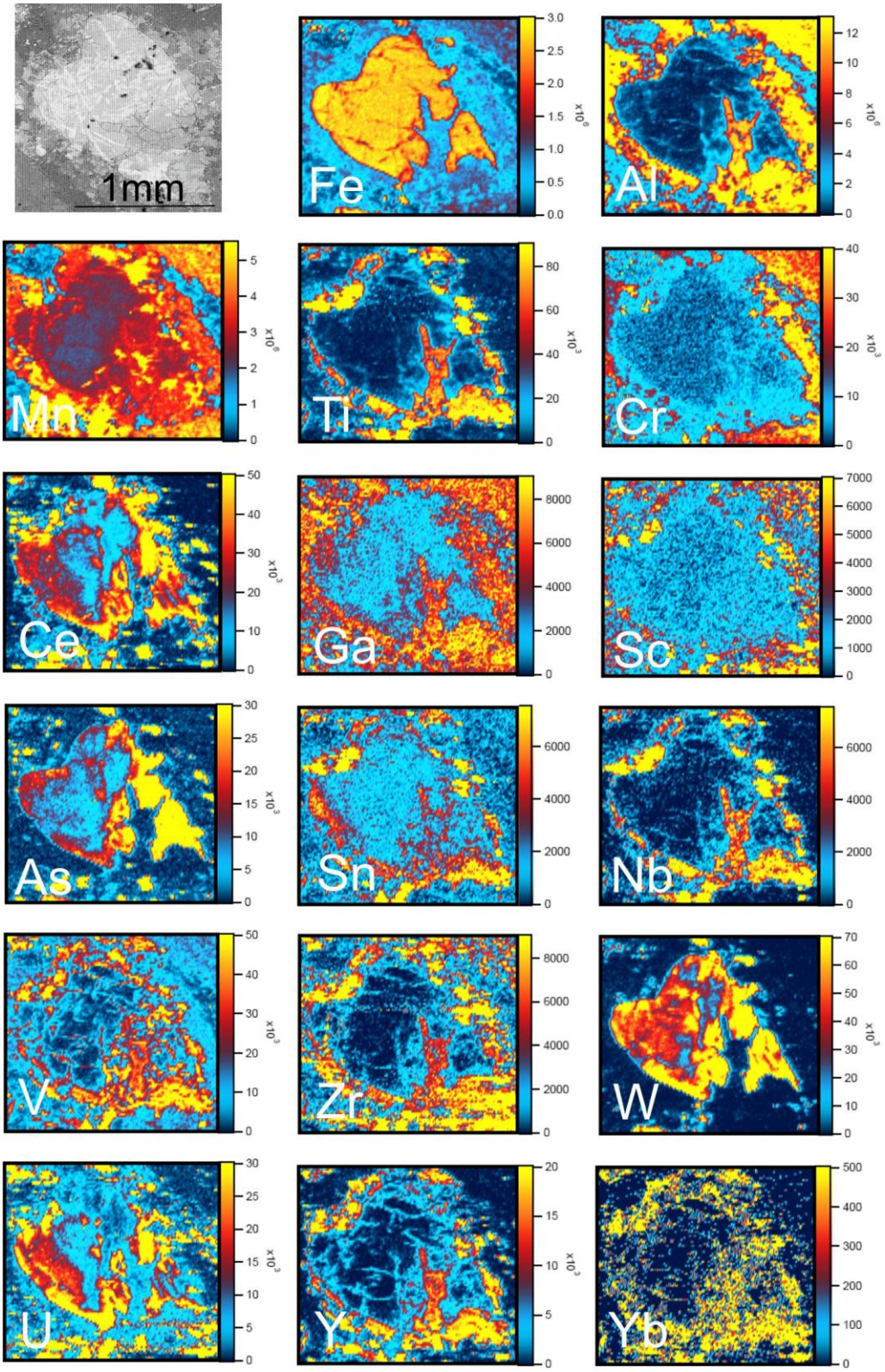


**Figure 18: LA-ICP-MS mineral element map of a course grained garnet from polished block sample GH6-898 with optical image of the same grain (top left). The grain shows a bright core with intermediate growth zones and an outermost rim. (*Element analysis in counts per second*)**

## APPENDIX E: SEM AND OPTICAL IMAGES

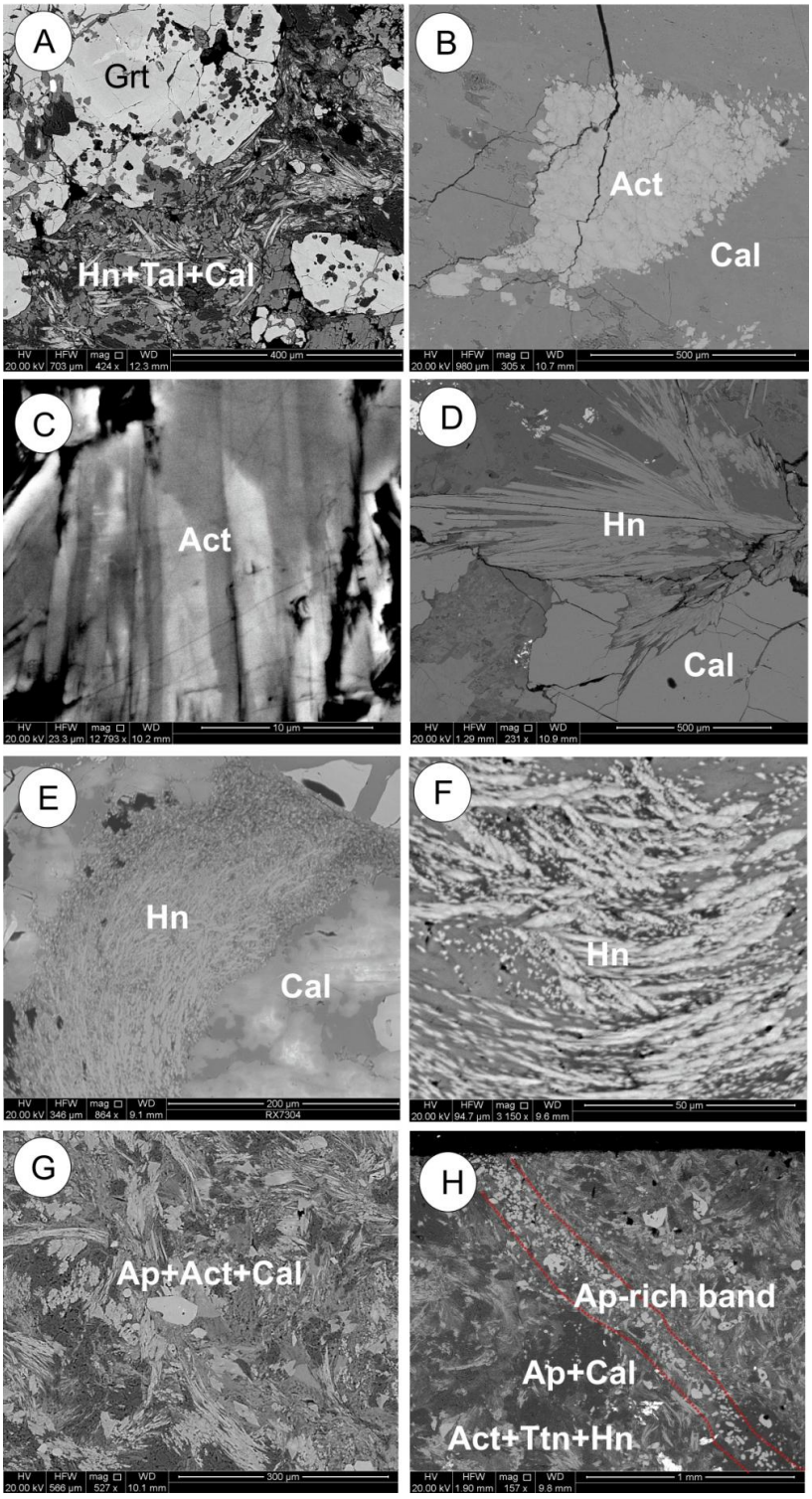


**Figure 19: backscatter electron image showing amphiboles throughout the matrix (apatite (Ap) + titanite (Ttn) + calcite (Cal)). (A) Association between hornblende (Hbl), talc (Tal) and calcite (Cal) with garnet (Grt). (B) Growth of actinolite within an area of course-grained calcite. (C) Close-up of a surface of zoned actinolite. (D) Elongated growths of Hbl within calcite. (E) Large growth of Hbl, forming needle-like shapes within calcite. (F) Close-up from image (E) showing elongated and oriented hbl within calcite. (G) Characteristic matrix of Punt Hill skarn comprising of apatite, elongated actinolite and calcite. (H) Less magnified view of image (G) including growths of matrix garnet and an apatite-rich band**

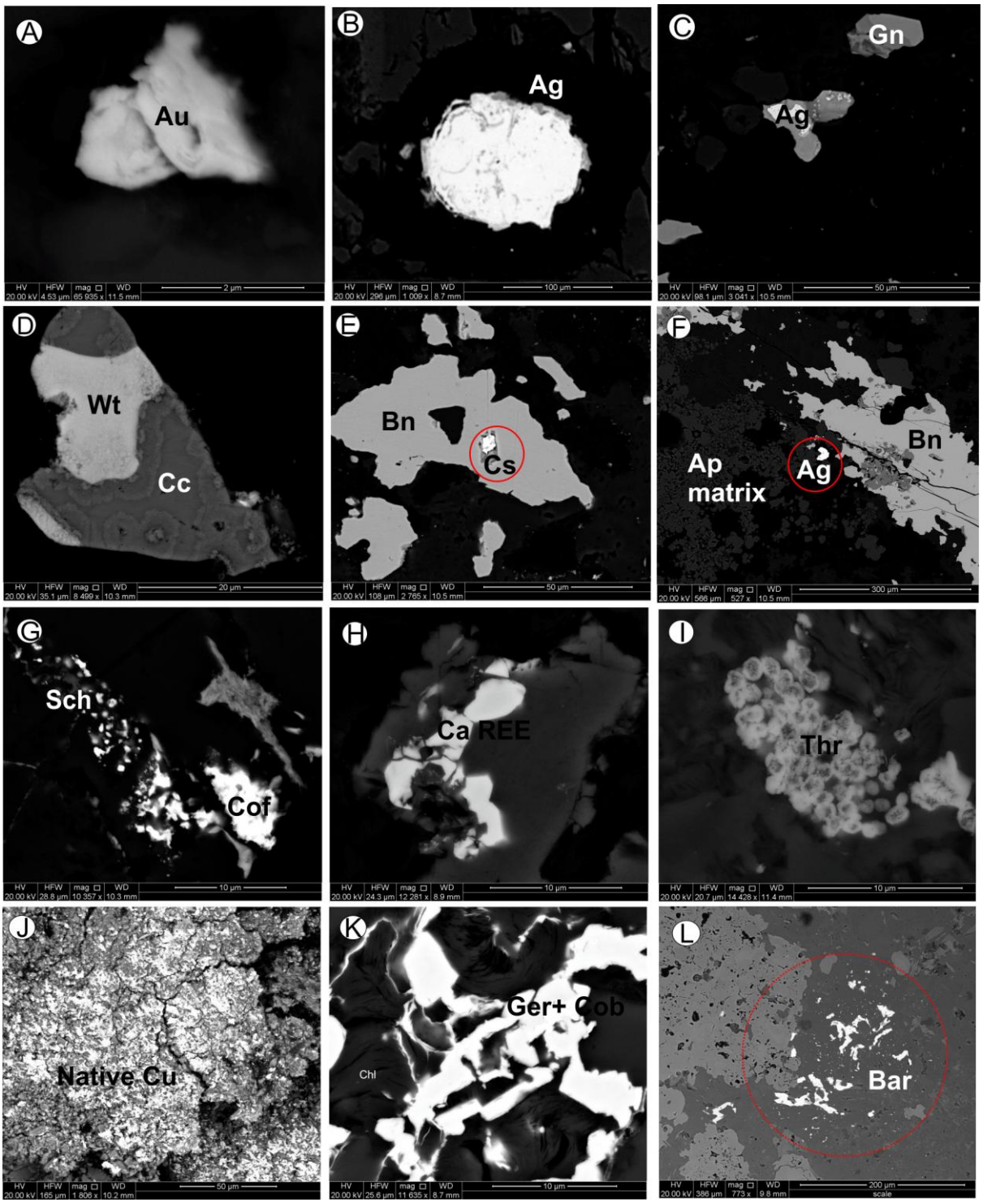


**Figure 20: Backscatter images showing (A) gold (Au) grain within a quartz vug. (B) Grain of silver (Ag) within an apatite and calcite matrix. (C) Galena (Gn) with inclusions of silver within an apatite-rich matrix. (D) Chalcocite (Cc) with inclusions of wittichenite (Wt) in quartz-rich matrix. (E) Irregular patch of bornite showing an inclusion of cassiterite (Cs) in an apatite-rich matrix. (F) Bornite within an apatite-matrix showing close association with silver. (G) A grain of coffenite (Cof) and scheelite (Sch) within a quartz vug. (H) Coarse-grained quartz hosting calcium-rich REE. (I) Thorite (Thr) grains forming within a patch within the K-feldspar-rich marker horizon (J) Native copper scattered (K) Association between chlorite and a mixture of gersdorffite (Ger) and cobaltite (Cob) located within the K-feldspar-rich marker horizon. (L) Irregular-formed patches of barite (Bar) located within the matrix and adjacent to garnet**

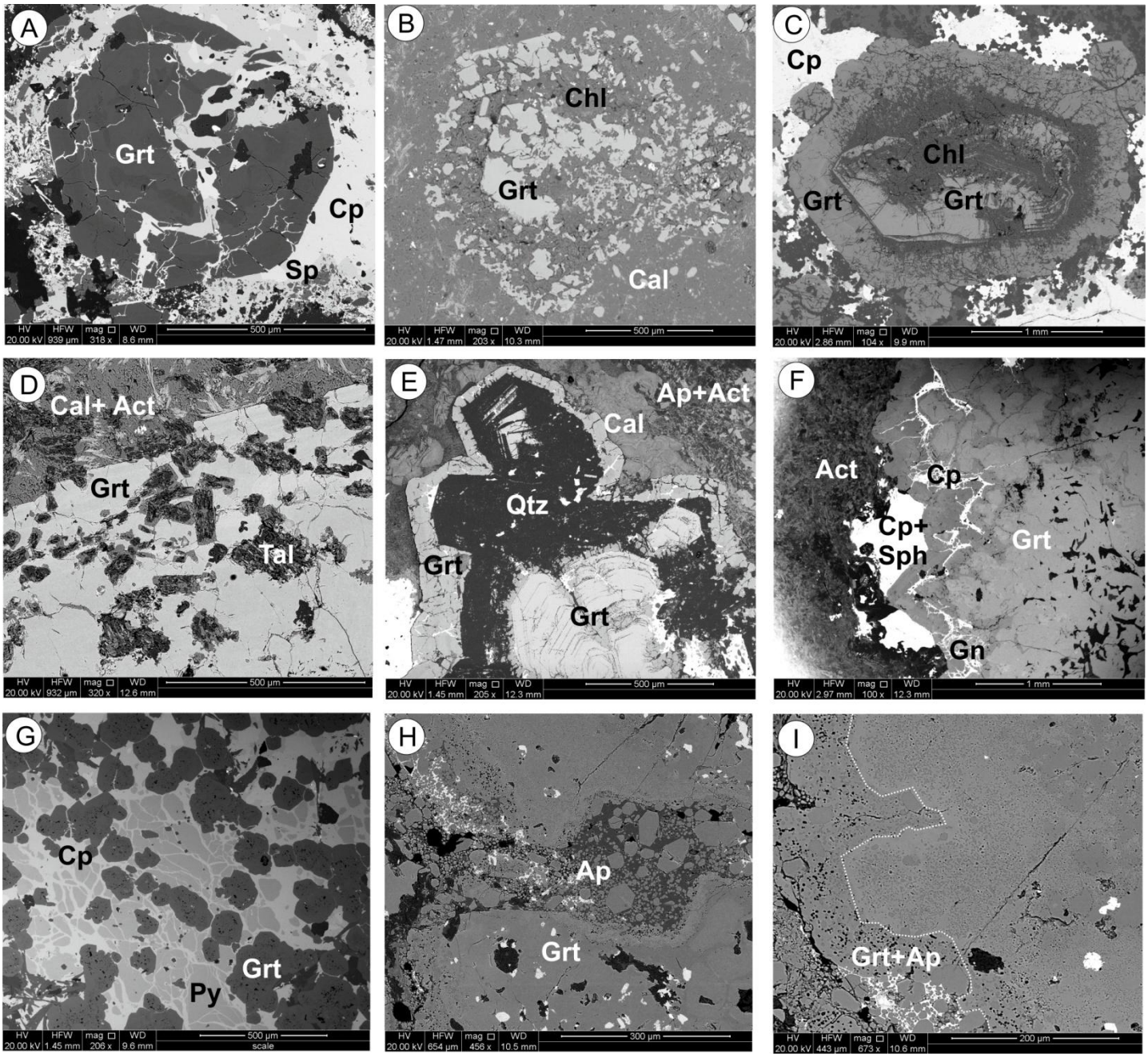


**Figure 21: Backscatter electron images showing (A) Brecciated garnet (Grt) with infill of later-formed chalcopyrite (Cp) that comprises the bulk of the matrix. Cp is accompanied by sphalerite (Sp). (B) A heavily brecciated garnet grain which shows almost complete replacement by late-chlorite. (C) Garnet displaying an early-formed core with oscillatory zoning (type I) being progressively replaced by chlorite and an outermost rim. Sulphides (Cp and Sp) comprise the bulk of the matrix with lesser calcite and actinolite. (D) A portion of a garnet grain showing retangular, elongated inclusions of talc (Tal) intergrown with quartz. (E) Garnet with replacement of dark zones by quartz (Qtz) within the oscillatory zoning and outermost rim. (F) Coarse-grained garnet crystal showing bright core with dark zones replaced by chalcopyrite and galena. Cp and Gn is also present interstitial to garnet. (G) Garnet grains within a matrix of pyrite (Py) and chalcopyrite. Pyrite is being progressively replaced by chalcopyrite. (H) Low magnification image of garnet with apatite emulsion. Large grains of apatite (Ap) are present surrounding the matrix and garnet. (I) Reaction of garnet with apatite creating an emulsion-like texture. Apatite grains approximately 2-20 microns in size**

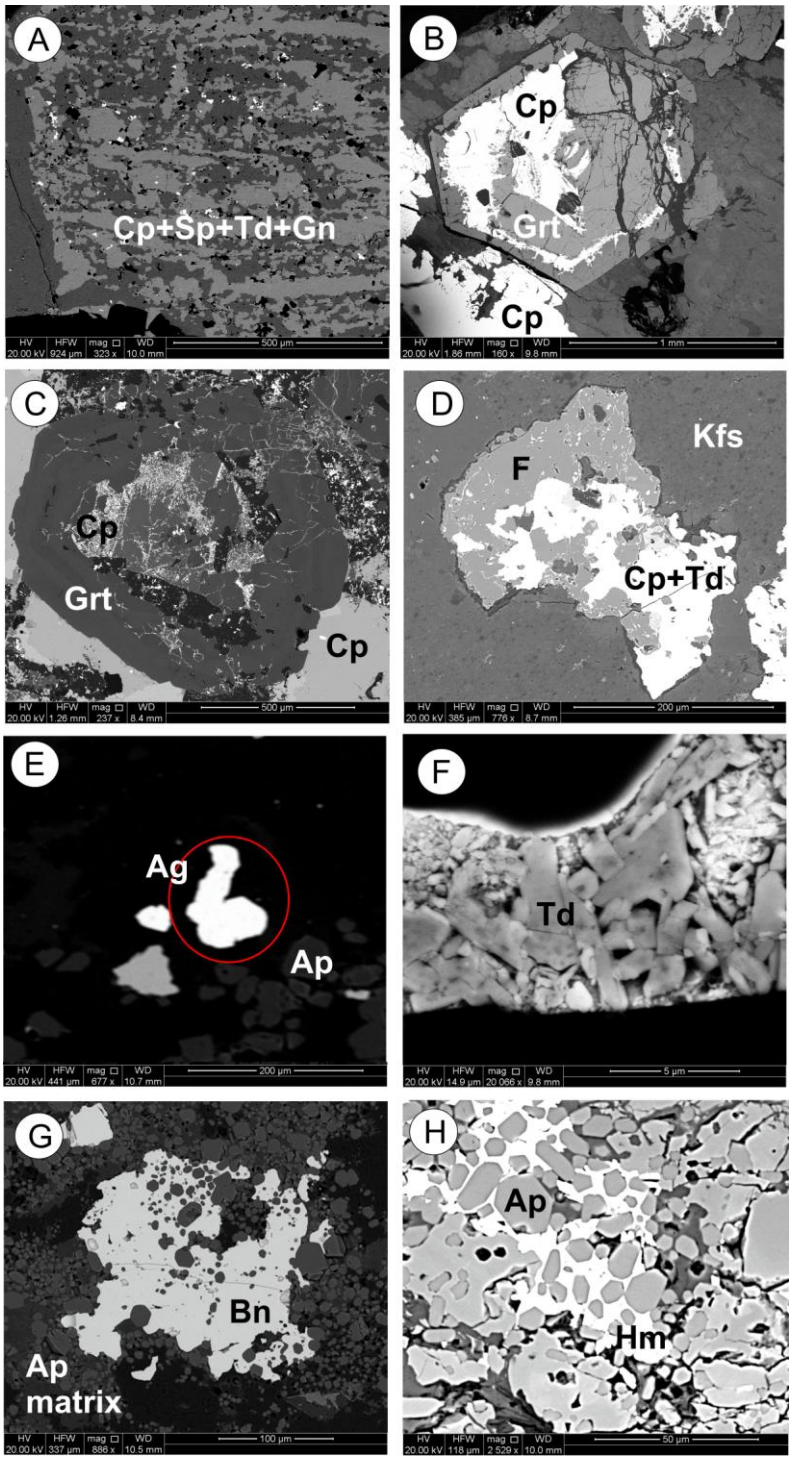


**Figure 22: Backscatter electron images depicting mineralization throughout skarn intervals. (A) Intergrowth texture between chalcopyrite (Cp), sphalerite (Sp), tetrahedrite (Td) and galena (Gn). (B) Idiomorphic oscillatory zoned garnet with chalcopyrite replacing dark zones. Chalcopyrite is also interstitial to the garnet grain, within a calcite matrix. (C) Weakly-zoned, brecciated garnet with infill of chalcopyrite within veinlets. Garnet grain is surrounded by a matrix of chalcopyrite and calcite. (D) Fluorite (F) with remobilised inclusions of chalcopyrite and tetrahedrite (Td) in K-feldspar-rich matrix (Kfs). (E) Grain of silver within an apatite and calcite-rich matrix. (F) Magnified view of tetrahedrite with distinct zoning patterns. (G) Irregular bornite (Bn) patch within an apatite-rich matrix. (H) Association between apatite (Ap) and late-stage infilling of hematite (Hm)**

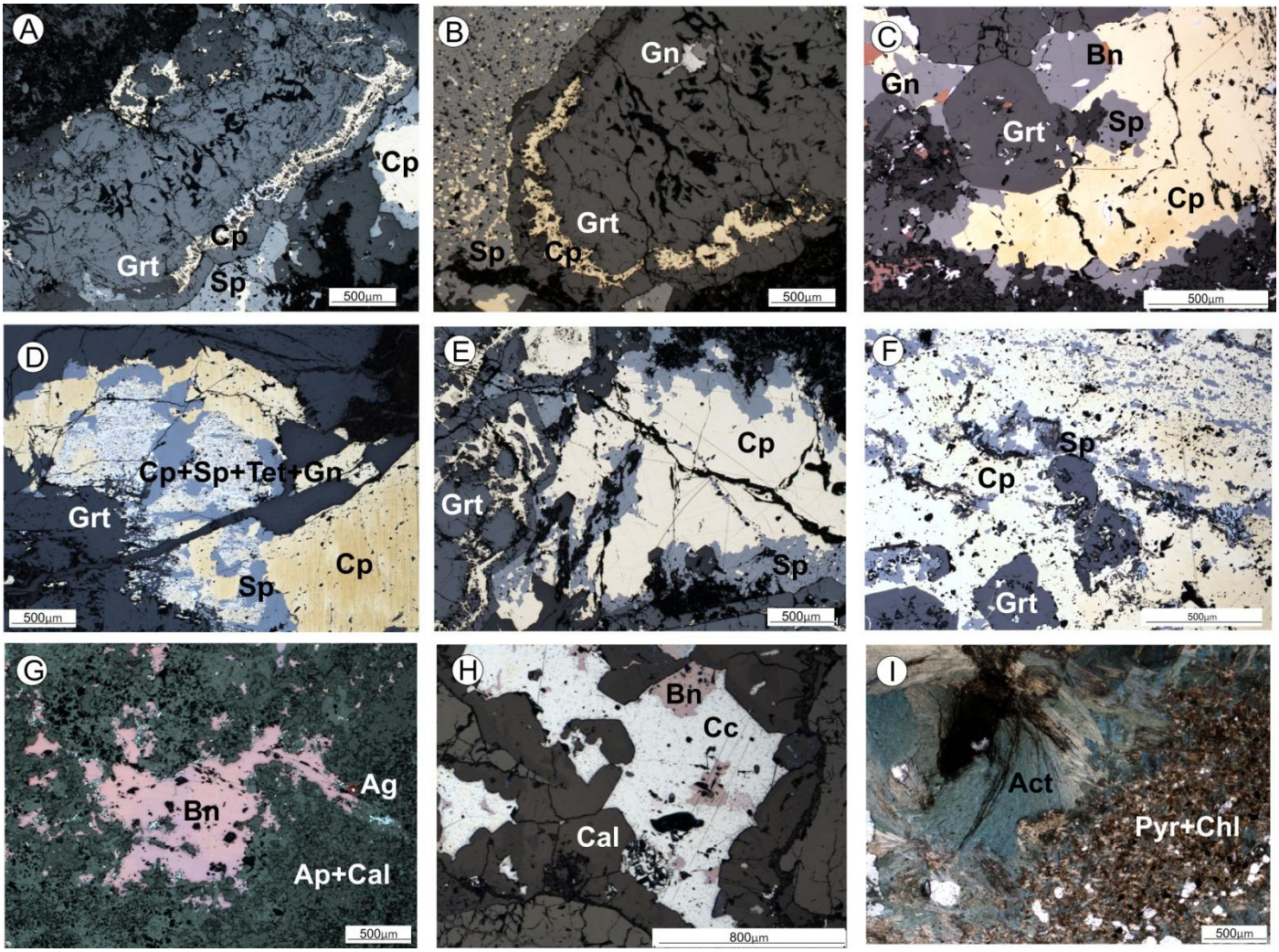


**Figure 23: Optical images showing mineralization throughout the skarn intervals. (A) Garnet grain showing replacement of oscillatory zoning by chalcopyrite (Cp) and galena (Gn) enclosed by an outermost rim. Chalcopyrite and sphalerite (Sp) are also adjacent to garnet in large patches. (B) A coarse-grained oscillatory-zoned garnet being replaced by chalcopyrite, enclosed by an outer rim. Sphalerite is adjacent to garnet and shows chalcopyrite disease (inclusions of Cp throughout). (C) Garnet grains surrounded by a matrix of chalcopyrite (Cp) rimmed by sphalerite (Sp) with inclusions of bornite (Bn) and galena (Gn). (D) Garnet with infill of sulphides, including large patches of chalcopyrite with intergrowths of sphalerite (Sp), tetrahedrite (Td) and galena (Gn). (E) Patches of chalcopyrite (Cp) rimmed by sphalerite (Sp), interstitial to garnet with enclosed skeletal chalcopyrite. (F) Islands of garnet within a chalcopyrite intergrown with sphalerite-rich matrix. (G) Large irregular patch of bornite (Bn) associated with inclusions of silver (Ag) in an apatite and calcite-rich matrix. (H) Chalcocite (Cc) intergrown with bornite (Bn), residing within a quartz vug in garnet. (I) Elongated actinolite (Act), within a fine-grained pyroxene (Pyr) and chlorite (Chl) matrix**